AD_____

Award Number: DAMD17-98-1-8627

TITLE: Mitochondrial Mechanisms of Neuronal Injury

PRINCIPAL INVESTIGATOR: Ian J. Reynolds, Ph.D.
Teresa G. Hastings, Ph.D.

CONTRACTING ORGANIZATION: University of Pittsburgh
Pittsburgh, Pennsylvania 15260

REPORT DATE: September 2000

TYPE OF REPORT: Annual

PREPARED FOR: U.S. Army Medical Research and Materiel Command
Fort Detrick, Maryland 21702-5012

DISTRIBUTION STATEMENT: Approved for public release;
Distribution unlimited

The views, opinions and/or findings contained in this report are those of the author(s) and should not be construed as an official Department of the Army position, policy or decision unless so designated by other documentation.

DTIC QUALITY INSPECTED 4

20001213 104

REPORT DOCUMENTATION PAGE

Form Approved
OMB No. 074-0188

Public reporting burden for this collection of information is estimated to average 1 hour per response, including the time for reviewing instructions, searching existing data sources, gathering and maintaining the data needed, and completing and reviewing this collection of information. Send comments regarding this burden estimate or any other aspect of this collection of information, including suggestions for reducing this burden to Washington Headquarters Services, Directorate for Information Operations and Reports, 1215 Jefferson Davis Highway, Suite 1204, Arlington, VA 22202-4302, and to the Office of Management and Budget, Paperwork Reduction Project (0704-0188), Washington, DC 20503

1. AGENCY USE ONLY (Leave blank)	2. REPORT DATE	3. REPORT TYPE AND DATES COVERED
	September 2000	Annual (1 Sep 99 - 31 Aug 00)

4. TITLE AND SUBTITLE
Mitochondrial Mechanisms of Neuronal Injury

5. FUNDING NUMBERS
DAMD17-98-1-8627

6. AUTHOR(S)
Ian J. Reynolds, Ph.D.
Teresa G. Hastings, Ph.D.

7. PERFORMING ORGANIZATION NAME(S) AND ADDRESS(ES)
University of Pittsburgh
Pittsburgh, Pennsylvania 15260

E-MAIL:
iannmda@pop.pitt.edu

8. PERFORMING ORGANIZATION REPORT NUMBER

9. SPONSORING / MONITORING AGENCY NAME(S) AND ADDRESS(ES)
U.S. Army Medical Research and Materiel Command
Fort Detrick, Maryland 21702-5012

10. SPONSORING / MONITORING AGENCY REPORT NUMBER

11. SUPPLEMENTARY NOTES
Report contains color graphics.

12a. DISTRIBUTION / AVAILABILITY STATEMENT
Approved for public release; distribution unlimited

12b. DISTRIBUTION CODE

13. ABSTRACT ***(Maximum 200 Words)***

This project is investigating the contribution of mitochondria to neuronal injury. Our previous studies have shown that glutamate mediated injury to neurons requires mitochondrial calcium accumulation. However, we know little about the magnitude of the mitochondrial calcium load that causes injury, or the mechanisms that link calcium to neuronal death. In this project we have now established a method for estimating calcium content in neuronal mitochondria following glutamate stimulation. We have also begun to investigate the mechanisms that regulate the production of reactive oxygen species in order to understand the effects of calcium on this process. Additional studies are investigating other aspects of mitochondrial function in relation to neuronal injury. We are characterizing a novel phenomenon of spontaneous mitochondrial depolarization in neurons to understand its involvement in neuronal injury. We are also investigating the properties of cytochrome c release in relation to apoptosis, which may be an important regulator of mitochondrial function. These studies are providing important new information related to the control of neuronal injury by mitochondrial function.

14. SUBJECT TERMS	15. NUMBER OF PAGES
Neurotoxin Mitochondria; neurodegeneration; excitotoxicity; apoptosis; stroke; Parkinson's disease	145 16. PRICE CODE

17. SECURITY CLASSIFICATION OF REPORT	18. SECURITY CLASSIFICATION OF THIS PAGE	19. SECURITY CLASSIFICATION OF ABSTRACT	20. LIMITATION OF ABSTRACT
Unclassified	Unclassified	Unclassified	Unlimited

Table of Contents

Mitochondrial Mechanisms of Neurotoxicity
DAMD17-98-1-8627
Ian J. Reynolds, Ph.D., Principal Investigator
Teresa G. Hastings, Ph.D., Co-P.I.

Introduction

This project is designed to investigate intracellular signaling mechanisms associated with neuronal cell injury. In the acute form, this injury accounts for neural injury following stroke and head trauma, while in the chronic phenotype, it may account for degenerative diseases such as Parkinson's disease. Our preliminary studies have suggested that mitochondria play a pivotal role in the signaling processes that result in neuronal death. Accordingly, we have designed a series of experiments that are intended to elucidate the mechanisms by which mitochondria contribute to neuronal death, with the ultimate goal of identifying strategies for neuroprotection that can be applied to both acute and chronic disease states. These studies are performed on cultured neurons and on tissue derived from mature rodents.

Progress Report.

The progress reported here relates to the revised statement of work dated 7/20/98. This SOW is now focused on the first two technical objectives of the original proposal, based on the recommendations provided by the review process. In the previous progress report we documented the set-up of the microscope system, and this has been fully functional over the last year. According to the statement of work we anticipated completing technical objective 1 and beginning work on technical objective 2. We have made substantial progress on technical objective 1, although the goals have not all been met because of interesting issues that we have encountered along the way. We have begun work on technical objective 2 as anticipated.

Objective 1. Glutamate Injury Model. The first technical objective is concerned with the mechanisms underlying the injurious effects of glutamate in neuronal cultures. Several of the approaches that we have used required further refinement to address the issues raised in this technical objective.
Intramitochondrial Ca^{2+} determination. We reported early findings last year of a novel approach to measuring mitochondrial calcium loading. This approach uses the protonophore FCCP to release calcium from mitochondria into the cytoplasm where it can be detected with one of several low affinity dyes. We have now completed the evaluation of this approach, which appears to be the best method currently available for monitoring glutamate-induced mitochondrial calcium changes in at least a semi-quantitative way. These findings have been submitted to the *Journal of Physiology*, and have received a positive review. We expect to submit a revised manuscript shortly. The original submission is provided in the appendix (Brocard et al., 2000). We have also investigated the sensitivity of mitochondrial calcium transport to CGP 37157, which is putatively an inhibitor of the main calcium efflux pathway from mitochondria. Although this drug clearly does block mitochondrial calcium efflux (White and Reynolds, 1997) we did not find major effects of the drug on neuronal physiology or

pathophysiology. These findings were recently submitted for publication (Scanlon et al., included in appendix).

We are extending these studies of mitochondrial calcium transport in two ways. Firstly, we are attempting to determine the mechanisms of calcium uptake and release under the conditions of these experiments. Based on experiments in isolated mitochondria we expect that the calcium uniporter is the main transport mechanism for both uptake and release (Gunter and Pfeiffer, 1990;Fiskum and Cockrell, 1985). However, establishing this in intact cells is proving difficult because the pharmacological tools are less than ideal. The best inhibitor of this process, Ru360 (Matlib et al., 1998) does not penetrate intact neurons at all. We have had some success in using the drug in isolated mitochondria, and have also applied it to the inside of neurons using a patch clamp electrode and have seen some effects, so we should ultimately be able to address the question of whether the uniporter is the key transport mechanism. This is important because the transport of calcium by mitochondria is critical to the injury process, and learning about the effects of prototype inhibitors will be valuable in designing therapeutic interventions to prevent injury. The second extension of the original findings will involve determining the sensitivity of calcium transport to inhibition of electron transport. Our early results suggest that certain complexes are much more sensitive to inhibition, reflected by a much more profound effect on mitochondrial calcium transport. For example, we can monitor effects of rotenone at concentrations as low as 10nM, suggesting that complex I is especially sensitive to inhibition. This will provide valuable insights into the modification of mitochondrial calcium transport in neurodegenerative disease states characterized by alteration in electron transport chain function (including Parkinson's disease, for example).

Characterization of MitoTracker dyes. We reported last year that we were working on a detailed characterization of the properties of the series of MitoTracker dyes. These tools have been proposed to be potential-sensitive fixable mitochondrial markers that are gaining in popularity. However, our studies show that the dye signals are very dependent on membrane potential, oxidation status and cell type, which makes them somewhat difficult to use. These findings have been submitted for publication and the manuscript is currently under revision for the *Journal of Neuroscience Methods*. A copy of the original manuscript is included in the appendix.

Measurements of $\Delta\psi m$. We reported last year that we had observed spontaneous mitochondrial depolarization in neurons. This is a previously unreported phenomenon in these cell cultures, although some evidence for this type of event has been published in other cells. We have made good progress in studying this unexpected property of neuronal mitochondria, and have also observed similar characteristics of mitochondria in primary astrocyte cultures. We have been able to measure the spontaneous mitochondrial depolarizations (SMDs) using both JC-1 and tetramethylrhodamine methylester (TMRM). We essentially use these two dyes in parallel to ensure that we are not studying a dye-specific artifact. The characteristics of SMDs are illustrated in figure 1 below. We have spent a considerable amount of time determining the best approach to studying SMDs quantitatively, and also in investigating the mechanism underlying SMDs. Using these quantitative approaches we have established that, in neurons, the SMDs are unrelated to action potential generation or glutamate receptor activation, which were the first suggestions to account for the phenomenon. Interestingly, however, SMDs are greatly attenuated

in neurons treated with the ATP synthase inhibitor oligomycin. This suggests that SMDs arise from the change in membrane potential associated with mitochondria switching from a resting state to one of active oxidative phosphorylation. SMDs in astrocytes are similar to those found in neurons, although the phenomenon is harder to analyze quantitatively because the astrocytic mitochondria do not have the same spatial constraints as mitochondria in neuronal processes, and thus move around in the cell to a much greater extent. This makes it difficult to distinguish between alterations in fluorescence intensity and signal variation resulting from mitochondria moving into and out of defined regions of interest used for measuring fluorescence intensity. We have also found that astrocyte mitochondria appear to be more sensitive to alterations in dye signal associated with phototoxicity, especially with TMRM, and this makes interpretation of some of the findings more difficult. Nevertheless, we have a much better understanding of the nature of this phenomenon and some insights into the mechanism. We feel that it will provide a useful marker of mitochondrial function in association with neuronal and astrocyte injury and are currently exploring paradigms that will alter SMD expression. We are currently preparing two manuscripts that will describe these findings, and have submitted an abstract that is included in the appendix (Buckman et al, 2000).

Mechanisms of ROS generation. Based on the prior findings of this laboratory and others, we anticipate that the generation of reactive oxygen species (ROS) by mitochondria may be a critical signaling event in glutamate mediated neuronal injury. However, the mechanisms of ROS generation under circumstances of glutamate stimulation are poorly understood. We have begun to characterize mitochondrial ROS generation in isolated brain mitochondria with an initial goal of establishing the fundamental mechanisms specific to neuronal mitochondria. We will then try to recapitulate the circumstances associated with glutamate receptor activation (high calcium load, increased sodium concentration and mitochondrial depolarization) to understand the mechanism of the glutamate mediated effect. We have so far established that neuronal mitochondria generate large quantities of peroxide when respiring on succinate. However, this ROS generation is very sensitive to small changes in mitochondrial membrane potential, so that depolarization substantially inhibits ROS formation (Figure 2). This suggests that at least some of the conditions associated with glutamate receptor activation should *inhibit* rather than stimulate ROS formation. We also found that mitochondria respiring on complex I substrates do not generate measurable ROS until complex I is substantially inhibited (Figure 2). We have no direct evidence that complex I is inhibited under conditions of glutamate exposure, but this may be a more plausible mechanism to account for the effects of glutamate. We hope to progress from studies in isolated mitochondria to experiments in permeabilized cells and finally to intact neurons to determine both the basic mechanisms of ROS generation as well as to understand the effects of glutamate.

Objective 2. Mechanism of "Death Factor" Release. We continued experiments this year directed at understanding the characteristics of the release of factors that cause neuronal injury.

Characterization of PTP in Brain. We previously reported a comparison of brain and liver mitochondria with respect to the properties of the permeability transition pore (PTP). These findings have now been published in *Experimental Neurology* (Berman et al, 2000) and are included in the appendix.

Tamoxifen Effects on Neurons. We previously reported a study of the effects of tamoxifen on

neuronal mitochondria. We found that it partially protected neurons from glutamate-induced mitochondrial depolarization. However, it did not prove to be protective, either *in vitro* or *in vivo*. This paper has now been published in the *Journal of Pharmacology and Experimental Therapeutics* and is included in the appendix (Hoyt et al., 2000).

Cytochrome c release. Clearly, one of the best candidate molecules for a mitochondrially released death factor is cytochrome c. We have been interested in developing assays for the release of cytochrome c that can be integrated into the other approaches used in this project. We have made some progress with these assays. We have been able to obtain adequate immunohistochemical staining for cytochrome c in our primary neuronal and astrocytic cultures (Figure 3) and have looked at alterations in the distribution of staining in relation to injury. However, although the pattern of staining is clearly different hours after an apoptosis-inducing injury, it is not clear that the changes specifically represent cytochrome c redistribution rather than simply morphological changes of the cells. We continue to develop this approach, although it is possible that the approach of using a GFP/cytochrome c fusion protein may ultimately be a better approach to these experiments (Heiskanen et al., 1999). We are also investigating cytochrome c release from isolated brain mitochondria using Western blotting approaches, with the goal of determining whether toxins such as dopamine and methamphetamine alter cytochrome c release as a mechanism of injury (Figure 3). We are making solid progress with the technical issues, but have not been able to effectively address the experimental questions at this stage. This will be one of the major goals of the coming year.

Figure 1. Spontaneous mitochondrial depolarization.

Reynolds, Ian J.

Images from neurons, 1 frame/30s

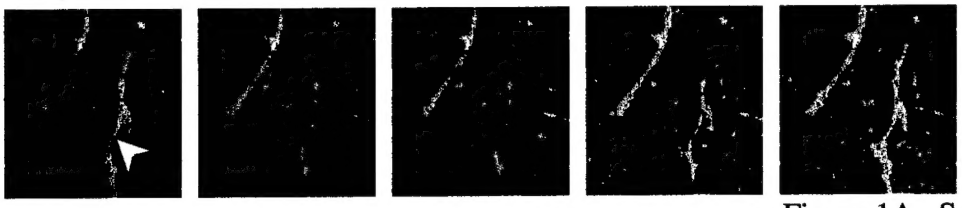

Images from astrocytes, 1 frame/30s

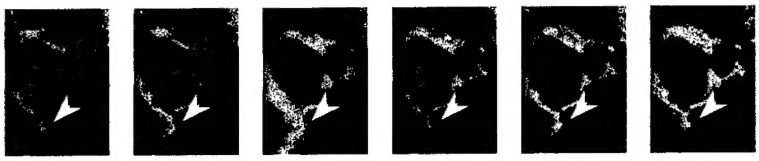

Figure 1A. Spontaneous mitochondrial depolarization in neurons and astrocytes measured with JC-1. The image sequences illustrates mitochondria that show several increases over the 2.5 minutes of this experiment.

Figure 1B. Illustration of an image of a field of neurons in which the qualified JC-1 aggregate signal (red) has been overlaid on the JC-1 monomer signal (green). The subsequent analysis measures the monomer signal associated with the regions under the areas defined by the aggregate signal. Note that the cell bodies are largely excluded from the analysis using this approach. This image contains about 2000 regions of interest.

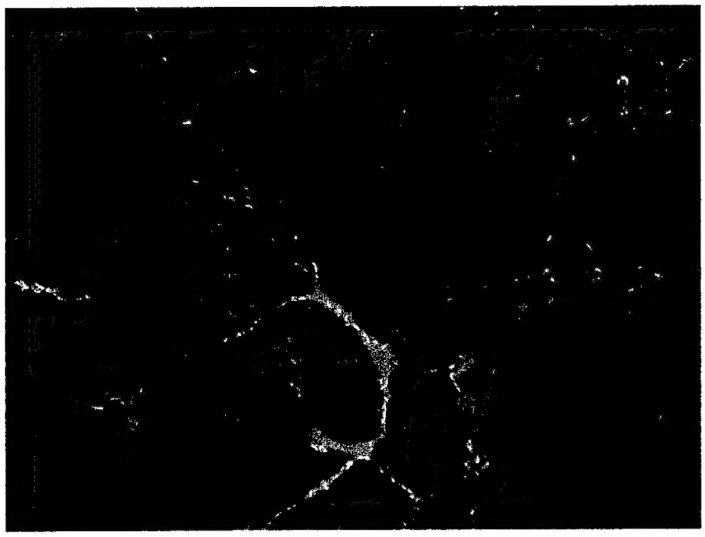

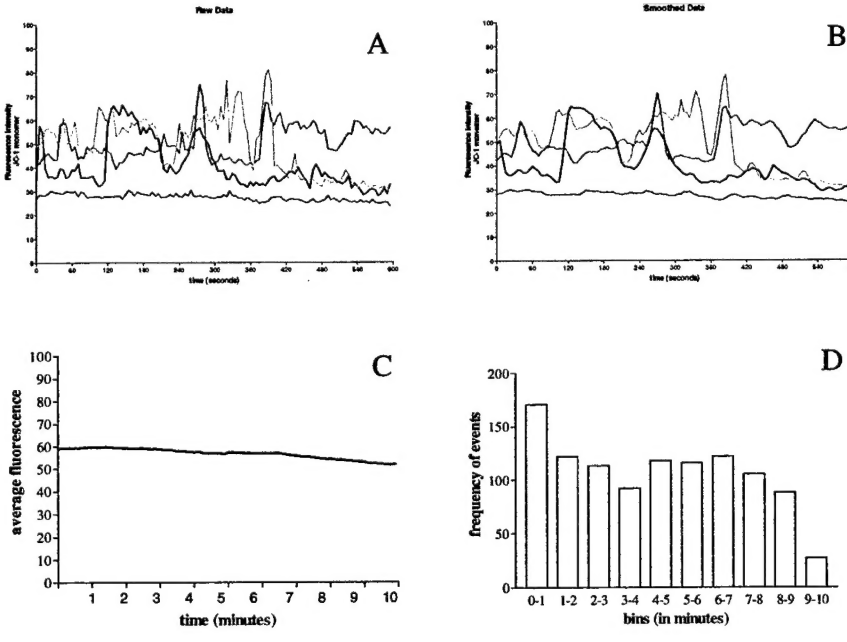

Figure 1C. As an example of the analysis of SMD's, these data show four sample traces from an experiment similar to that shown in figure C1.2. Each trace in panels A and B represent a single ROI and shows the fluctuations in the JC-1 monomer signal over time. Panel B is the smoothed version of the traces in panel A. Panel C shows the overall fluorescence across the entire field over the same experiment, and illustrates the point that the net change in the monomer signal is rather small while there are quite substantial changes in individual ROI's. Panel D is a histogram representing the number of events per one minute bin during this 10 minute experiment.

Figure 2. Mitochondrial ROS generation.

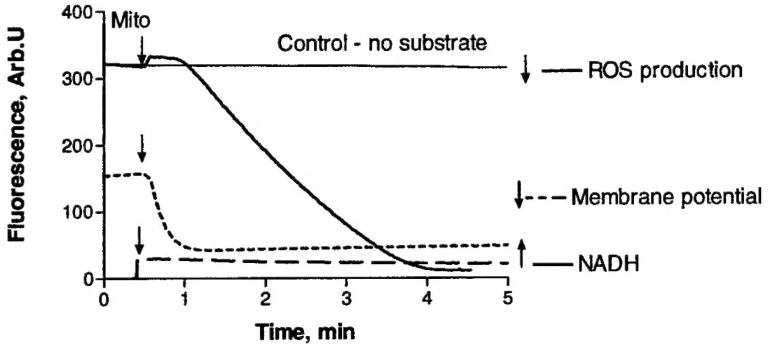

Figure 2A ROS generation by brain mitochondria respiring on succinate. 0.2 mg/ml mitochondria were added as indicated to a cuvette containing scopoletin (ROS production, safranine O (membrane potential) or buffer alone (NADH).

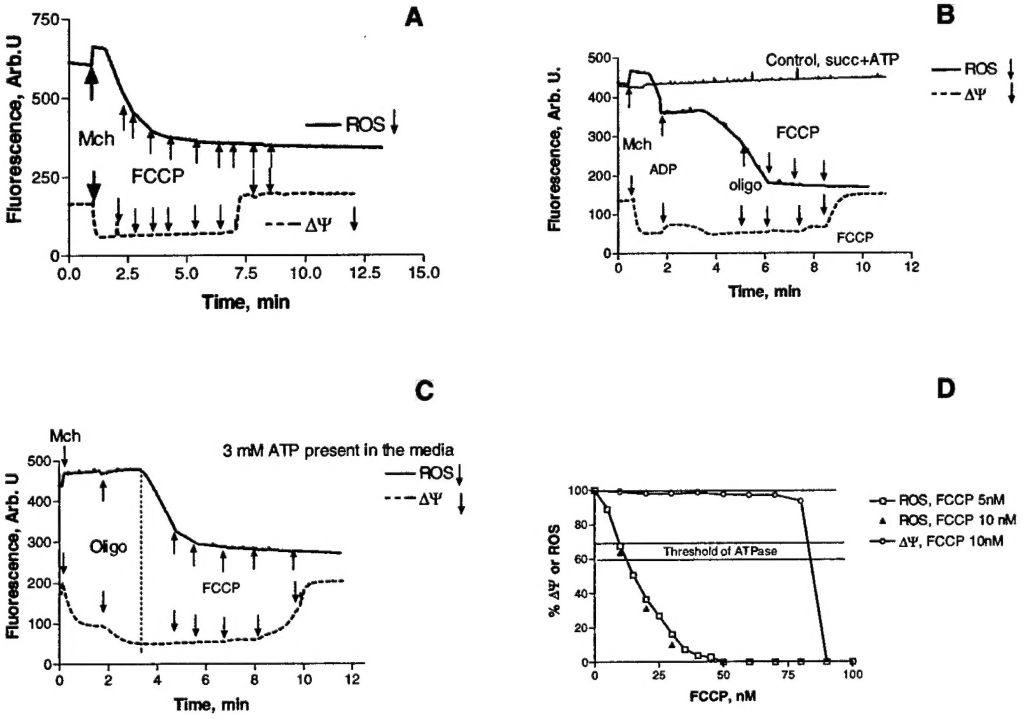

Figure 2B. (A) Addition of FCCP inhibits ROS production. FCCP was added in 10nM increments as indicated by the arrows. (B) Addition of ADP to trigger ATP synthesis depolarizes sufficiently to inhibit ROS generation. ROS production resumes when the ADP is consumed and the membrane potential hyperpolarizes again. (C) Similarly, by blocking ATP synthesis with oligomycin (100nM) hyperpolarization occurs and ROS production is stimulated. (D) This summary graph illustrates the sensitivity of succinate driven ROS generation to very low concentrations of FCCP, and shows that the depolarization associated with ATP synthesis is sufficient to block ROS production.

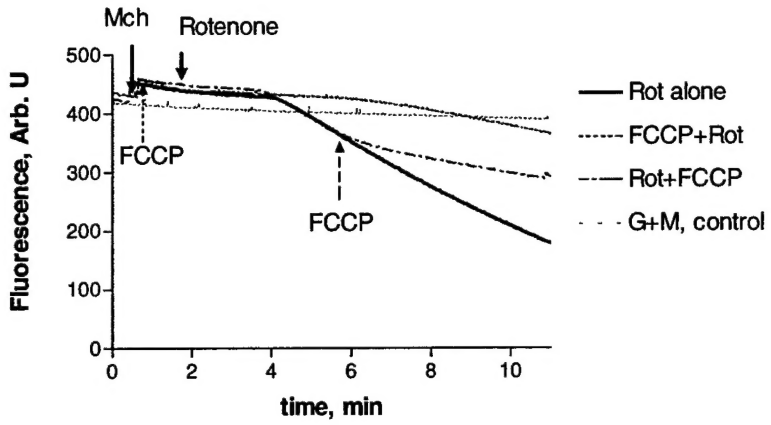

Figure 2C. ROS production driven by glutamate and malate (G+M). In the presence of G+M, ROS production is only evident after the addition of rotenone (2μM). The effects of rotenone are inhibited by FCCP (150nM). The effects of rotenone and FCCP are the same, regardless of the order of addition.

Table 1. Effect of electron transport chain inhibitors on ROS generation by isolated brain mitochondria.

	Rate of Peroxide Production, pmol/min/mg protein (mean ±SEM)				
Substrate	Control	+Antimycin	+Rotenone	+Myxothiazole	+FCCP
Succinate	1388±58.9	274.6±18.0	173.9±17.9	40.2±2.3	-
G+M + Rotenone	434.2±9.2	434.8±21.1*	-	-	140.0±19.9
G+M + Antimycin	227.6±5.6	-	1328±128.1	50.5±9.6	282.8 ±8.24

*Includes FCCP.
Values are the mean ±S.E.M. of 4-23 determinations from different mitochondrial preparations. Peroxide production was determined using the scopoletin/horseradish peroxidase technique which was calibrated using known concentrations of hydrogen peroxide.

Figure 3. Cytochrome c immunohistochemistry.

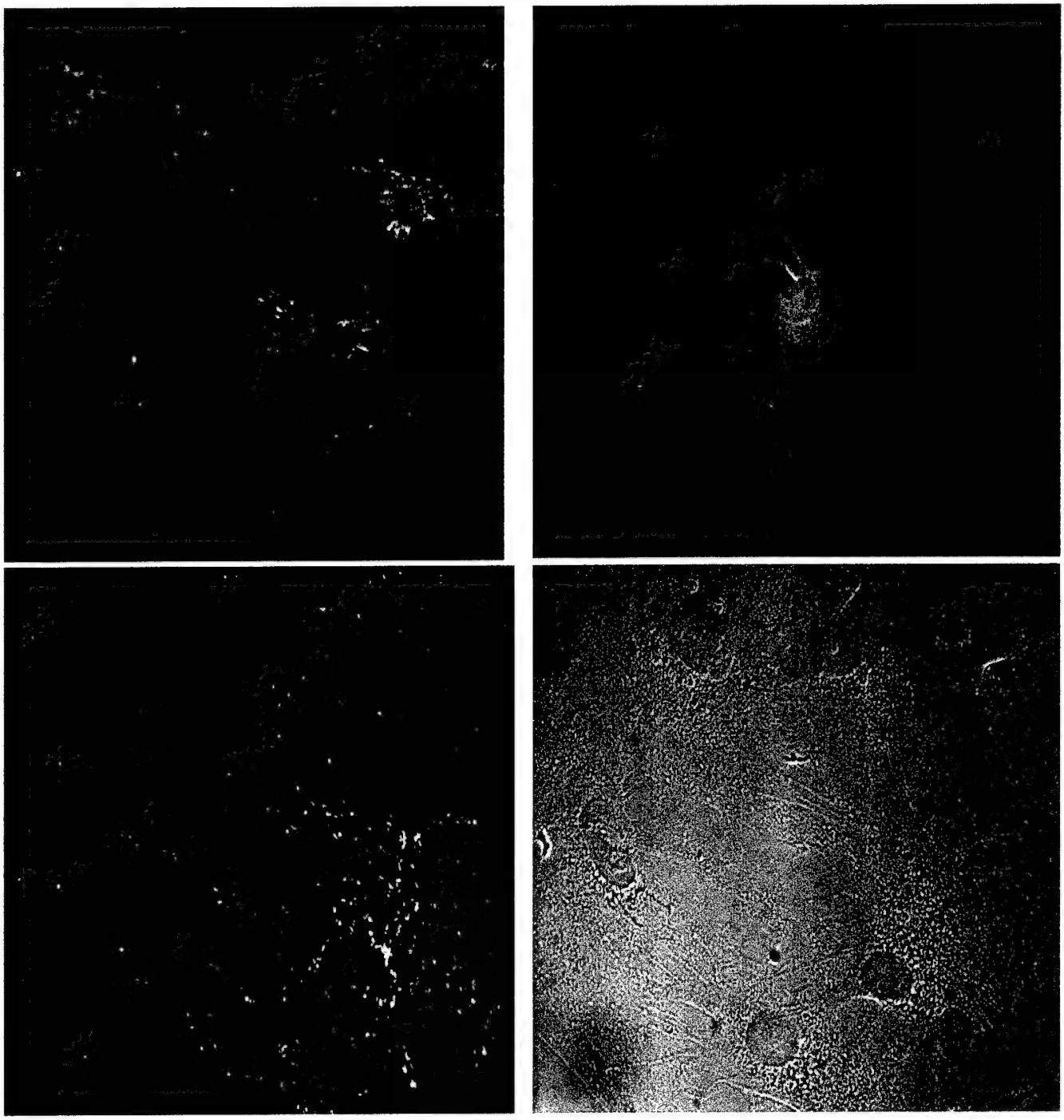

The top pair of panels shows cytochrome c immunohistochemistry in control astrocytes on the left, and the corresponding phase contrast image on the right. The lower pair of images show cytochrome c staining 24h after exposure to a combination of zinc and the ionophonre pyrithione, which is sufficient to cause apoptotic injury. Note that the cytochrome c staining remains punctate following injury even though the distribution is clearly not the same as the control This illustrates the difficulty of using this approach in studying the mitochondrial contribution to apoptotic injury.

Key Research Accomplishments.

- Completed a study characterizing the properties of mitochondrial calcium transport after glutamate receptor activation.
- Completed a study of the properties of the mitochondrial sodium calcium exchange inhibitor CGP 37157 in neurons
- Characterized the properties of spontaneous mitochondrial depolarization in neuronal and astrocytic cultures
- Characterized the properties of ROS generation by neuronal mitochondria

Reportable Outcomes.

All of the papers and abstracts cited here are included in the appendix.

The following papers have been published:

Berman, S.B., Watkins, S.C. and Hastings, T.G. Quantitative biochemical and ultrastructural comparison of mitochondrial permeability transition in isolated brain and liver mitochondria: evidence for reduced sensitivity of brain mitochondria. Exp. Neurol. 164:415-425 (2000).

Hoyt, K.R., McLaughlin, B.A., Higgins, D.S. and Reynolds, I.J. Inhibition of glutamate-induced mitochondrial depolarization by tamoxifen in cultured neurons. J. Pharmacol. Exp.Ther. 293 480-486 (2000).

The following paper is in press:

Reynolds, I.J and Hastings, T.G. The role of the permeability transition in glutamate-mediated neuronal injury. In: Mitochondria and pathogenesis, Lemasters, J.J. and Nieminen, A.-L. (Eds), Plenum Press, New York. (2000).

The following papers have been submitted:

Buckman, J.F., Hernández, H., Kress, G.J., Votyakova, T., Pal, S. and Reynolds, I.J. MitoTracker labeling in primary neuronal and astrocytic cultures: influence of mitochondrial membrane potential and oxidants. Under revision, J. Neurosci. Meth. (2000).

Brocard, J.B., Tassetto, M. and Reynolds, I.J. Quantitative evaluation of mitochondrial calcium content following an NMDA receptor stimulation in rat cortical neurones. Under revision J. Physiol. (2000).

Scanlon, J.M., Brocard, J.B., Stout, A.K. and Reynolds, I.J. Pharmacological investigation of mitochondrial Ca^{2+} transport in central neurons: studies with CGP-37157, an inhibitor of the

mitochondrial Na^+/Ca^{2+} exchanger. Submitted to Cell Calcium (2000).

The following abstracts have been published.

Brocard, J.B., Tassetto, M. and Reynolds, I.J. Quantitative evaluation of mitochondrial calcium content following NMDA receptor stimulation. Society for Neuroscience, 26: 1013, (2000).

Buckman, J.F., Han, Y. and Reynolds, I.J. Spontaneous mitochondrial depolarizations and motility in neurons. Society for Neuroscience, 26: 1016, (2000).

Votyakova, T.V. and Reynolds, I.J. $\Delta\psi$m-dependent and -independent ROS production by rat brain mitochondria. Society for Neuroscience, 26: 1016, (2000).

Kress, G.K., Dineley, K.E. and Reynolds, I.J. Intracellular Fe^{2+} fluorescence measurements and intracellular Fe^{2+} induced neurotoxicity. Society for Neuroscience, 26: 930, 2071(2000).

Conclusions.

We are making solid progress towards the goals laid out in the initial objectives. Our advances in understanding of the quantitative characteristics of neuronal mitochondrial calcium transport will allow unprecedented insight into this critical parameter that regulates neuronal injury. In addition, our studies of the mechanisms of ROS generation are revealing some surprising and important features of this process that are critical to understand when evaluating the mechanisms of glutamate toxicity. The study of spontaneous mitochondrial depolarizations in neurons and astrocytes is an unexpected and exciting development. We are not at all sure of the full implications of this phenomenon. At the least it is likely to represent an interesting and overlooked aspect of mitochondrial physiology in neurons, and it may also provide a critical insight into alterations in mitochondrial function that is associated with the onset of injury.

These experiments help to provide a more complete and accurate picture of the operation of mitochondria in neurons, both under physiological and pathological conditions. Mitochondria obviously have a critical role in normal cell function in generating ATP from glucose. Understanding the ways in which it is possible to interrupt the pathological processes in which mitochondria participate without altering the normal physiological function will be essential if mitochondria are to represent a viable therapeutic target. We feel that the initial findings reported here will help to provide those necessary insights.

References.

1. Fiskum G, Cockrell RS (1985) Uncoupler-stimulated release of Ca^{2+} from Ehrlich ascites tumor cell mitochondria. Arch Biochem Biophys 240: 723-733.

2. Gunter TE, Pfeiffer DR (1990) Mechanisms by which mitochondria transport calcium. Am J Physiol Cell Physiol 258: C755-C786.

3. Heiskanen KM, Bhat MB, Wang HW, Ma JJ, Nieminen AL (1999) Mitochondrial depolarization accompanies cytochrome *c* release during apoptosis in PC6 cells. J Biol Chem 274: 5654-5658.

4. Matlib MA, Zhou Z, Knight S, Ahmed S, Choi KM, Krause-Bauer J, Phillips R, Altschuld R, Katsube Y, Sperelakis N, Bers DM (1998) Oxygen-bridged dinuclear ruthenium amine complex specifically inhibits Ca^{2+} uptake into mitochondria *in vitro* and *in situ* in single cardiac myocytes. J Biol Chem 273: 10223-10231.

5. White RJ, Reynolds IJ (1997) Mitochondria accumulate Ca^{2+} following intense glutamate stimulation of cultured rat forebrain neurones. J Physiol (Lond) 498: 31-47.

DAMD17-98-1-8627

Ian J. Reynolds, Ph.D., P.I.
Teresa G. Hastings, Ph.D., Co-P.I.

Mitochondrial mechanisms of neuronal injury

Year 2 Progress Report - Appendix.

Contains:

2 published reprints

3 submitted manuscripts

4 meeting abstracts

Experimental Neurology **164,** 415–425 (2000)
doi:10.1006/exnr.2000.7438, available online at http://www.idealibrary.com on IDEAL®

Quantitative Biochemical and Ultrastructural Comparison of Mitochondrial Permeability Transition in Isolated Brain and Liver Mitochondria: Evidence for Reduced Sensitivity of Brain Mitochondria

Sarah B. Berman,* Simon C. Watkins,† and Teresa G. Hastings*,‡

**Department of Neuroscience, †Department of Cell Biology and Physiology, and ‡Department of Neurology, University of Pittsburgh, Pittsburgh, Pennsylvania 15213*

Received November 15, 1999; accepted March 23, 2000

Opening of the mitochondrial permeability transition pore has increasingly been implicated in excitotoxic, ischemic, and apoptotic cell death, as well as in several neurodegenerative disease processes. However, much of the work directly characterizing properties of the transition pore has been performed in isolated liver mitochondria. Because of suggestions of tissue-specific differences in pore properties, we directly compared isolated brain mitochondria with liver mitochondria and used three quantitative biochemical and ultrastructural measurements of permeability transition. We provide evidence that brain mitochondria do not readily undergo permeability transition upon exposure to conditions that rapidly induce the opening of the transition pore in liver mitochondria. Exposure of liver mitochondria to transition-inducing agents led to a large, cyclosporin A-inhibitable decrease in spectrophotometric absorbance, a loss of mitochondrial glutathione, and morphologic evidence of matrix swelling and disruption, as expected. However, we found that similarly treated brain mitochondria showed very little absorbance change and no loss of glutathione. The absence of response in brain was not simply due to structural limitations, since large-amplitude swelling and release of glutathione occurred when membrane pores unrelated to the transition pore were formed. Additionally, electron microscopy revealed that the majority of brain mitochondria appeared morphologically unchanged following treatment to induce permeability transition. These findings show that isolated brain mitochondria are more resistant to induction of permeability transition than mitochondria from liver, which may have important implications for the study of the mechanisms involved in neuronal cell death. © 2000 Academic Press

Key Words: **mitochondria; permeability transition; neurodegeneration; apoptosis; excitotoxicity; oxidative stress.**

INTRODUCTION

The important role of mitochondria in normal cellular functioning has long been recognized, and not surprisingly, abnormalities in mitochondrial function are increasingly found to play a significant role in cell death. This has become of particular importance in the brain, where investigations into the mechanisms responsible for neurodegenerative diseases and neurotoxic events have begun to focus on the potential contributions of mitochondrial dysfunction (for review, see 23, 37). Mitochondrial dysfunction has been associated with the mechanisms of several forms of neuronal cell death, including excitotoxicity, apoptosis, ischemia, and hypoglycemia-induced death (20, 22, 27–28, 34, 42, 45, 48, 53, 57, 59, 61–64). Mitochondrial alterations have also been implicated in several neurodegenerative diseases, including Parkinson's disease, Alzheimer's disease, and amyotrophic lateral sclerosis (see 12).

One mitochondrial process that has been increasingly implicated in many of these neurotoxic and neurodegenerative conditions is the opening of a proteinaceous pore in the inner mitochondrial membrane, the permeability transition pore (PTP). The opening of the PTP, termed permeability transition, allows the normally impermeable inner membrane of mitochondria to become nonselectively permeable to solutes with a molecular mass of 1500 Daltons or less. This leads to mitochondrial membrane depolarization, release of small solutes and proteins, osmotic swelling, and a loss of oxidative phosphorylation (see 6, 31). Much of the early work characterizing the properties of the mitochondrial PTP has been performed in liver and heart cells, and opening of the PTP has been linked to many forms of cell death (7). Interest in potential involvement of the PTP in neuronal cell death led to investigations of permeability transition in glial and neuronal cells (21, 32), under conditions of glutamate exposure (53, 62), hypoglycemia (27), and ischemia (42, 59). In

0014-4886/00 $35.00
Copyright © 2000 by Academic Press
All rights of reproduction in any form reserved.

these studies, the pharmacological PTP inhibitor cyclosporin A (CsA) was shown to be protective against the neurotoxic insults. However, interpretation is complicated by the fact that CsA has other cellular effects such as inhibiting calcineurin (56), which may also play an important role in cell death (2, 54).

To avoid such confounds, PTP properties have been characterized directly, by utilizing preparations of isolated mitochondria, most often liver mitochondria, where environmental factors can be controlled and actions of CsA are less ambiguous (see 6, 31 and references therein). Factors that affect pore opening such as calcium concentration, phosphate (Pi), pH, surface potential, oxidants, and free fatty acids have been well described in this system, and many more regulators of the PTP are being actively studied (6). Investigations have also shown different tissue-specific properties. For example, heart mitochondria are much less sensitive than liver to permeability transition induced by calcium alone, and require either higher concentrations of calcium or an additional inducer such as Pi (40, 44). In addition, permeability transition in skeletal muscle mitochondria has been shown to have different sensitivity than liver to modulation by Complex I substrates of the electron transport chain (24).

These data suggest that differences may also exist in pore properties in brain mitochondria. In fact, many variations in mitochondrial function and the cellular environment of brain and liver mitochondria would support this hypothesis. We have previously shown that dopamine oxidation induced opening of the PTP, as evidenced by CsA-inhibitable mitochondrial swelling (4). However, this occurs to a far lesser extent in isolated brain mitochondria than in liver mitochondria (4). Other studies of the PTP in brain utilizing whole cells (21, 32) or isolated mitochondria (1, 32) also report findings that differ from previously noted properties in liver mitochondria. These data suggest the possibility that assumptions about the role of the PTP in brain based on properties developed in liver mitochondria, which has occurred, for example, in studies of the parkinsonian neurotoxin 1-methyl-4-phenylpyridinium (13–14, 43), may not be entirely valid. Thus, it is critical to more fully elucidate PTP characteristics in brain mitochondria, given the growing interest in its involvement in neuronal degeneration. However, no systematic characterization of pore properties in brain mitochondria had been undertaken, nor had any direct comparison of brain mitochondria to the very well-characterized properties of the PTP in liver mitochondria been performed.

Therefore, in this study, we directly compared the effects of exposure to known inducers of the PTP in liver mitochondria to those in identically isolated brain mitochondria. Using three different measures of pore opening: mitochondrial swelling, glutathione (GSH) release, and ultrastructural changes, we provide evidence that the majority of brain mitochondria do not readily undergo permeability transition after exposure to conditions that rapidly induce permeability transition in liver mitochondria. These findings present the possibility that regulatory processes in brain differ from those in liver mitochondria and have important implications for the study of the mechanisms involved in neuronal cell death.

MATERIALS AND METHODS

Mitochondrial isolation. Brain mitochondria from male Sprague–Dawley rats (300–350 g; Hilltop Laboratories, Scottdale, PA), were isolated by differential centrifugation using a medium containing 225 mM mannitol, 75 mM sucrose, 5 mM K-Hepes, 1 mg/ml BSA, and 1 mM EGTA (pH 7.4), according to the method of Rosenthal *et al.* (49). This method uses 0.02% digitonin to free mitochondria from the synaptosomal fraction. Digitonin binds cholesterol and permeabilizes cell membranes such as those of synaptosomes, but has little effect on mitochondria, which contain less cholesterol than cellular membranes (e.g., 55). In order to maintain identical conditions, liver mitochondria were isolated from rat liver (1.5–1.75 g tissue) using the exact procedure as that for brain mitochondria. Mitochondrial protein yields for a single rat, determined by the method of Bradford (10), were approximately 8–12 mg protein for brain and 20–25 mg protein for liver.

To ensure that the preparation contained healthy, functioning mitochondria, mitochondrial respiration was measured prior to the start of experiments (49). Respiration measurements were determined polarographically with a thermostatically controlled (37°C) Clark oxygen electrode (Yellow Springs Instrument Co., Yellow Springs, OH) in medium containing 125 mM KCl, 2 mM K_2HPO_4, 1 mM $MgCl_2$, 5 mM K-Hepes (pH 7.0), 1 mM EGTA, 5 mM glutamate, and 5 mM malate. Mitochondria were only used if the ratios of State 3 respiration (using 0.25 mM ADP) to State 4 respiration (using 2 μg/ml oligomycin) were determined to be at least 7.5. Rates of respiration (ng O/min/mg protein) were similar in brain and liver mitochondria.

Mitochondrial swelling. Mitochondrial swelling was measured spectrophotometrically by monitoring the decrease in absorbance at 540 nm over 10 min similar to previously described methods (11). Mitochondria (1 mg protein) were incubated in 2 ml of media containing 213 mM mannitol, 70 mM sucrose, 3 mM Hepes (pH 7.4), 10 mM succinate, and 1 μM rotenone. In studies of the transition pore, $CaCl_2$ (70 μM) was added after 30 s, and other indicated compounds were added at 2 min. When cyclosporin A (CsA; 850 nM) was used, it was added to the buffer prior to the addition of the mitochondria. Data were quantified and

compared by calculating the total decrease in absorbance from 2 min (the time the indicated inducers were added) to 10 min. In studies utilizing mastoparan, it was added after 30 s, and data were quantified by calculating the total decrease in absorbance from 30 s to 10 min.

GSH measurements. Mitochondria were incubated as described for the swelling measurements. After the 10-min incubation, mitochondria were reisolated via centrifugation at 12,000*g* for 10 min at 4°C. The supernatant was removed, and protein was precipitated from the mitochondrial pellet via sonication in 0.1 N perchloric acid with 0.2 mM sodium bisulfite followed by centrifugation at 18,000*g* for 10 min at 4°C. The resulting supernatant, containing GSH from inside the mitochondria, was removed and stored at −70°C until the time of the GSH assay. Total GSH (oxidized and reduced) was measured via the enzyme-coupled spectrophotometric method of Griffith (29).

Electron microscopy. Mitochondria were prepared for electron microscopy either directly after the final centrifugation of the isolation procedure or following treatment with $CaCl_2$ and Pi as described for swelling experiments, followed by centrifugation at 12,000*g* for 10 min. Electron microscopy methods are well established and only will be discussed briefly. Mitochondrial pellets were prepared and fixed in 2.5% glutaraldehyde in PBS. Following fixation, the samples were cut into small (1 mm^3) cubes, postfixed with 1% osmium tetroxide, dehydrated, and embedded in Epon. Sections were cut using a Reichert Ultracut E ultramicrotome (Leica, Deerfield, IL), mounted on grids, and double-stained with 2% uranyl acetate (7 min) and 1% lead citrate (3 min). Observation was with either a Jeol 100CXII or Jeol 1210 TEM (Peabody, MA). To quantify the proportion of mitochondria affected by treatment with $CaCl_2$ and Pi, mitochondrial profiles were counted from randomly selected images collected at 25,000. Negatives from the two populations were coded and mixed and examined. The mitochondrial profiles were assigned either a normal or aberrant morphology by an experienced microscopist (SCW).

Statistical analysis. Analyses were performed by one-way ANOVA followed by Tukey's *post hoc* comparisons. A probability of $P < 0.05$ was considered significant. N values reported refer to data obtained from separate experiments.

RESULTS

Mitochondrial swelling. Induction of permeability transition has been shown to lead to swelling of mitochondria (31), which can be measured spectrophotometrically. In this study, known inducers of the PTP were tested for their ability to cause mitochondrial swelling in liver and brain mitochondria isolated by identical procedures. Similar to previously reported studies (see 31), exposure of liver mitochondria to 70 μM $CaCl_2$, followed by the addition of the inducers, Pi (3 mM K_2HPO_4), phenylarsenoxide (PhAsO, 5 μM), or tert-butylhydroperoxide (tBOOH, 1 mM) led to large decreases in absorbance, indicative of mitochondrial swelling (Fig. 1A). Cyclosporin A (CsA) has been shown to prevent the opening of the PTP in liver and heart mitochondria (11, 19, 25). We also found that pretreatment of liver mitochondria with CsA (850 nM) largely prevented the swelling caused by the pore inducers (Fig. 1A). In contrast, exposure of brain mitochondria to the same compounds led to much smaller changes in absorbance (Fig. 1B), with less potent inhibition by CsA. Expansion of the scale, as shown in Fig. 1C, clearly reveals that the inducers caused some changes in absorbance in brain mitochondria albeit much smaller than those in liver.

Table 1 shows the quantified results of these treatments. The change in absorbance from the time the inducing agent was added (2 min) until the end of the experiments (10 min) was determined for each condition in liver and brain mitochondria. All of the inducers tested led to a significantly larger absorbance change over time in liver mitochondria as compared to control conditions. CsA pretreatment significantly reduced the absorbance change after exposure to the inducers, by 89% with Pi, 72% with PhAsO, and 74% with tBOOH, indicative of a decrease in the amount of swelling. Exposure to the inducers in brain resulted in changes in absorbance that were 10–14% of responses observed in liver. However, the small responses were still statistically significant for Pi and PhAsO, although not for exposure to tBOOH (Table 1). Effects of CsA pretreatment also differed in brain as compared to liver, preventing only 46% of the change in absorbance caused by Pi and 51% of the change caused by PhAsO (Table 1).

Increasing the mitochondrial calcium load either by the presence of CGP 37157, an inhibitor of sodium-dependent calcium efflux from mitochondria (16, 18), or by exposure to higher concentrations of calcium did not increase the amount of swelling in brain mitochondria (data not shown). These results were also similar whether Complex I substrates in a KCl-based respiration medium, longer incubation times, or combinations of inducers were utilized (data not shown).

Loss of GSH. To begin to determine whether the differences between liver and brain swelling were due to differences in pore function or simply in the swelling properties of the different types of mitochondria, a second measure of pore opening, loss of mitochondrial GSH, was investigated. GSH is a small molecule that is accumulated in the mitochondrial matrix, and the loss of GSH from the matrix has been shown to occur upon pore opening (51). Although GSH exists in both a re-

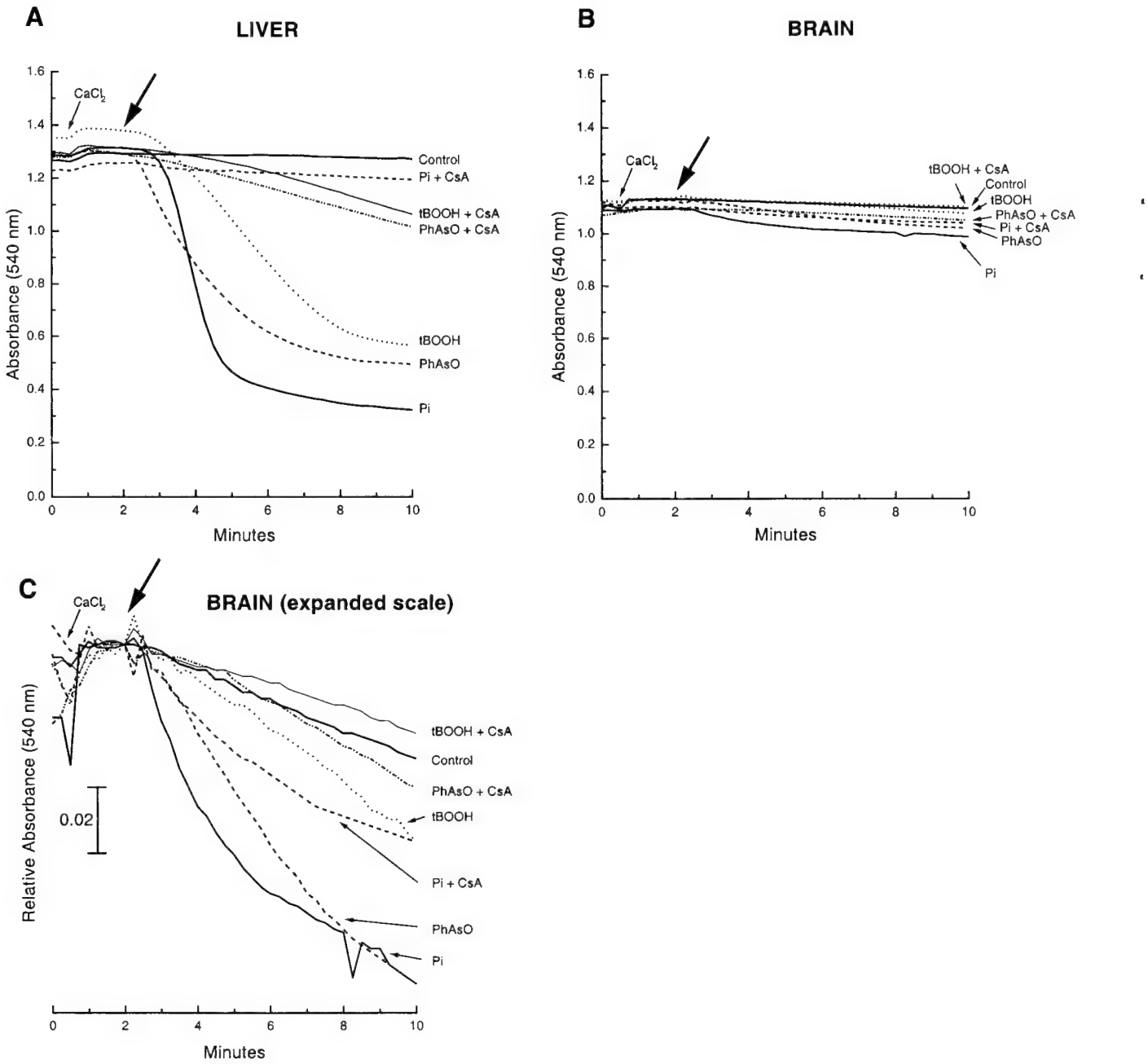

FIG. 1. Representative traces of mitochondrial swelling induced by various agents, assessed spectrophotometrically. $CaCl_2$ (70 μM) was added after 30 s, and other compounds were added at 2 min [phosphate (Pi; 3 mM), phenylarsenoxide (PhAsO; 5 μM), and tert-butylhydroperoxide (tBOOH; 1 mM)]. When used, cyclosporin A (CsA; 850 nM) was present at the beginning of the incubation. Control samples were exposed only to $CaCl_2$. (A) Liver; (B) brain; (C) brain (expanded scale). Arrow indicates the time that the inducers were added.

duced and oxidized form, nearly all of the intramitochondrial GSH has been shown to be in the reduced state (58). Liver and brain mitochondria contain comparable amounts of GSH following isolation and exposure to control conditions containing only $CaCl_2$ (Fig. 2). We found that treatment of liver mitochondria with $CaCl_2$ (70 μM) followed by Pi (3 mM) resulted in a profound loss (−82%) of mitochondrial GSH (Fig. 2). CsA (850 nM) was able to completely prevent this effect. In brain mitochondria, however, $CaCl_2$ and Pi did not result in any loss of GSH (Fig. 2). Incubation with $CaCl_2$ (70 μM) and CsA had no significant effect on GSH levels in either brain or liver mitochondria as compared to controls.

Effects of mastoparan on swelling and GSH release. As a positive control, we tested the effects of the peptide mastoparan on mitochondrial swelling and GSH

TABLE 1

Quantification of Mitochondrial Swelling after Exposure to Permeability Transition Inducing Agents

	Liver		Brain	
Treatment[a]	n	Decrease in absorbance (540 nm)[b]	n	Decrease in absorbance (540 nm)[b]
Control	3	0.024 ± 0.003	8	0.032 ± 0.003
Pi (3 mM)	5	0.958 ± 0.014[c]	3	0.130 ± 0.012[c]
Pi (3 mM) + CsA	4	0.095 ± 0.019[d]	4	0.074 ± 0.006[d]
PhAsO (5 μM)	3	0.853 ± 0.069[c]	3	0.099 ± 0.007[c]
PhAsO (5 μM) + CsA	3	0.230 ± 0.030[d]	3	0.049 ± 0.002[d]
tBOOH (1 mM)	3	0.550 ± 0.150[c]	3	0.052 ± 0.003
tBOOH (1 mM) + CsA	3	0.143 ± 0.059[d]	2	0.024 ± 0.004

[a] Mitochondria were exposed to $CaCl_2$ (70 μM) at 30 s, followed by the indicated agents at 2 min. When utilized, CsA (850 nM) was present prior to the addition of mitochondria.

[b] Values are the absolute change in absorbance from the time the inducing agent was added (2 min) to 10 min (mean ± SEM).

[c] Significantly different than control values ($P < 0.05$).

[d] Significantly different than the same condition without CsA ($P < 0.05$).

release in liver and brain. Although at lower concentrations, mastoparan can induce the PTP (46), at higher concentrations, such as the concentration used in this study (20 μM), mastoparan produces pores in the mitochondrial membrane in a non-CsA-dependent manner, thought to be unrelated to PTP opening (38, 46). We observed that mastoparan caused large-amplitude swelling in both liver and brain mitochondria (Figs. 3A and 3B). In liver, maximal change in absorbance approximated that induced by permeability transition, whereas in brain, the change in absorbance was approximately threefold greater than with presumed inducers of the pore and averaged 40% that of liver (Fig. 3B). In addition, mastoparan caused the complete loss of GSH from both brain and liver mitochondria. Levels of GSH in brain and liver mitochondria under the same control conditions as in the swelling experiments were 2.94 ± 0.17 and 3.03 ± 0.33 nmol/mg protein, respectively (mean ± SEM; $n = 3$). Levels of GSH following exposure to mastoparan (20 μM) were nondetectable in both tissues.

Electron microscopy. Figure 4 shows the typical fine structural morphology of mitochondrial preparations used within this study. In untreated preparations of brain mitochondria (Fig. 4A), the predominant morphology shows small mitochondria with numerous electron dense branching cristae (arrow). The only contaminant in these preparations is free synaptosomes (chevron). In approximately 10% of mitochondria, vesiculated cristae may be seen (arrowhead). Following exposure to $CaCl_2$ (70 μM) and Pi (3 mM) (Fig. 4B), large numbers of normal brain mitochondria are still seen (arrow) as well as synaptosomes. However, mitochondria showing fragmentation and vesiculation of cristae (arrowhead) now represent a larger (quantitatively 45%) proportion of the mitochondrial fraction in these preparations. Liver mitochondria prepared in the same fashion show a somewhat different morphology (Fig. 4C): the intracristal volume appears reduced when compared with the brain mitochondria, principally due to an increased volume fraction of matrix within the mitochondria. Apart from occasional free membrane derived from the endoplasmic reticulum, there is very little contamination of this preparation. Treatment of liver mitochondria with $CaCl_2$ and Pi completely disrupts the mitochondrial morphology (Fig. 4D). Although discrete membrane bound profiles persist, no recognizable structures are present within the mitochondria apart from free protein aggregates.

DISCUSSION

This study is the first to directly compare properties of the mitochondrial PTP in brain mitochondria with those of the well-characterized liver mitochondria, using both biochemical and ultrastructural measurements. We found that brain and liver mitochondria behave biochemically and morphologically different after exposure to agents that have previously been shown to induce permeability transition in liver mitochondria.

Using three different measures, we provide evidence that isolated brain mitochondria are more resistant to undergoing permeability transition upon exposure to conditions that rapidly induce the opening of the PTP in liver mitochondria. Exposure to transition-inducing agents led to a large, CsA-inhibitable decrease in spectrophotometric absorbance, a loss of mitochondrial GSH, and morphologic evidence of matrix swelling and disruption in liver mitochondria, as has been reported

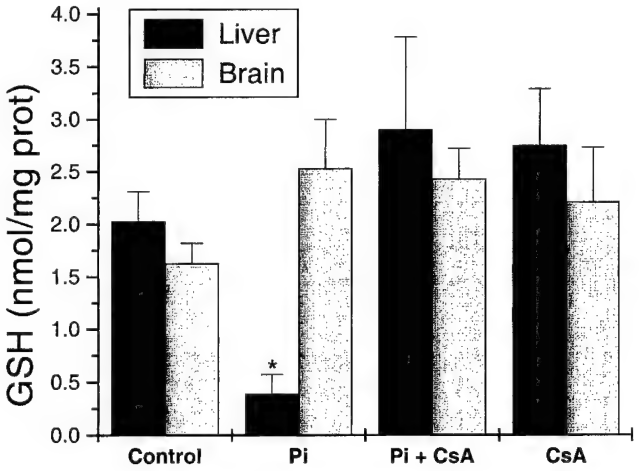

FIG. 2. GSH remaining in the mitochondria was measured following a 10-min incubation period (mean ± SEM; $n = 3$–9). $CaCl_2$ (70 μM) was added to all samples after 30 s of incubation, and Pi (3 mM) was added where indicated after 2 min.

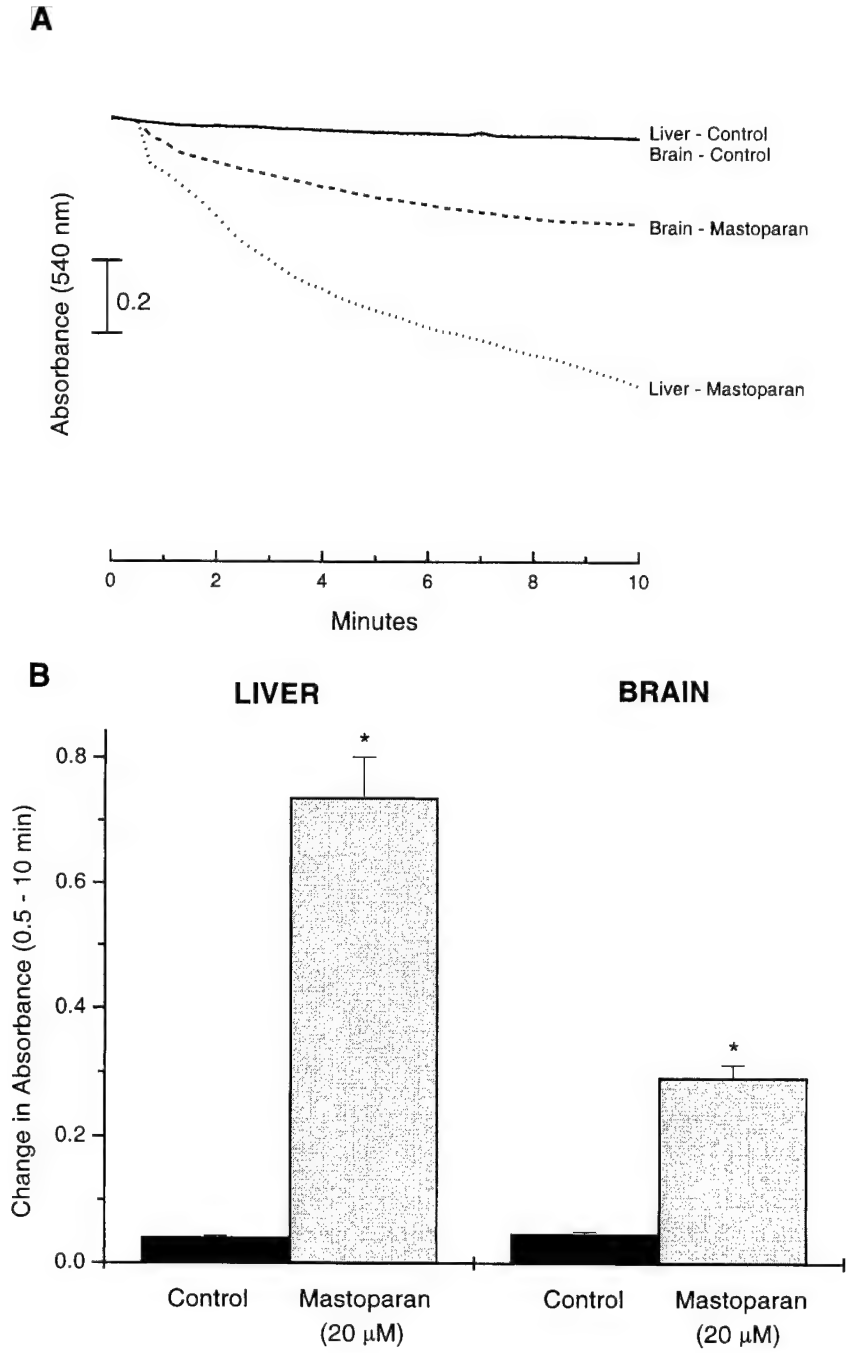

FIG. 3. (A) Representative traces of mitochondrial swelling induced by mastoparan (20 μM), added at 30 s compared to control. (B) Quantification of absorbance changes calculated as the absolute change in absorbance from 30 s to 10 min (mean ± SEM; n = 3–4).

previously (e.g., 8, 51, 52). However, we found that similarly treated brain mitochondria showed very little absorbance change as compared to liver and no loss of GSH. The absence of these responses in brain was not simply due to structural limitations, since large-amplitude swelling and release of GSH were induced when membrane pores unrelated to the PTP were formed by high concentrations of mastoparan. As additional evidence, electron microscopy revealed that the majority of the brain mitochondria appeared morphologically unchanged following treatments to induce PTP. The morphological changes that did occur were more subtle and did not reflect the complete disruption of structure that was observed in liver mitochondria.

Comparison to previous studies of isolated brain mitochondria. We have previously noted a similar differential swelling response of liver and brain mitochon-

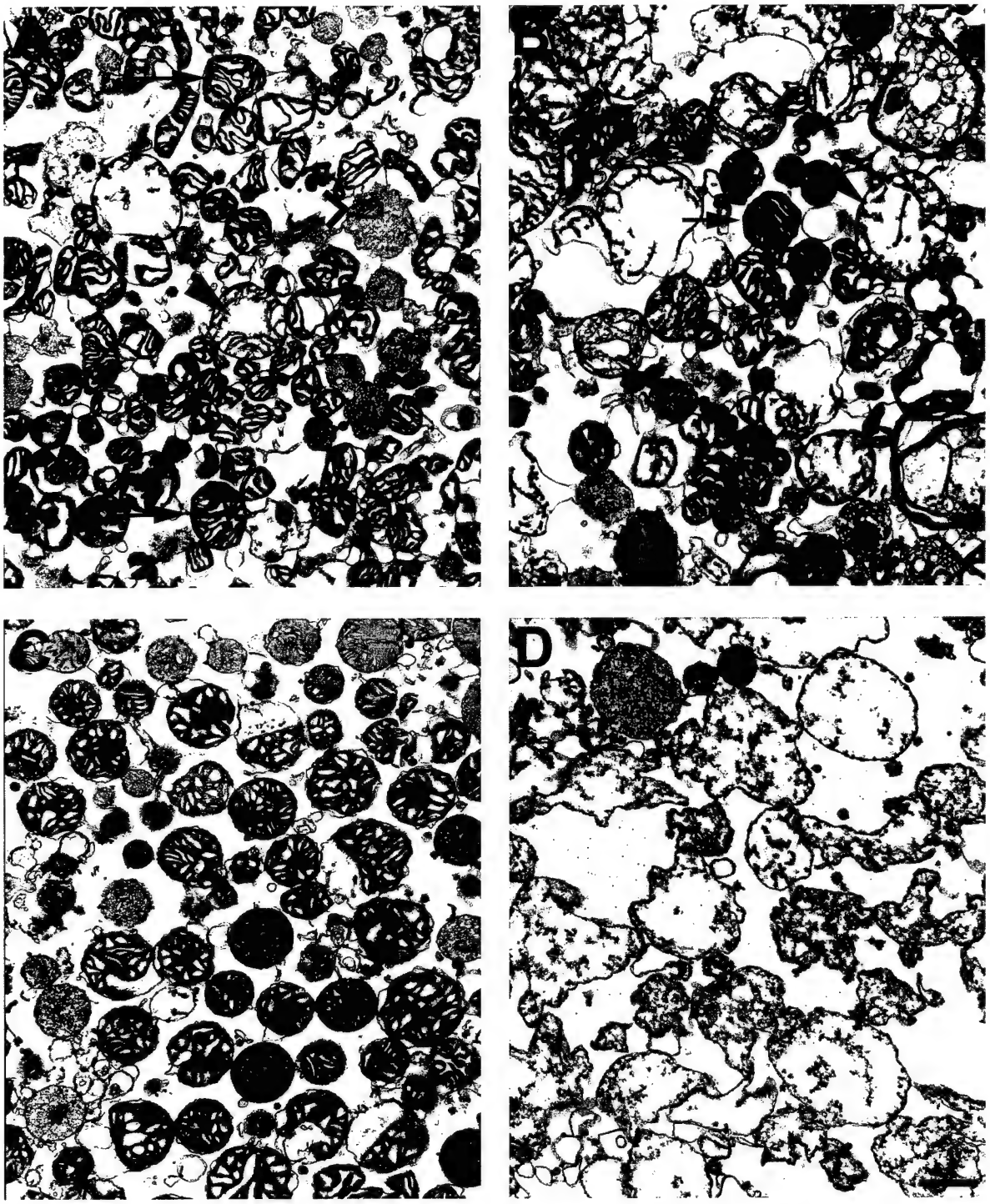

FIG. 4. Electron micrographs of mitochondria from brain (A and B) and liver (C and D), isolated and prepared as described under Materials and Methods. Mitochondria either were untreated (A and C) or were incubated with $CaCl_2$ (70 μM) and Pi (3 mM) for 10 min as described in the legend of Fig. 2 (B and D). In A and B, normal brain mitochondria (arrow), larger mitochondria with fragmented cristae (arrowhead), and a small amount of contaminating synaptosomes (chevron) are observed. In liver mitochondria (C and D), nearly all mitochondria appear normal when untreated (C) and are completely disrupted when treated (D). Bar, 0.5 μm.

dria after exposure to the products of dopamine oxidation (4). Many other recent studies have provided evidence for swelling of isolated brain mitochondria after exposure to pore-inducing agents (1, 26, 27, 32). However, none of these studies quantified the degree of swelling, nor compared it to the degree of swelling observed in liver mitochondria. Where quantitative inferences can be made (32), it appears that the degree of

swelling observed is similar to the small amount of swelling found in our study. In fact, Andreyev *et al.* (1) also noted that when swelling did occur upon exposure to pore inducers, the degree of swelling was incomplete. Thus, these studies support our findings of decreased sensitivity of brain mitochondria to permeability transition.

Similar to findings reported by Kristal and Dubinsky (32), we also found that inhibition of mitochondrial swelling by CsA was incomplete in brain mitochondria, yet we observed a much greater degree of inhibition of swelling and GSH release by CsA in liver. In contrast to our results, Andreyev *et al.* (1) reported release of GSH from brain mitochondria upon pore induction. Although the reason for this apparent difference is unclear, the total mitochondrial GSH in that study was not determined, and thus, it is not known what fraction of the total GSH was released.

Possible mechanisms involved in tissue-specific differences. Our evidence suggests, then, that brain mitochondria do not readily undergo permeability transition under the same conditions that have been well-characterized for liver mitochondria. The reason for this difference is not known, but several possible explanations exist. One possibility is that only a fraction of mitochondria in the brain preparation are able to undergo permeability transition. Although the degree of swelling in brain mitochondria after exposure to Pi or PhAsO was small compared to liver, approximately half of the swelling was prevented by CsA, suggesting that this portion may be due to the PTP. The accompanying release of GSH from the mitochondria that undergo transition would then be only a very small amount compared to that still remaining inside the intact mitochondria and therefore, may be difficult to detect. In addition, since mitochondria are able to take up GSH (30, 33, 36), any released GSH could potentially be transported into the intact mitochondria, masking a small effect.

The heterogeneous brain preparation includes mitochondria from both glia and neurons, and it is not known which population of mitochondria might be more susceptible to PTP induction. It is possible that one cell type or cells from specific regions in brain contain mitochondria that will undergo permeability transition, while others do not. The proportion of mitochondria from glial and neuronal cells in our preparation is not definitively known, but it is likely that there is a substantial proportion from both cell types. The method utilized in our studies is similar to isolation procedures for brain mitochondria which isolate both glial and neuronal (nonsynaptosomal) mitochondria (e.g., 17). However, the current method adds digitonin to the synaptosomal/mitochondrial fraction, which permeabilizes synaptosomal membranes, increasing the neuronal mitochondrial yield (49). The overall mitochondrial yield increases from approximately 3–4 mg mitochondrial protein/brain in standard procedures (e.g., 17) to 8–10 mg mitochondrial protein/brain in this preparation. Thus, it is likely that there is a substantial population of neuronal mitochondria as well as glial mitochondria. It is interesting to speculate whether the small degree of swelling observed in our study reflects the population of mitochondria from specific regions of the brain or from specific cell types that are susceptible to degeneration via mechanisms suggested to involve the PTP. In fact, Friberg *et al.* (26) found that sensitivity to calcium-induced mitochondrial swelling varies in different regions of the brain, correlating with sensitivity to ischemic damage.

It is also possible that differences in protein expression between liver and brain could be responsible for the differences observed in this study. For example, recent evidence suggests that creatine kinase, which is present in high amounts in brain but not liver mitochondria, is a potent inhibitor of the PTP (9, 41). In addition, members of the bcl-2 family of proteins are known to be inhibitors and activators of permeability transition (47), and thus, differential expression of these proteins in liver and brain could contribute to altered sensitivity. Protein expression may also indirectly affect pore opening by altering environmental factors that are known to regulate the PTP, such as intramitochondrial pH, the oxidation state of pyridine nucleotides and GSH, calcium load, or matrix magnesium (5). For example, oxidized pyridine nucleotides are known to increase the probability of PTP opening (15), and evidence suggests that the ability of pyridine nucleotides to be oxidized may be lower in brain mitochondria than in other tissues, due to differences in peroxidase activity (3, 35, 50).

Certainly, other differences in mitochondria from liver and brain have been identified. For example, liver and brain mitochondria use diverse mechanisms to transport calcium; calcium efflux from brain mitochondria is primarily through sodium-dependent transport, whereas liver mainly utilizes a sodium-independent mechanism (31). Likewise, as stated previously, different PTP characteristics have also been identified in other tissues, such as heart mitochondria, which are less sensitive than liver (40, 44) and skeletal muscle mitochondria, which show differential sensitivity to substrate modulators (24). Brain mitochondria appear to be even less sensitive than heart, since exposure to calcium with inducers, higher concentrations of calcium, calcium efflux blockade, or even combinations of several inducers over longer periods of time did not result in large-scale opening of the PTP. The composition of the PTP and its regulatory proteins is still under debate (see 6), and until it is fully defined, it will be difficult to specifically determine the potential mechanisms leading to these tissue-specific differences.

Conclusions. This study is the first to directly examine pore properties in brain mitochondria and compare them to the properties that have previously been well-described in other tissues. It is clear from our findings that considerable differences exist in measures of PTP properties between isolated brain and liver mitochondria and that sensitivity to variations in mitochondria from one tissue to another is critical. This is important to note, since previously it has been thought that pore properties are similar, and studies of isolated liver mitochondria have been utilized to extrapolate to brain (13, 14, 43).

In addition, it is very likely that heterogeneity exists between glial and neuronal mitochondria, between mitochondria from different regions of the brain, or even within different regions of a single neuron. With reports suggesting a potential role for the PTP in neuronal injury due to excitotoxicity (39, 53, 62), ischemia (42, 59, 60), dopamine-induced toxicity (4), the parkinsonian neurotoxin, 1-methyl-4-phenylpyridinium (13, 14, 43), and some forms of apoptosis (65), better characterization of the properties and regulatory mechanisms of the PTP specific to brain mitochondria is critical.

ACKNOWLEDGMENTS

Preliminary reports of these findings were presented at the 28th meeting of the Society for Neuroscience, Los Angeles, CA, November 7–12, 1998 (Berman *et al.,* 1998). We thank Dr. Anne Murphy for her helpful discussions and technical expertise and Dr. Ian Reynolds for critical reading of the manuscript. In addition, we thank Dr. Donna Beer Stolz for providing the EM analysis. This work was supported in part by USPHS Grants NS19068 and DA09601 and USAMRMC Grant 98292027.

REFERENCES

1. Andreyev, A. Y., B. Fahy, and G. Fiskum. 1998. Cytochrome *c* release from brain mitochondria independent of the mitochondrial permeability transition. *FEBS Lett.* **439:** 373–376.
2. Ankarcrona, M., J. M. Dypbukt, S. Orrenius, and P. Nicotera. 1996. Calcineurin and mitochondrial function in glutamate-induced neuronal cell death. *FEBS Lett.* **439:** 321–324.
3. Beatrice, M. C., D. L. Stiers, and D. R. Pfeiffer. 1984. The role of glutathione in the retention of Ca^{2+} by liver mitochondria. *J. Biol. Chem.* **259:** 1279–1287.
4. Berman, S. B., and T. G. Hastings. 1999. Dopamine oxidation alters mitochondrial respiration and induces permeability transition in brain mitochondria: Implications for Parkinson's disease. *J. Neurochem.* **73:** 1127–1137.
5. Bernardi, P. 1995. The permeability transition pore. History and perspectives of a cyclosporin A-sensitive mitochondrial channel. *Prog. Cell Res.* **5:** 119–123.
6. Bernardi, P. 1999. Mitochondrial transport of cations: Channels, exchangers, and permeability transition. *Physiol. Rev.* **79:** 1127–1155.
7. Bernardi, P., L. Scorano, R. Colonna, V. Petronilli, and F. Di Lisa. 1999. Mitochondria and cell death: Mechanistic aspects and methodological issues. *Eur. J. Biochem.* **264:** 687–701.
8. Bernardi, P., S. Vassanelli, P. Veronese, R. Colonna, I. Szabó, and M. Zoratti. 1992. Modulation of the mitochondrial permeability transition pore: Effect of protons and divalent cations. *J. Biol. Chem.* **267:** 2934–2939.
9. Beutner, G., A. Ruck, B. Riede, and D. Brdiczka. 1998. Complexes between porin, hexokinase, mitochondrial creatine kinase and adenylate translocator display properties of the permeability transition pore. Implication for regulation of permeability transition by the kinases. *Biochim. Biophys. Acta.* **1368:** 7–18.
10. Bradford, M. A. 1976. A rapid and sensitive method for the quantitation of microgram quantities of protein utilizing the principle of protein-dye binding. *Anal. Biochem.* **72:** 248–254.
11. Broekemeier, K. M., M. E. Dempsey, and D. R. Pfeiffer. 1989. Cyclosporin A is a potent inhibitor of the inner membrane permeability transition in liver mitochondria. *J. Biol. Chem.* **264:** 7826–7830.
12. Cassarino, D. S., and J. P. Bennett. 1999. An evaluation of the role of mitochondria in neurodegenerative diseases: Mitochondrial mutations and oxidative pathology, protective nuclear responses, and cell death in neurodegeneration. *Brain Res. Rev.* **29:** 1–25.
13. Cassarino, D. S., C. P. Fall, T. S. Smith, and J. P. Bennett. 1998. Pramipexole reduces reactive oxygen species production *in vivo* and *in vitro* and inhibits the mitochondrial permeability transition produced by the parkinsonian neurotoxin methylpyridinium ion. *J. Neurochem.* **71:** 295–301.
14. Cassarino, D. S., J. K. Parks, W. D. Parker Jr., and J. P. Bennett Jr. 1999. The parkinsonian neurotoxin MPP+ opens the mitochondrial permeability transition pore and releases cytochrome c in isolated mitochondria via an oxidative mechanism. *Biochim. Biophys. Acta.* **1453:** 49–62.
15. Chernyak, B. V., and P. Bernardi. 1996. The mitochondrial permeability transition pore is modulated by oxidative agents through both pyridine nucleotides and glutathione at two separate sites. *Eur. J. Biochem.* **238:** 623–630.
16. Chiesi, M., R. Schwaller, and K. Eichenberger. 1988. Structural dependency of the inhibitory action of benzodiazepines and related compounds on the mitochondrial Na^+-Ca^{2+} exchanger. *Biochem. Pharmacol.* **37:** 4399–4403.
17. Clark, J. B., and W. J. Nicklas. 1970. The metabolism of rat brain mitochondria: Preparation and characterization. *J. Biol. Chem.* **245:** 4724–4731.
18. Cox, D. A., L. Conforti, N. Sperelakis, and M. A. Matlib. 1993. Selectivity of inhibition of $Na(^+)$-Ca^{2+} exchange of heart mitochondria by benzothiazepine CGP-37157. *J. Cardiovasc. Pharmacol.* **21:** 595–599.
19. Crompton, M., H. Ellinger, and A. Costi. 1988. Inhibition by cyclosporin A of a Ca^{2+}-dependent pore in heart mitochondria activated by inorganic phosphate and oxidative stress. *Biochem. J.* **255:** 357–360.
20. Deckwerth, T. L., and E. M. Johnson. 1993. Temporal analysis of events associated with programmed cell death (apoptosis) of sympathetic neurons deprived of nerve growth factor. *J. Cell Biol.* **123:** 1207–1222.
21. Dubinsky, J. M., and Y. Levi. 1998. Calcium-induced activation of the mitochondrial permeability transition in hippocampal neurons. *J. Neurosci. Res.* **53:** 728–741.
22. Ellerby, M. H., S. J. Martin, L. M. Ellerby, S. S. Naiem, S. Rabizadeh, G. S. Salvesen, C. A. Casiano, N. R. Cashman, D. R. Green, and D. E. Bredesen. 1997. Establishment of a cell-free

system of neuronal apoptosis: Comparison of premitochondrial, mitochondrial, and postmitochondrial phases. *J. Neurosci.* **17:** 6165–6178.

23. Fiskum, G., A. N. Murphy, and M. F. Beal. 1999. Mitochondria in neurodegeneration: Acute ischemia and chronic neurodegenerative diseases. *J. Cereb. Blood Flow Metab.* **19:** 351–369.
24. Fontaine, E., O. Eriksson, F. Ichas, and P. Bernardi. 1998. Regulation of the permeability transition pore in skeletal muscle mitochondria: Modulation by electron flow through the respiratory chain complex I. *J. Biol. Chem.* **273:** 12662–12668.
25. Fournier, N., G. Ducet, and A. Crevat. 1987. Action of cyclosporine on mitochondrial calcium fluxes. *J. Bioenerg. Biomembr.* **19:** 297–303.
26. Friberg, H., C. Connern, A. P. Halestrap, and T. Wieloch. 1999. Differences in the activation of the mitochondrial permeability transition among brain regions in the rat correlate with selective vulnerability. *J. Neurochem.* **72:** 2488–2497.
27. Friberg, H., M. Ferrand-Drake, F. Bengtsson, A. P. Halestrap, and T. Wieloch. 1998. Cyclosporin A, but not FK506, protects mitochondria and neurons against hypoglycemic damage and implicates the mitochondrial permeability transition in cell death. *J. Neurosci.* **18:** 5151–5159.
28. Green, D. R., and J. C. Reed. 1998. Mitochondria and apoptosis. *Science* **281:** 1309–1312.
29. Griffith, O. W. 1980. Determination of glutathione and glutathione disulfide using glutathione reductase and 2-vinylpyridine. *Anal. Biochem.* **106:** 207–212.
30. Griffith, O. W., and A. Meister. 1985. Origin and turnover of mitochondrial glutathione. *Proc. Natl. Acad. Sci. USA* **82:** 4668–4672.
31. Gunter, T. E., and D. R. Pfeiffer. 1990. Mechanisms by which mitochondria transport calcium. *Am. J. Physiol.* **258:** C755–786.
32. Kristal, B. S., and J. M. Dubinsky. 1997. Mitochondrial permeability transition in the central nervous system: Induction by calcium cycling-dependent and -independent pathways. *J. Neurochem.* **69:** 524–538.
33. Kurosawa, K., N. Hayashi, N. Sato, T. Kamada, and K. Tagawa. 1990. Transport of glutathione across the mitochondrial membranes. *Biochem. Biophys. Res. Commun.* **167:** 367–372.
34. Liu, X., C. N. Kim, J. Yang, R. Jemmerson, and X. Wang. 1996. Induction of apoptotic program in cell-free extracts: Requirement for dATP and cytochrome c. *Cell* **86:** 147.
35. Lötscher, R. R., K. H. Winterhalter, E. Carafoli, and C. Richter. 1979. Hydroperoxides can modulate the redox state of pyridine nucleotides and the calcium balance in rat liver mitochondria. *Proc. Natl. Acad. Sci. USA* **76:** 4340–4344.
36. Martensson, J., J. C. K. Lai, and A. Meister. 1990. High-affinity transport of glutathione is part of a multicomponent system essential for mitochondrial function. *Proc. Natl. Acad. Sci. USA* **87:** 7185–7189.
37. Murphy, A. N., G. Fiskum, and M. F. Beal. 1999. Mitochondria in neurodegeneration: Bioenergetic function in cell life and death. *J. Cereb. Blood Fl. Metab.* **19:** 231–245.
38. Nicolay, K., F. D. Laterveer, and W. Laurens Van Heerde. 1994. Effects of amphipathic peptides, including presequences, on the functional integrity of rat liver mitochondrial membranes. *J. Bioenerg. Biomembr.* **26:** 327–334.
39. Nieminen, A-L., T. G. Petrie, J. J. Lemasters, and W. R. Selman. 1996. Cyclosporin A delays mitochondrial depolarization induced by *N*-methyl-D-aspartate in cortical neurons: Evidence of the mitochondrial permeability transition. *Neuroscience* **75:** 993–997.
40. Novgorodov, S. A., T. I. Gudz, Y. M. Milfrom, and G. P. Brierley. 1992. The permeability transition in heart mitochondria is regulated synergistically by ADP and cyclosporin A. *J. Biol. Chem.* **267:** 16274–16282.
41. O'Gorman, E., G. Beutner, M. Dolder, A. P. Koretsky, D. Brdiczka, and T. Wallimann. 1997. The role of creatine kinase in inhibition of mitochondrial permeability transition. *FEBS Lett.* **414:** 253–257.
42. Ouyang, Y. B., S. Kuroda, T. Kristian, and B. K. Siesjö. 1997. Release of mitochondrial aspartate aminotransferase (MAST) following transient focal cerebral ischemia suggests the opening of a mitochondrial permeability transition pore. *Neurosci. Res. Commun.* **20:** 167–173.
43. Packer, M. A., R. Miesel, and M. P. Murphy. 1996. Exposure to the parkinsonian neurotoxin 1-methyl-4-phenylpyridinium (MPP^+) and nitric oxide simultaneously causes cyclosporin A-sensitive mitochondrial calcium efflux and depolarization. *Biochem. Pharmacol.* **51:** 267–273.
44. Palmer, J. W., and D. R. Pfeiffer. 1981. The control of Ca^{2+} release from heart mitochondria. *J. Biol. Chem.* **256:** 6742–6750.
45. Petit, P. X., H. Lecoeur, E. Zorn, C. Duguet, B. Mignotte, and M. L. Gougeon. 1995. Alterations of mitochondrial structure and function are early events of dexamethasone-induced thymocyte apoptosis. *J. Cell Biol.* **130:** 157–167.
46. Pfeiffer, D. R., T. I. Gudz, S. A. Novgorodov, and W. L. Erdahl. 1995. The peptide mastoparan is a potent facilitator of the mitochondrial permeability transition. *J. Biol. Chem.* **270:** 4923–4932.
47. Reed, J. C., J. M. Jurgensmeier, and S. Matsuyama. 1998. Bcl-2 family proteins and mitochondria. *Biochim. et Biophys. Acta.* **1366:** 127–137.
48. Reynolds, I. J., J. M. Scanlon, and A. K. Stout. 1998. Mitochondrial mechanisms of neuronal injury. In *Pharmacology of Cerebral Ischemia 1998* (Krieglstein, J., Ed), pp. 89–95. Elsevier Science, New York.
49. Rosenthal, R. E., F. Hamud, G. Fiskum, P. J. Varghese, and S. Sharpe. 1987. Cerebral ischemia and reperfusion: Prevention of brain mitochondrial injury by lidoflazine. *J. Cereb. Blood Flow Metab.* **7:** 752–758.
50. Satrustegui, J., and C. Richter. 1984. The role of hydroperoxides as calcium release agents in rat brain mitochondria. *Arch. Biochem. Biophys.* **233:** 736–740.
51. Savage, M. K., D. P. Jones, and D. J. Reed. 1991. Calcium- and phosphate-dependent release and loading of glutathione by liver mitochondria. *Arch. Biochem. Biophys.* **290:** 51–56.
52. Savage, M. K., and D. J. Reed. 1994. Release of mitochondrial glutathione and calcium by a cyclosporin A-sensitive mechanism occurs without large amplitude swelling. *Arch. Biochem. Biophys.* **315:** 142–152.
53. Schinder, A. F., E. C. Olson, N. C. Spitzer, and M. Montal. 1996. Mitochondrial dysfunction is a primary event in glutamate neurotoxicity. *J. Neurosci.* **16:** 6125–6133.
54. Shibasaki, F., and F. McKeon. 1995. Calcineurin functions in Ca^{2+}-activated cell death in mammalian cells. *J. Cell Biol.* **131:** 735–743.
55. Sims, N. R., and J. P. Blass. 1986. Expression of classical mitochondrial respiratory responses in homogenates of rat forebrain. *J. Neurochem.* **47:** 496–505.
56. Snyder, S. H., and D. M. Sabatini. 1995. Immunophilins and the nervous system. *Nature Med.* **1:** 32–37.
57. Susin, S. A., N. Zamzami, M. Castedo, T. Hirsh, P. Marchetti, A. Macho, E. Daugas, M. Geuskens, and G. Kroemer. 1996. Bcl-2 inhibits the mitochondrial release of an apoptogenic protease. *J. Exp. Med.* **184:** 1331–1341.

58. Traber, J., M. Suter, P. Walter, and C. Richter. 1992. *In vivo* modulation of total and mitochondrial glutathione in rat liver: Depletion by phorone and rescue by *N*-acetylcysteine. *Biochem. Pharmacol.* **43:** 961–964.

59. Uchino, H., E. Elmér, K. Uchino, O. Lindvall, and B. K. Siesjö. 1995. Cyclosporin A dramatically ameliorates CA1 hippocampal damage following transient forebrain ischaemia in the rat. *Acta Physiol. Scand.* **155:** 469–471.

60. Uchino, H., E. Elmer, K. Uchino, P. A. Li, Q. P. He, M. L. Smith, and B. K. Siesjo. 1998. Amelioration by cyclosporin A of brain damage in transient forebrain ischemia in the rat. *Brain Res.* **812:** 216–226.

61. Vayssière, J-L., P. X. Petit, Y. Risler, and B. Mignotte. 1994. Commitment to apoptosis is associated with changes in mitochondrial biogenesis and activity in cell lines conditionally immortalized with simian virus 40. *Proc. Natl. Acad. Sci. USA* **91:** 11752–11756.

62. White, R. J., and I. J. Reynolds. 1996. Mitochondrial depolarization in glutamate-stimulated neurons: An early signal specific to excitotoxin exposure. *J. Neurosci.* **16:** 5688–5697.

63. Zamzami, N., P. Marchetti, M. Castedo, C. Zanin, J-L. Vayssière, P. X. Petit, and G. Kroemer. 1995a. Reduction in mitochondrial potential constitutes an early irreversible step of programmed lymphocyte death in vivo. *J. Exp. Med.* **181:** 1661–1672.

64. Zamzami, N., P. Marchetti, M. Castedo, D. Decaudin, A. Maho, T. Hirsch, S. A. Susin, P. X. Petit, B. Mignotte, and G. Kroemer. 1995b. Sequential reduction of mitochondrial transmembrane potential and generation of reactive oxygen species in early programmed cell death. *J. Exp. Med.* **182:** 367–377.

65. Zamzami, N., S. A. Susin, P. Marchetti, T. Hirsch, I. Gómez-Monterrey, M. Castedo, and G. Kroemer. 1996. Mitochondrial control of nuclear apoptosis. *J. Exp. Med.* **183:** 1533–1544.

0022-3565/00/2932-0480$03.00/0
THE JOURNAL OF PHARMACOLOGY AND EXPERIMENTAL THERAPEUTICS
Copyright © 2000 by The American Society for Pharmacology and Experimental Therapeutics
JPET 293:480–486, 2000 /2189/817868

Vol. 293, No. 2
Printed in U.S.A.

Inhibition of Glutamate-Induced Mitochondrial Depolarization by Tamoxifen in Cultured Neurons[1]

KARI R. HOYT,[2] BETH ANN MCLAUGHLIN, DONALD S. HIGGINS JR., and IAN J. REYNOLDS[3]

Departments of Pharmacology (K.R.H, I.J.R.) and Neurobiology (B.A.M.), University of Pittsburgh School of Medicine, Pittsburgh, Pennsylvania; and Department of Neurology (D.S.H.), The Ohio State University College of Medicine, Columbus, Ohio

Accepted for publication January 9, 2000 This paper is available online at http://www.jpet.org

ABSTRACT

In central neurons, glutamate receptor activation causes massive calcium influx and induces a mitochondrial depolarization, which is partially blocked by cyclosporin A, suggesting a possible activation of the mitochondrial permeability transition pore (PTP) as a mechanism. It has been recently reported that tamoxifen (an antiestrogen chemotherapeutic agent) blocks the PTP in isolated liver mitochondria, similar to cyclosporin A. In this study, we tested whether tamoxifen inhibits the mitochondrial depolarization induced by glutamate receptor activation in intact cultured neurons loaded with the fluorescent dye 5,5′,6,6′-tetrachloro-1,1′,3,3′-tetraethylbenzimidazolylcarbocyanine iodide. This dye reports disruptions in mitochondrial membrane potential, which can be caused by PTP activation. We found that glutamate (100 μM for 10 min) causes a robust mitochondrial depolarization that is partially inhibited by tamoxifen. The maximum inhibitory concentration of tamoxifen was 0.3 μM, with concentrations higher and lower than 0.3 μM being less effective. However, although tamoxifen (0.3 μM) blocked glutamate-induced mitochondrial depolarization, it did not inhibit glutamate-induced neuronal death, in contrast to the PTP inhibitor cyclosporin A. A relatively high concentration of tamoxifen (100 μM) caused mitochondrial depolarization itself and was neurotoxic. These data suggest that tamoxifen may be an inhibitor of the PTP in intact neurons. However, the lack of specificity of most PTP inhibitors, and the difficulty in measuring PTP in intact cells, preclude definite conclusions about the role of PTP in excitotoxic injury.

Activation of the mitochondrial permeability transition pore (PTP) has been identified as a possible common effector of the cell death of numerous cell types in response to both necrotic and apoptotic stimuli (Lemasters et al., 1997; Kroemer et al., 1998). The PTP includes proteins located in both the inner and outer mitochondrial membranes and, when opened, allows mitochondrial constituents <1.5 kD to cross the inner membrane. In isolated mitochondria this results in swelling, loss of the protonmotive force, and the loss of low molecular weight compounds such as glutathione (Savage and Reed, 1994; Zoratti and Szabo, 1995). Increases in matrix Ca^{2+} and oxidant levels are important inducers of the PTP. Cyclosporin A is among the most potent inhibitors of the PTP (Broekemeier et al., 1989).

The PTP has been suggested to be involved in the neurotoxicity caused by overactivation of neuronal glutamate receptors (Nieminen et al., 1996; Schinder et al., 1996; White and Reynolds, 1996). Glutamate-induced neurotoxicity is involved in the cell loss caused by stroke and trauma, as well as chronic neurodegenerative diseases (Choi, 1988). Activation of the various subtypes of glutamate receptor leads to opening of an integral ion channel and influx of Na^+, and for the *N*-methyl-D-aspartate (NMDA) subtype and certain α-amino-3-hydroxy-5-methyl-4-isoxazolepropionic acid/kainate subtypes, Ca^{2+} (Mayer and Westbrook, 1987). Robust Ca^{2+} accumulation and the subsequent mitochondrial Ca^{2+} loading are critical for the expression of NMDA receptor-mediated injury, although the events that link mitochondrial Ca^{2+} changes to toxicity have not been firmly established (Budd and Nicholls, 1996; Stout et al., 1998). Reactive oxygen species are generated by mitochondria in response to NMDA receptor-mediated Ca^{2+} influx (Dugan et al., 1995; Reynolds and Hastings, 1995; Bindokas et al., 1996). The massive Ca^{2+} loading caused by NMDA receptor activation also induces a Ca^{2+}-dependent depolarization of the mitochondrial membrane potential ($\Delta\psi_m$) that is partially blocked by the PTP inhibitor cyclosporin A (Ankarcrona et al., 1996; Schinder et

Received for publication October 11, 1999.
[1] This study was supported by DAMD17-98-1-8627 (to I.J.R.), the American Heart Association (to I.J.R.), AG 00751 (to D.S.H.), NS 07391 (to B.A.M.), and NS 07291 (to K.R.H.).
[2] Current address: Department of Neurology, 190 Medical Research Facility, 420 West 12th Ave., The Ohio State University, Columbus, OH 43210. E-mail: hoyt.31@osu.edu
[3] I.J.R. is an Established Investigator of the American Heart Association.

ABBREVIATIONS: PTP, mitochondrial permeability transition pore; NMDA, *N*-methyl-D-aspartate; $\Delta\psi_m$, mitochondrial membrane potential; JC-1, 5,5′,6,6′-tetrachloro-1,1′,3,3′-tetraethylbenzimidazolylcarbocyanine iodide; HBSS, HEPES-buffered salt solution; FCCP, carbonyl cyanide *p*-trifluoromethoxyphenylhydrazone; LDH, lactate dehydrogenase.

al., 1996; White and Reynolds, 1996) as well as other PTP blockers such as trifluoperazine and dibucaine (Hoyt et al., 1997). Cyclosporin A also inhibits toxicity caused by glutamate receptor activation, although this effect may be mediated by calcineurin inhibition rather than PTP activation (Dawson et al., 1993; Ankarcrona et al., 1996; Schinder et al., 1996; White and Reynolds, 1996). Indeed, it has proven difficult to establish the role of the PTP in excitotoxicity because of the lack of potent and selective inhibitors.

It has been recently reported that tamoxifen, a widely used antiestrogen chemotherapeutic and chemoprevention agent, blocks Ca^{2+}-induced PTP activation in isolated liver mitochondria, with effects similar to those caused by cyclosporin A (Custodio et al., 1998). In addition to its estrogen receptor-blocking effects, tamoxifen is a lipophilic peroxyl radical scavenger (Custodio et al., 1994). However, it does not appear that its antioxidant function is related to its ability to block PTP because the PTP-inducing conditions (Ca^{2+} and phosphate treatment) with which tamoxifen was tested did not alter mitochondrial oxidized glutathione levels (an indication of oxidation) (Custodio et al., 1998).

Tamoxifen rapidly induces apoptosis in neural cell lines (Ellerby et al., 1997; Hashimoto et al., 1997). Whole-cell extracts from cultures treated with 100 μM tamoxifen induced assymetric chromatin formations indicative of apoptosis in naïve isolated nuclei within 1 h. This rapid morphological change was accompanied by caspase cleavage of nuclear substrates (Ellerby et al., 1997). These effects were not blocked by inhibitors of caspases 1 and 4 and could not be reproduced if nuclei were treated with only mitochondrial and cytosolic fractions from tamoxifen-primed cells. This apparent requirement for cellular components other than the mitochondria and cytosol would suggest that tamoxifen does not initiate cell death by directly impairing mitochondrial membrane potential, although this hypothesis has not been directly tested. It also remains to be determined if this compound can provide neuroprotection by altering PTP activation in primary neuronal cultures at concentrations similar to those that inhibit PTP in liver mitochondria (5–25 μM) (Custodio et al., 1998).

There are relatively few drugs available to study PTP activation in intact cells, and we were interested to see whether tamoxifen would be as effective in neurons as it is in isolated mitochondria. We tested whether tamoxifen inhibits the $\Delta\psi_m$ depolarization induced by glutamate receptor activation in cultured neurons. $\Delta\psi_m$ was monitored in neurons loaded with the $\Delta\psi_m$-sensitive fluorescent dye 5,5′,6,6′-tetrachloro-1,1′,3,3′-tetraethylbenzimidazolylcarbocyanine iodide (JC-1), as an indirect indication of PTP activation, because PTP activation necessarily results in a loss of $\Delta\psi_m$. We also determined the effect of tamoxifen on glutamate-induced neuronal death, both in vitro and in vivo.

Materials and Methods

Primary Neuronal Culture. Forebrain neurons were cultured from embryonic day 17 Sprague-Dawley rat pups as described in White and Reynolds (1995). Pregnant rats were deeply anesthetized with diethyl ether and were not allowed to regain consciousness. Embryos were then taken and used to obtain forebrain neurons. All animal handling procedures for isolation of neurons for cell culture were approved by the Institutional Animal Care and Use Committee of the University of Pittsburgh. Brain tissue was dissociated with trypsin, and then plated on to poly(D-lysine)-coated glass coverslips at a density of 450,000 cells ml^{-1} in Dulbecco's modified Eagle's medium with 10% fetal bovine serum, 24 U ml^{-1} penicillin, and 24 μg ml^{-1} streptomycin. Twenty-four hours after plating, the media were removed and replaced with Dulbecco's modified Eagle's medium that contained horse serum in place of fetal bovine serum, and the coverslips were inverted to suppress glial proliferation. Neurons were kept in a 37°C, 5% CO_2-humidified incubator for 12 to 18 days until use. All recordings were made with a HEPES-buffered salt solution (HBSS) that contained 137 mM NaCl, 5 mM KCl, 0.9 mM $MgSO_4$, 1.4 mM $CaCl_2$, 3 mM $NaHCO_3$, 0.6 mM Na_2HPO_4, 0.4 mM KH_2PO_4, 5.6 mM glucose, and 20 mM HEPES; pH was adjusted to 7.4 with NaOH. All glutamate solutions contained 1 μM glycine. Tamoxifen was dissolved in methanol ($\leq$0.02% final methanol concentration) and all control conditions contained 0.02% methanol.

Measurements of $\Delta\psi_m$. $\Delta\psi_m$ was estimated in individual neurons loaded with the $\Delta\psi_m$-sensitive fluorescent dye JC-1 (Molecular Probes, Eugene, OR; White and Reynolds, 1996). Neurons were loaded with the JC-1 (3 μM) for 20 min at 37°C, rinsed with dye-free HBSS for 20 min at room temperature, and then mounted in a recording chamber on the stage of an ACAS 570c laser scanning confocal microscope (Meridian Instruments, Okemos, MI). Fields of neurons were illuminated with the 488-nm line of an argon laser, and emission at 530 and 590 nm was monitored. Solution changes in this protocol were made by rapidly aspirating and replacing the contents of the recording chamber. The fluorescence emission wavelength of JC-1 depends on the aggregation of the JC-1 molecules that in turn depends on the $\Delta\psi_m$ (i.e., the greater the $\Delta\psi_m$, the greater the aggregation; Reers et al., 1991). By monitoring JC-1 fluorescence at 590 nm (aggregate) and 530 nm (monomer), one can assess relative changes in $\Delta\psi_m$. Ratio values were obtained by dividing the signal at 590 nm by the signal at 530 nm after background subtraction on a cell-by-cell basis and normalized to a starting value of 1 for comparison between cells. With this approach, a decrease in the normalized ratio represents mitochondrial depolarization, which was confirmed by titration with increasing concentrations of the protonophore carbonyl cyanide *p*-trifluoromethoxyphenylhydrazone (FCCP; 20–750 nM), resulting in graded, concentration-dependent decreases in the JC-1 ratio (K. R. Hoyt and I. J. Reynolds, unpublished observations).

$[Ca^{2+}]_i$ Measurements. $[Ca^{2+}]_i$ was measured from individual neurons loaded with the Ca^{2+}-sensitive fluorescent dye indo-1 (White and Reynolds, 1995). Neurons were rinsed with HBSS and then loaded with 5 μM indo-1 AM (Molecular Probes) in HBSS containing 5 mg/ml BSA for 50 min at 37°C, and incubated in dye-free HBSS for a further 20 min at 37°C to allow for dye cleavage. Coverslips were then mounted in a recording chamber (1-ml volume) on the stage of a Nikon Diaphot microscope. Cells were illuminated at 350 nm with light from a 75-W mercury arc lamp. Indo-1 emission was simultaneously monitored at 405 and 490 nm with a dual photomultiplier system. Background subtracted ratios were converted to $[Ca^{2+}]_i$ with parameters from an in situ calibration.

In Vitro Toxicity Assay. For neuronal viability experiments, coverslips were washed once in HBSS that had been prewarmed to 37°C, inverted, and transferred to new plates. Cells were then washed twice more in HBSS and incubated in toxin. Cells were exposed to glutamate (100 μM) and glycine (1 μM) or HBSS in the presence or absence of tamoxifen (0.3 μM) and returned to the incubator for 10 min. Glutamate exposure was terminated by washing cells twice with HBSS. After rinsing with HBSS, cells were maintained in the presence or absence of tamoxifen (0.3 μM) in minimal essential medium. For high-dose tamoxifen experiments, cells were maintained in 100 μM tamoxifen in minimal essential medium. Neuronal viability was determined 18 to 20 h later for all experiments by measuring lactate dehydrogenase (LDH) release with an in vitro toxicology assay kit (Sigma Chemical Co., St. Louis, MO). Forty-microliter samples of medium were assayed spectrophotometrically according to the manufacturer's protocol to obtain a measure of cytoplasmic LDH released from dead and dying neurons

(Hartnett et al., 1997). LDH results were confirmed qualitatively by visual inspection of the cells. Chromatin staining of tamoxifen-treated cells also was performed as described in McLaughlin et al. (1998). After incubation with tamoxifen, the cultures were washed briefly with PBS, fixed in 4% paraformaldehyde (pH 7.4) for 5 min, and incubated in 5 μg/ml Hoechst 33342 (Molecular Probes) for 10 min. Cells were then washed twice in PBS and mounted on glass slides. Fluorescence of stained chromatin was evaluated with a Nikon Diaphot fluorescence microscope.

Striatal Malonate Lesions. Male Sprague-Dawley rats (275–350 g) were maintained in a 12-h light/dark cycle with free access to standard rat chow and water. All animal procedures were in accordance with the National Institutes of Health Guide for the Care and Use of Laboratory Animals and have been approved by the Institutional Laboratory Animal Care and Use Committee of The Ohio State University. Rats were anesthetized with equithesin, then placed in a Kopf small animal stereotaxic apparatus. A midline incision was made and the confluence of the sagittal and coronal sutures was identified (bregma). Malonate (3 μmol in 2 μl of 0.9 N NaCl) was administered via a 26-gauge Hamilton syringe at a rate of 0.2 μl/min at the following coordinates relative to bregma: 0.7 mm anterior, 2.8 mm lateral, and 5.0 mm ventral. The needle remained in place for an additional 5 min to limit regurgitation up the needle tract. Tamoxifen or vehicle (dimethyl sulfoxide) treatments were administered i.p. 2 h before and 4 h after malonate exposure. Seven days after malonate exposure, all animals were euthanized with chloral hydrate (500 mg/kg) and rapid decapitation. The cranial contents were removed, coated with embedding matrix, frozen under powdered dry ice, and stored at −70°C until sectioning.

Coronal sections (25 μm) were gathered at 250-μm intervals through the rostrocaudal extent of the striatum with a cryostat and were thaw-mounted onto poly(lysine)-treated slides. Tissue sections were then processed for cytochrome oxidase histochemistry.

Cytochrome Oxidase Histochemistry. Sections were incubated in 100 mM sodium phosphate buffer (pH 7.4) with cytochrome *c* (10 μM) and 3,3′-diaminobenzidine (1 mM) for 2 h at 37°C in the dark. Sections were postfixed in 10% formalin (10 min), dehydrated in graded alcohol, and coverslipped from xylene. Analysis of striatal lesion volume of cytochrome oxidase-stained sections was performed on a microcomputer based image analysis program (Imaging Research, St. Catherines, Ontario, Canada) with area standards to provide a calibration from which three-dimensional volume (cubic millimeters) of the lesioned striatum was estimated.

Results

Exposure of neurons to excitotoxic concentrations of glutamate (100 μM) causes a decrease in $\Delta\psi_m$ that can be monitored with the $\Delta\psi_m$-sensitive fluorescent probe JC-1. A decrease in the ratio of JC-1 fluorescence emission at 590 nm relative to the emission at 530 nm indicates $\Delta\psi_m$ depolarization (Fig. 1A). We have previously shown this depolarization is mediated primarily by the NMDA subtype of glutamate receptor and is Ca^{2+}-dependent (White and Reynolds, 1996). When tamoxifen (0.3 μM) was included during the glutamate exposure (Fig. 1A), there was a notable attenuation of the $\Delta\psi_m$ depolarization caused by glutamate. A protonophore FCCP, which collapses the $\Delta\psi_m$, was added at the end of the fluorescence recording and demonstrates a small additional depolarization that was not affected by tamoxifen. A higher tamoxifen concentration (20 μM) did not inhibit glutamate-induced mitochondrial depolarization (Fig. 1B). We tested a range of tamoxifen concentrations (0.001–20 μM) on the glutamate-induced $\Delta\psi_m$ depolarization (Fig. 1, A and B). As an expression of the magnitude of the effect of tamoxifen, we took the difference between the mean normalized JC-1 ratios after 5 min of exposure to glutamate (100 μM) in the presence or absence of tamoxifen (Fig. 1C). The inhibitory effect of tamoxifen on glutamate-induced $\Delta\psi_m$ depolarization was maximal at 0.3 μM. Tamoxifen was less effective at concentrations higher or lower than 0.3 μM, suggesting an additional effect of higher tamoxifen concentrations on $\Delta\psi_m$.

We tested whether tamoxifen alone affected $\Delta\psi_m$ and found no effect of tamoxifen at lower concentrations (<1 μM) and an apparent increase in $\Delta\psi_m$ induced by higher tamoxifen concentrations (10 or 20 μM) (Fig. 2A). Prolonged exposure to a relatively high concentration of tamoxifen (100 μM) resulted in an apparent $\Delta\psi_m$ hyperpolarization followed by a marked depolarization (Fig. 2B).

We tested whether tamoxifen inhibits glutamate receptor activity as a possible mechanism of its inhibition of glutamate-induced $\Delta\psi_m$ depolarization. Tamoxifen (0.3 μM) did not inhibit glutamate-induced increases in $[Ca^{2+}]_i$ measured in indo-1-loaded neurons, indicating that tamoxifen does not directly inhibit glutamate receptor activation (Fig. 3A). Specifically, the glutamate-induced (3 μM for 15 s) peak $[Ca^{2+}]_i$ increase was 2.1 ± 0.4 μM (n = 7 neurons) and 1.7 ± 0.2 μM in the presence of 0.3 μM tamoxifen (n = 7 neurons; not significantly different from control, Student's t test). Tamoxifen (0.3 μM) also did not affect the rate of Ca^{2+} recovery from a longer, more intense glutamate stimulus (100 μM for 5 min) (Fig. 3C). The time required to recover to twice basal Ca^{2+} levels in Ca^{2+}-free HBSS was 47.1 ± 9.5 min (n = 8 neurons) and 42.5 ± 8.3 min in the presence of 0.3 μM tamoxifen for the 2 min after glutamate exposure (n = 6 neurons; not significantly different from control, Student's t test). Agents that alter mitochondrial and plasma membrane Ca^{2+}-buffering mechanisms affect the rate of Ca^{2+} recovery after glutamate (White and Reynolds, 1995, 1997; Hoyt and Reynolds, 1998; Hoyt et al., 1998). The lack of effect of tamoxifen on $[Ca^{2+}]_i$ or on Ca^{2+} recovery suggests that it does not inhibit glutamate-induced $\Delta\psi_m$ depolarization because of major alterations in $[Ca^{2+}]_i$ handling in response to glutamate.

It has been proposed that PTP activation is involved in the neurotoxicity of glutamate receptor activation, so we were interested to see whether tamoxifen had a neuroprotective action. Tamoxifen (0.3 μM; present during and after glutamate exposure) had no effect on the neuronal death caused by glutamate (100 μM for 10 min) as measured by LDH release from damaged neurons into the media during the 20 h after glutamate exposure (Fig. 4A). Because tamoxifen has been reported to rapidly induce apoptosis in neural cell lines, we tested a higher concentration (100 μM) of tamoxifen alone on neuronal viability and found that a 30-min exposure resulted in significant cell loss expressed 20 h later (Fig. 4B). Continuous exposure of neurons to 100 μM tamoxifen for 3 h also caused an increase in the number of apoptotic nuclei visualized with the fluorescent nuclear dye Hoechst 33342 from 3% in controls to 23% for cells treated with tamoxifen, consistent with previous findings in a neural cell line (Ellerby et al., 1997). It appears, therefore, that a low concentration of tamoxifen does not protect cells from excitotoxic injury and that high concentrations of tamoxifen are neurotoxic to primary cultured neurons.

We also tested whether tamoxifen was neuroprotective in an in vivo model of excitotoxic neuronal death. Malonate, an inhibitor of succinate dehydrogenase, causes metabolic inhi-

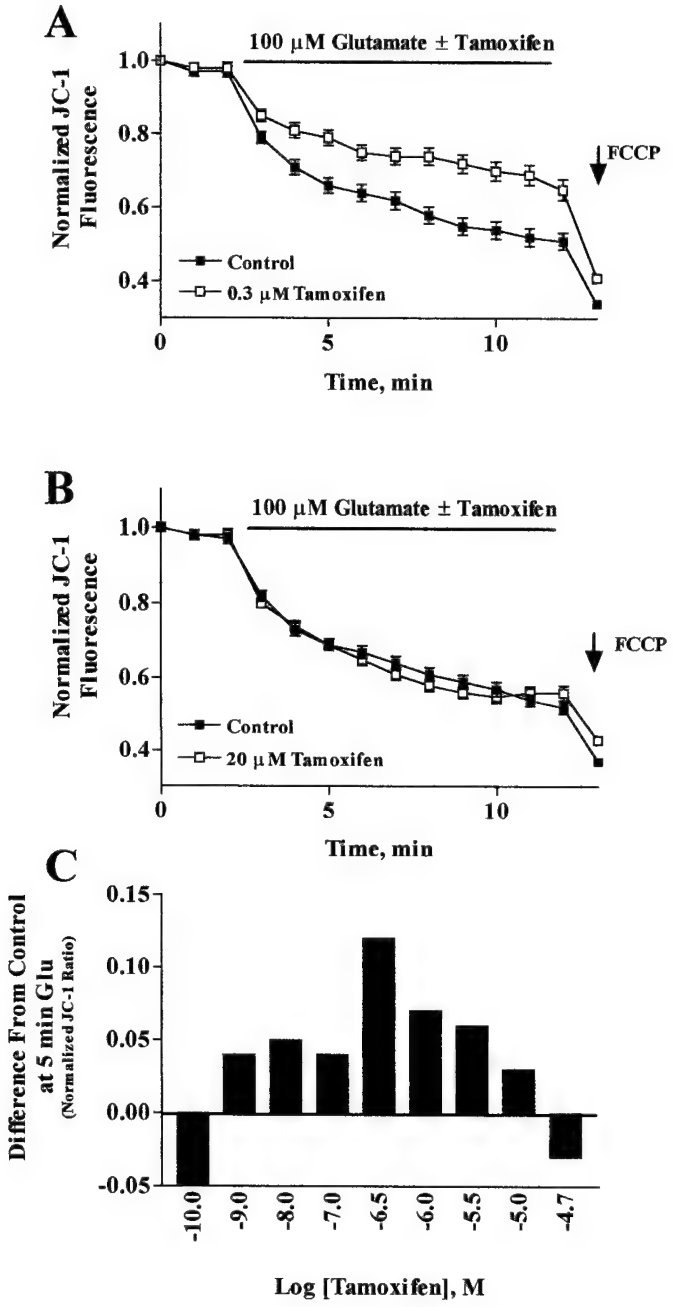

Fig. 1. Tamoxifen inhibits glutamate-induced mitochondrial depolarization in neurons loaded with JC-1. A, application of 100 μM glutamate (■) caused a decrease in the normalized 590:530 nm JC-1 emission ratio, reflecting mitochondrial depolarization. Addition of 0.3 μM tamoxifen (□) during the glutamate exposure substantially reduced the extent of the loss of $\Delta\psi_m$ caused by glutamate. Data represent the mean ± S.E. of 54 to 70 neurons per condition. FCCP (750 nM), a protonophore that depolarizes $\Delta\psi_m$, was added at the end of the experiment for comparison. B, a higher tamoxifen concentration (20 μM) did not inhibit the glutamate-induced decrease in $\Delta\psi_m$ when included during the glutamate exposure. Data represent the mean ± S.E. of 51 to 61 neurons per condition. C, concentration dependence of the inhibition of glutamate-induced mitochondrial depolarization by tamoxifen. Data are expressed as the difference between the normalized JC-1 ratio for tamoxifen-treated versus untreated cells after 5 min of glutamate exposure. Because these data points are not paired, we cannot calculate individual standard error values for these data. As an indication of variability, we report that the range of the standard error for the data points from which the differences were calculated was 0.018 to 0.025 normalized JC-1 fluorescence units. As the tamoxifen concentration was increased, there was a decrease in the inhibitory effect on glutamate-induced depolarization. Data were collected from a total of 41 to 70 neurons.

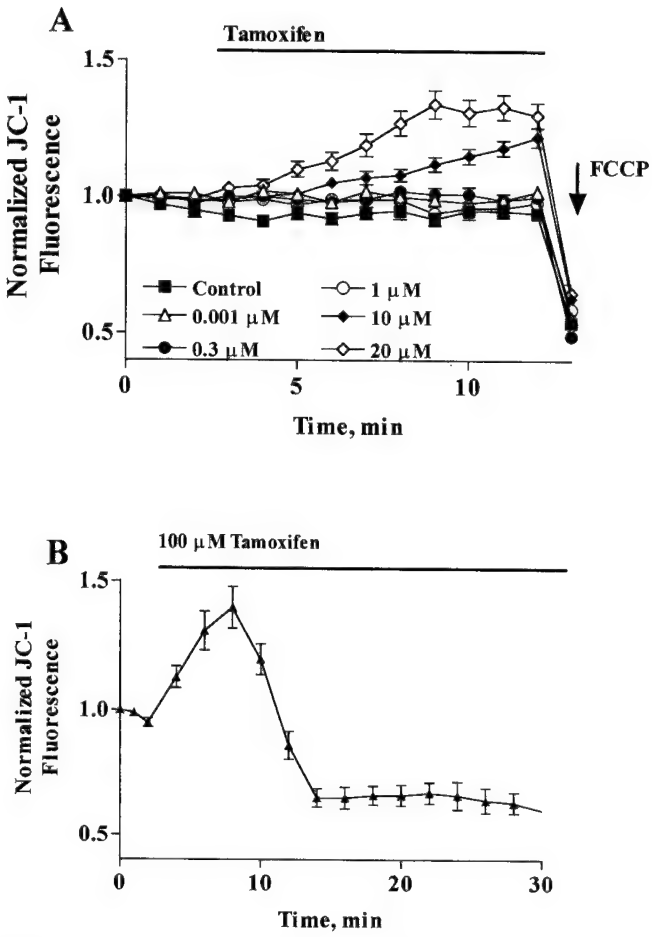

Fig. 2. Tamoxifen, at relatively high concentrations, increases the apparent $\Delta\psi_m$. A, a range of tamoxifen concentrations was tested on the $\Delta\psi_m$ in JC-1-loaded neurons. Concentrations of tamoxifen <1 μM had little direct effect on $\Delta\psi_m$, whereas higher concentrations (>10 μM) caused an increase in the JC-1 ratio, presumably reflecting an increase in $\Delta\psi_m$. Data represent the mean ± S.E. of 21 to 41 neurons per condition. B, a prolonged exposure to tamoxifen (100 μM) causes an increase in the $\Delta\psi_m$ followed by a pronounced decrease in $\Delta\psi_m$. Data represent the mean ± S.E. of 14 neurons from a single culture date and are representative of data collected from a total of three experiments.

bition and neuronal damage when injected into the striatum (Fig. 5A). Glutamate receptor antagonists inhibit this neuronal damage, reflecting an excitotoxic component of this neuronal injury (data not shown) (Greene and Greenamyre, 1995; Schulz et al., 1996). Tamoxifen (2 mg/kg i.p. 2 h before and 4 h after striatal malonate injection) did not reduce the volume of the striatal lesion (Fig. 5B). Doses of tamoxifen from 1 to 20 mg/kg were tested and none prevented the striatal damage caused by malonate (Fig. 5C).

Discussion

We found that glutamate (100 μM) causes a robust mitochondrial depolarization that is partially inhibited by tamoxifen. The maximum inhibitory concentration of tamoxifen was 0.3 μM, with concentrations higher and lower than 0.3 μM being less effective. Tamoxifen (0.3 μM) did not inhibit glutamate receptor-activated increases in intracellular Ca^{2+}, suggesting that it does not directly inhibit receptor activation, nor does it appear to inhibit $[Ca^{2+}]_i$ buffering after a glutamate stimulus. Therefore, a decrease in glutamate-in-

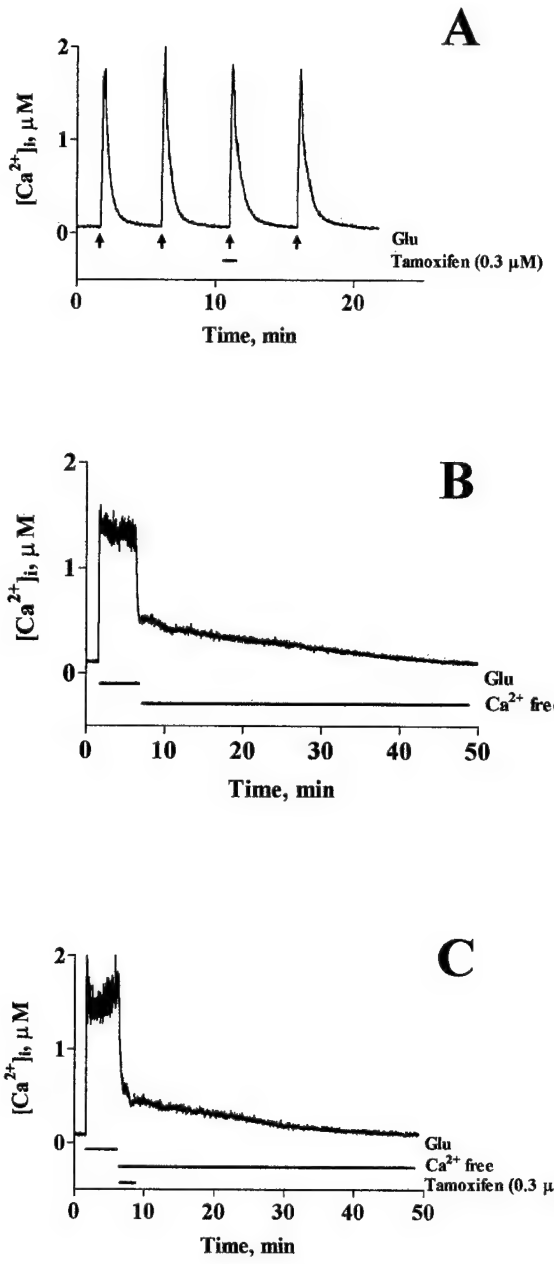

Fig. 3. Tamoxifen did not inhibit glutamate-induced increases in $[Ca^{2+}]_i$. A, indo-1-loaded neurons were exposed to 15-s pulses of 3 μM glutamate/1 μM glycine (arrows). When tamoxifen (0.3 μM) was included before and during the glutamate stimulus, there was no alteration in the $[Ca^{2+}]_i$ increase induced by glutamate. Data are representative of Ca^{2+} traces collected from seven neurons. B, tamoxifen does not affect $[Ca^{2+}]_i$ recovery after a glutamate stimulus. Neurons were exposed to 100 μM glutamate/1 μM glycine for 5 min and then immediately exposed to Ca^{2+}-free HBSS or tamoxifen (0.3 μM) in Ca^{2+}-free HBSS for 2 min immediately after glutamate exposure. Note that there is no apparent effect of tamoxifen on the rate or shape of the $[Ca^{2+}]_i$ recovery. Data are representative of Ca^{2+} traces collected from five to seven additional neurons.

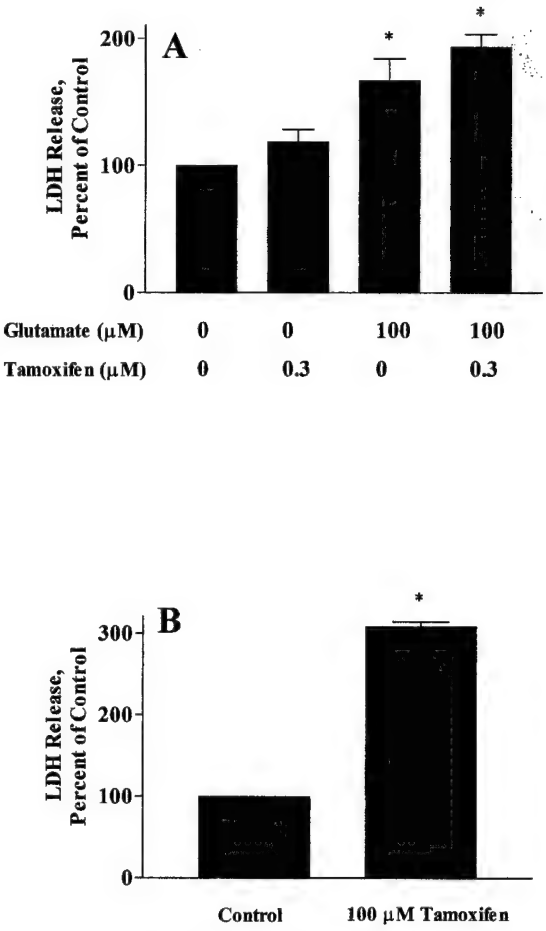

Fig. 4. Effects of tamoxifen on neuronal viability and on excitotoxicity in vitro. A, tamoxifen (0.3 μM) does not inhibit glutamate-induced neuronal death. Neurons were exposed to 100 μM glutamate for 10 min in the presence or absence of 0.3 μM tamoxifen, and neuronal death was assessed 20 h later by LDH release into the media as a measure of neuronal damage. Tamoxifen treatment did not significantly change glutamate neurotoxicity ($P > .05$). *$P < .01$, significantly different from untreated control, ANOVA with Bonferroni correction for multiple comparisons. B, a relatively high concentration of tamoxifen (100 μM) causes neuronal death. Neurons were exposed to 100 μM tamoxifen for 30 min and LDH release was assayed 20 h later. Data represent the mean ± S.E. collected from at least three culture dates. *$P < .01$, significantly different from untreated control, Student's t test.

duced $[Ca^{2+}]_i$ levels by tamoxifen is unlikely to explain the inhibitory effect of tamoxifen on mitochondrial $\Delta\psi_m$ depolarization.

Tamoxifen did not completely inhibit glutamate-induced $\Delta\psi_m$ depolarization. This is similar to what we have previously reported for other PTP inhibitors, namely, cyclosporin A, trifluoperazine, and dibucaine (White and Reynolds, 1996; Hoyt et al., 1997; Scanlon and Reynolds, 1998). This may be a matter of time of onset of action of the particular drug, or its duration of action. There are other Ca^{2+}-stimulated effects on mitochondria in addition to activation of the PTP that would result in dissipation of $\Delta\psi_m$, including mitochondrial Ca^{2+} cycling (Nicholls and Akerman, 1982) and ATP synthesis. Because we are not measuring PTP activation directly and are unable to do so as yet in intact neurons, we cannot differentiate between PTP activation and other direct effects of glutamate receptor activation on $\Delta\psi_m$. Therefore, definitive conclusions about the role of PTP activation in glutamate-induced mitochondrial depolarization cannot be drawn from the results presented herein. The numerous additional effects of these agents on other cellular signal transduction mechanisms such as calcineurin, calmodulin, and protein kinase C complicate the interpretation of effects of these drugs (Levin and Weiss, 1979; Liu et al., 1991; Rowlands et al., 1995; Gundimeda et al., 1996).

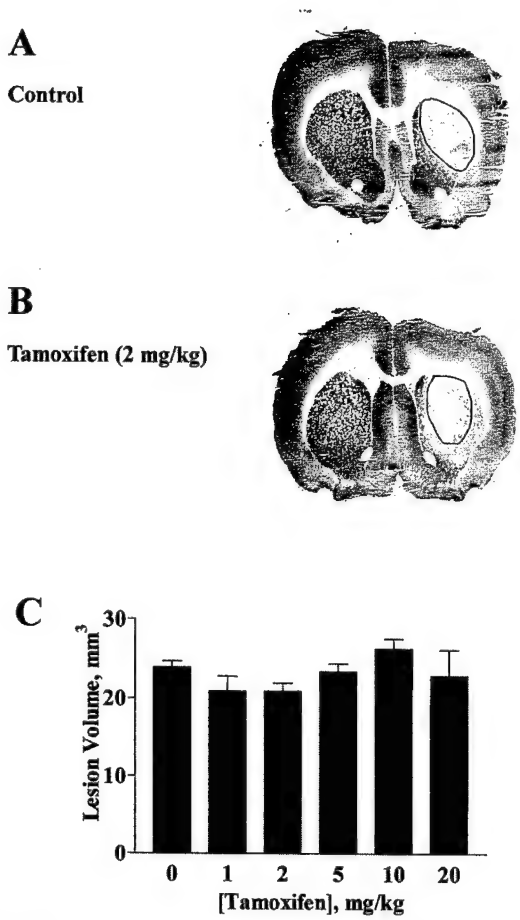

Fig. 5. Tamoxifen does not inhibit formation of striatal lesions induced by malonate. A, injection of malonate into the rat striatum induces a lesion that was visualized 7 days postinjection by staining for cytochrome oxidase. B, treatment with 2 mg/kg tamoxifen 2 h before and 4 h after malonate injection did not decrease the size of the malonate-induced lesion. C, a range of tamoxifen doses (1–20 mg/kg) did not protect against striatal malonate lesion formation. Data represent the mean ± S.E. collected from 3 to 13 rats per condition.

The lack of inhibition of glutamate-induced depolarization by tamoxifen at higher concentrations is puzzling. It is possible that at lower concentrations, tamoxifen has a relatively selective effect on glutamate-mediated $\Delta\psi_m$ depolarization, whereas at higher concentrations, its membrane-disruptive effects interact with the glutamate-induced mitochondrial dysfunction, leading to a lack of inhibition at these tamoxifen concentrations. These higher tamoxifen concentrations caused an increase in $\Delta\psi_m$. It is possible that tamoxifen affects one of a number of mitochondrial functions that could result in hyperpolarization. Among these possibilities are inhibition of the mitochondrial Na^+/Ca^{2+} exchanger, the F_1F_o-ATPase or a direct ionophore effect similar to nigericin (White and Reynolds, 1996; Hoyt et al., 1997), or inhibition of spontaneous depolarizing events (Duchen et al., 1998). These possible mechanisms remain to be tested. High micromolar concentrations of tamoxifen induce rapid apoptotic death in neural cell lines (a finding that we confirmed in our primary cultures) (Ellerby et al., 1997; Hashimoto et al., 1997). The inability of tamoxifen-primed mitochondria to initiate apoptosis in naïve cell extracts suggests that nuclear or cell membrane associated caspases mediate the major component of tamoxifen-induced programmed cell death (Ellerby et al., 1997).

Cyclosporin A inhibits glutamate-induced neuronal death in vitro, although the interpretation of the mechanism of this neuroprotective effect is complicated by the multiple effects that cyclosporin A has on cellular function, including inhibition of PTP as well as calcineurin activation (Dawson et al., 1993; Ankarcrona et al., 1996; Schinder et al., 1996; White and Reynolds, 1996). Because tamoxifen inhibited glutamate-induced $\Delta\psi_m$ depolarization in a manner similar to that of cyclosporin A, we were interested to see whether tamoxifen protected neurons from glutamate-induced injury. Tamoxifen did not inhibit glutamate-induced neuronal death, suggesting that PTP activation is not a major contributor to the death caused by glutamate and that other actions of cyclosporin A explain its neuroprotective effect. We also tested whether tamoxifen could lessen the neuronal injury caused by excitotoxic injury to the striatum in an intact animal. Tamoxifen was not an effective inhibitor of striatal injury at the doses tested (1–20 mg/kg). Clinical doses of tamoxifen in humans are 0.4 to 0.8 mg/kg, causing an acute serum concentration of ~0.07 μM and chronic (after 3 months) steady-state concentrations of ~0.2 μM (Physicians' Desk Reference, 1997). Because tamoxifen is very lipophilic, it is likely that tissue concentrations are higher than the serum concentration. It is possible that a higher and more prolonged tamoxifen exposure than used herein would be neuroprotective. The lack of effect in primary culture argued against further testing this in vivo.

The inhibition of glutamate-induced mitochondrial depolarization by tamoxifen is consistent with its reported action as an inhibitor of PTP activation, although processes other than PTP activation may explain the decrease in $\Delta\psi_m$ caused by glutamate receptor activation. Given the lack of specificity of tamoxifen and other PTP inhibitors and the difficulties in measuring PTP in intact cells, conclusions about the role of PTP in glutamate-induced mitochondrial depolarization and excitotoxic injury are not yet possible and await the development of selective PTP inhibitors, as well as a reliable assay for PTP activation in intact cells.

Acknowledgments

We thank Geraldine Kress for preparation of neuronal cultures and Dr. Kendall Wallace for helpful discussion.

References

Ankarcrona M, Dypbukt JM, Orrenius S and Nicotera P (1996) Calcineurin and mitochondrial function in glutamate-induced neuronal cell death. *FEBS Lett* **394:** 321–324.

Bindokas VP, Jordan J, Lee CC and Miller RJ (1996) Superoxide production in rat hippocampal neurons: Selective imaging with hydroethidine. *J Neurosci* **16:**1324–1336.

Broekemeier KM, Dempsey ME and Pfeiffer DR (1989) Cyclosporin A is a potent inhibitor of the inner membrane permeability transition in liver mitochondria. *J Biol Chem* **264:**7826–7830.

Budd SL and Nicholls DG (1996) Mitochondria, calcium regulation, and acute glutamate excitotoxicity in cultured cerebellar granule cells. *J Neurochem* **67:**2282–2291.

Choi DW (1988) Glutamate neurotoxicity and diseases of the nervous system. *Neuron* **1:**623–634.

Custodio JB, Dinis TC, Almeida LM and Madeira VM (1994) Tamoxifen and hydroxytamoxifen as intramembraneous inhibitors of lipid peroxidation. Evidence for peroxyl radical scavenging activity. *Biochem Pharmacol* **47:**1989–1998.

Custodio JBA, Moreno AJM and Wallace KB (1998) Tamoxifen inhibits induction of the mitochondrial permeability transition by Ca^{2+} and inorganic phosphate. *Toxicol Appl Pharmacol* **152:**10–17.

Dawson TM, Steiner JP, Dawson VL, Dinerman JL, Uhl GR and Snyder SH (1993) Immunosuppressant FK506 enhances phosphorylation of nitric oxide synthase and protects against glutamate neurotoxicity. *Proc Natl Acad Sci USA* **90:**9808–9812.

Duchen MR, Leyssens A and Crompton M (1998) Transient mitochondrial depolarizations reflect focal sarcoplasmic reticular calcium release in single rat cardiomyocytes. *J Cell Biol* **142:**975–988.

Dugan LL, Sensi SL, Canzoniero LM, Handran SD, Rothman SM, Lin TS, Goldberg MP and Choi DW (1995) Mitochondrial production of reactive oxygen species in cortical neurons following exposure to *N*-methyl-D-aspartate. *J Neurosci* **15:**6377–6388.

Ellerby HM, Martin SJ, Ellerby LM, Naiem SS, Rabizadeh S, Salvesen GS, Casiano CA, Cashman NR, Green DR and Bredesen DE (1997) Establishment of a cell-free system of neuronal apoptosis: Comparison of premitochondrial, mitochondrial, and postmitochondrial phases. *J Neurosci* **17:**6165–6178.

Greene JG and Greenamyre JT (1995) Characterization of the excitotoxic potential of the reversible succinate dehydrogenase inhibitor malonate. *J Neurochem* **64:**430–436.

Gundimeda U, Chen ZH and Gopalakrishna R (1996) Tamoxifen modulates protein kinase C via oxidative stress in estrogen receptor-negative breast cancer cells. *J Biol Chem* **271:**13504–13514.

Hartnett KA, Stout AK, Rajdev S, Rosenberg PA, Reynolds IJ and Aizenman E (1997) NMDA receptor-mediated neurotoxicity: A paradoxical requirement for extracellular Mg^{2+} in Na^+/Ca^{2+}-free solutions in rat cortical neurons in vitro. *J Neurochem* **68:**1836–1845.

Hashimoto M, Inoue S, Muramatsu M and Masliah E (1997) Estrogens stimulate tamoxifen-induced neuronal cell apoptosis in vitro: A possible nongenomic action. *Biochem Biophys Res Commun* **240:**464–470.

Hoyt KR and Reynolds IJ (1998) Alkalinization prolongs recovery from glutamate-induced increases in intracellular Ca^{2+} concentration by enhancing Ca^{2+} efflux through the mitochondrial Na^+/Ca^{2+} exchanger in cultured rat forebrain neurons. *J Neurochem* **71:**1051–1058.

Hoyt KR, Sharma TA and Reynolds IJ (1997) Trifluoperazine and dibucaine-induced inhibition of glutamate-induced mitochondrial depolarization in rat cultured forebrain neurones. *Br J Pharmacol* **122:**803–808.

Hoyt KR, Stout AK, Cardman JM and Reynolds IJ (1998) The role of intracellular Na^+ and mitochondria in buffering of kainate-induced intracellular free Ca^{2+} changes in rat forebrain neurones. *J Physiol (Lond)* **509:**103–116.

Kroemer G, Dallaporta B and Resche-Rigon M (1998) The mitochondrial death/life regulator in apoptosis and necrosis. *Annu Rev Physiol* **60:**619–642.

Lemasters JJ, Nieminen AL, Qian T, Trost LC and Herman B (1997) The mitochondrial permeability transition in toxic, hypoxic and reperfusion injury. *Mol Cell Biochem* **174:**159–165.

Levin RM and Weiss B (1979) Selective binding of antipsychotics and other psychoactive agents to the calcium-dependent activator of cyclic nucleotide phosphodiesterase. *J Pharmacol Exp Ther* **208:**454–459.

Liu J, Farmer JD Jr, Lane WS, Friedman J, Weissman I and Schreiber SL (1991) Calcineurin is a common target of cyclophilin-cyclosporin A and FKBP-FK506 complexes. *Cell* **66:**807–815.

Mayer ML and Westbrook GL (1987) The physiology of excitatory amino acids in the vertebrate central nervous system. *Prog Neurobiol* **28:**197–276.

McLaughlin BA, Nelson D, Erecinska M and Chesselet MF (1998) Toxicity of dopamine to striatal neurons in vitro and potentiation of cell death by a mitochondrial inhibitor. *J Neurochem* **70:**2406–2415.

Nicholls D and Akerman K (1982) Mitochondrial calcium transport. *Biochim Biophys Acta* **683:**57–88.

Nieminen AL, Petrie TG, Lemasters JJ and Selman WR (1996) Cyclosporin A delays mitochondrial depolarization induced by *N*-methyl-D-aspartate in cortical neurons—Evidence of the mitochondrial permeability transition. *Neuroscience* **75:**993–997.

Physicians' Desk Reference (1997) Medical Economics Company, Montvale, NJ.

Reers M, Smith TW and Chen LB (1991) J-aggregate formation of a carbocyanine as a quantitative fluorescent indicator of membrane potential. *Biochemistry* **30:**4480–4486.

Reynolds IJ and Hastings TG (1995) Glutamate induces the production of reactive oxygen species in cultured forebrain neurons following NMDA receptor activation. *J Neurosci* **15:**3318–3327.

Rowlands MG, Budworth J, Jarman M, Hardcastle IR, McCague R and Gescher A (1995) Comparison between inhibition of protein kinase C and antagonism of calmodulin by tamoxifen analogues. *Biochem Pharmacol* **50:**723–726.

Savage MK and Reed DJ (1994) Release of mitochondrial glutathione and calcium by a cyclosporin A-sensitive mechanism occurs without large amplitude swelling. *Arch Biochem Biophys* **315:**142–152.

Scanlon JM and Reynolds IJ (1998) Effects of oxidants and glutamate receptor activation on mitochondrial membrane potential in rat forebrain neurons. *J Neurochem* **71:**2392–2400.

Schinder AF, Olson EC, Spitzer NC and Montal M (1996) Mitochondrial dysfunction is a primary event in glutamate neurotoxicity. *J Neurosci* **16:**6125–6133.

Schulz JB, Matthews RT, Henshaw DR and Beal MF (1996) Neuroprotective strategies for treatment of lesions produced by mitochondrial toxins: Implications for neurodegenerative diseases. *Neuroscience* **71:**1043–1048.

Stout AK, Raphael HM, Kanterewicz BI, Klann E and Reynolds IJ (1998) Glutamate-induced neuron death requires mitochondrial calcium uptake. *Nat Neurosci* **1:**366–373.

White RJ and Reynolds IJ (1995) Mitochondria and Na^+/Ca^{2+} exchange buffer glutamate-induced calcium loads in cultured cortical neurons. *J Neurosci* **15:**1318–1328.

White RJ and Reynolds IJ (1996) Mitochondrial depolarization in glutamate-stimulated neurons—An early signal specific to excitotoxin exposure. *J Neurosci* **16:**5688–5697.

White RJ and Reynolds IJ (1997) Mitochondria accumulate Ca^{2+} following intense glutamate stimulation of cultured rat forebrain neurons. *J Physiol (Lond)* **498.1:**31–47.

Zoratti M and Szabo I (1995) The mitochondrial permeability transition. *Biochim Biophys Acta* **1241:**139–176.

Send reprint requests to: Ian J. Reynolds, Ph.D., Department of Pharmacology, University of Pittsburgh School of Medicine, E1354 Biomedical Science Tower, Pittsburgh, PA 15261. E-mail: iannmda@pop.pitt.edu

11 012

MitoTracker labeling in primary neuronal and astrocytic cultures: influence of mitochondrial membrane potential and oxidants

Jennifer F. Buckman, Hélène Hernández, Geraldine J. Kress, Tatyana V. Votyakova, Sumon Pal, Ian J. Reynolds

Department of Pharmacology, University of Pittsburgh, E1354 Biomedical Science Towers, Pittsburgh, PA 15261.

Corresponding Author:

Ian J. Reynolds, Ph.D.

Department of Pharmacology

University of Pittsburgh

E1354 Biomedical Sciences Tower

Pittsburgh, PA 15261

(412) 648-2134

(412) 624-0794

iannmda+@pitt.edu

Abstract: MitoTracker dyes are fluorescent mitochondrial markers that covalently bind free sulfhydryls. In this study, we investigated the impact of alterations in mitochondrial membrane potential ($\Delta\Psi_m$) and oxidant stress on MitoTracker staining in mitochondria in primary cultures of neurons and astrocytes. FCCP significantly decreased MitoTracker loading, except in the case of MitoTracker Green in neurons and MitoTracker Red in astrocytes. Treatment with FCCP after loading increased fluorescence intensity and caused a relocalization of the dyes. The magnitude of these effects was contingent on which MitoTracker, cell type and dye concentration were used. Oxidative stress induced by H_2O_2 pretreatment appeared to increase the fluorescence intensity of MitoTracker Orange and Red in neurons and MitoTracker Green in astrocytes. Exposure to H_2O_2 following loading increased MitoTracker Red fluorescence in astrocytes. Moreover, the MitoTracker dyes, at high concentrations, uncoupled respiration in state 4 (20-50%) and inhibited maximal respiration (30-40%). Thus, loading and mitochondrial localization of the MitoTracker dyes can be influenced by loss of $\Delta\Psi_m$ and increased oxidant burden. These dyes can also directly inhibit respiration. Thus, care must be taken in interpreting data collected using MitoTrackers dyes as these dyes have several potential limitations. Although MitoTrackers may have some value in identifying the location of mitochondria within cultured neurons and astrocytes, their sensitivity to $\Delta\Psi_m$ and oxidation negates their use as markers of mitochondrial dynamics in healthy cultures.

Key Words: Fluorescence imaging – mitochondria – oxidative stress

Running Title: MitoTrackers in neurons and astrocytes

There is an emerging appreciation for a role of mitochondria in excitotoxic injury pathways as well as injury mechanisms manifested as apoptotic or necrotic death processes. The development of novel mitochondrion-specific fluorescent dyes is necessary to explore the significance of mitochondria in these cell death pathways. Although some mitochondrial fluorescent probes are available that allow the assessment of mitochondrial membrane potential ($\Delta\Psi_m$), most fluorescent dyes that measure ions, such as calcium, magnesium and zinc, or reactive oxygen species (ROS) generation and pH are not specific to mitochondria. Moreover, dyes that can detect activity at the elusive permeability transition pore (PTP) in cultured neurons are currently unavailable.

The MitoTracker dyes, developed commercially by Molecular Probes (Eugene, OR), are structurally novel fluorescent probes that have been used to measure $\Delta\Psi_m$ (15), $\Delta\Psi_m$-independent mitochondrial mass (13) and photosensitisation (18). The MitoTracker dyes (MitoTracker Green FM, MitoTracker Orange CMTMRos, MitoTracker Red CMXRos) contain chloromethyl moieties that are thought to react with free sulfhydryls within the cell. MitoTracker Green has been suggested to be $\Delta\Psi_m$-insensitive and capable of loading and remaining within depolarized mitochondria, which implies that it would be an exceptional tool of assessing mitochondrial mass (22). MitoTrackers Orange and Red are positively charged rosamine derivatives that are rapidly taken up into the negatively charged mitochondria, suggesting that their loading would be dependent on $\Delta\Psi_m$, but their localization should be mitochondrial specific. However, MitoTracker Orange and Red, at least in their reduced state, may be strongly influenced by the presence of ROS (20, 21) and MitoTracker Orange may directly inhibit the respiratory chain at complex I and induce permeability transition (PT) (24). All three MitoTracker probes are believed to be fixable due to the membrane-impermeant dye complex that is created when the dyes enters the mitochondria. However, the sensitivity of these dyes to $\Delta\Psi_m$ and oxidant status and their permeability through the mitochondrial membrane has not been fully explored in unfixed cultured neurons and astrocytes.

Our laboratory is interested in identifying fluorescent dyes that can specifically label mitochondria in the central nervous system under a variety of conditions. The aim of the present study was to characterize the MitoTracker dyes in primary forebrain neurons and astrocytes to determine their dependency on $\Delta\Psi_m$ and oxidant status, especially given the widespread interest in using these dyes as fixable markers of $\Delta\Psi_m$. In addition, we addressed whether the MitoTrackers altered respiratory chain activity in isolated brain mitochondria to determine whether these dyes altered mitochondrial physiology.

MATERIALS AND METHODS

Cell culture

All procedures were in strict accordance with the NIH Guide for the Care and Use of Laboratory Animals and were approved by the University of Pittsburgh's Institutional Animal Care and Use Committee. Primary forebrain neurons were prepared as previously described (25). Briefly, forebrains from embryonic day-17 Sprague Dawley rats were removed and dissociated. Cells were plated on poly-D-lysine coated 31mm glass coverslips at a density of 450,000/ml (1.5mls/coverslip) and inverted after 24 hours to decrease glial growth. Experiments were performed when cells were 14 - 17 days in culture.

Primary forebrain astrocytes were prepared as described by McCarthy and DeVellis (17) with minor modifications. Briefly, forebrains from postnatal day-1 Sprague Dawley rats were dissociated and plated in 75cm^2 plastic flasks at a density of 860,000 cells/ml (10mls/flask). Media was changed every other day. Cells were grown to the point of confluency, at which point the flasks were orbitally shaken for 15-18 hours at 37°C. Adherent cells were then plated onto poly-D-lysine coated 31mm glass coverslips and fed every other day and used for up to 5 days in culture.

Solutions

Coverslips were perfused with a HEPES-buffered salt solution (HBSS) with (in mM): NaCl (137), KCl (5), $NaHCO_3$ (10), HEPES (20), glucose (5.5), KH_2PO_4 (0.6), Na_2HPO_4 (0.6), $CaCl_2$ (1.4), $MgSO_4$ (0.9), pH adjusted to 7.4 with NaOH. The protonophore and mitochondrial uncoupler carbonyl cyanide p-(trifluoromethoxy) phenyl-hydrazone (FCCP) was used at a concentration of 750nM (diluted in HBSS from a 750μM stock in methanol). Hydrogen peroxide (H_2O_2) was diluted in HBSS to concentrations ranging from 10μM – 3mM (from a 30% w/w stock solution). Oligomycin was used at a 2μM concentration (diluted from a 10mM stock in methanol).

Fluorescence imaging

For all experiments, individual coverslips were rinsed twice in HBSS and loaded with 10 – 500nM concentrations of MitoTracker Green FM, MitoTracker Orange (CMTMRos) or MitoTracker Red (CMXRos) (Molecular Probes, Eugene, OR) for 15 minutes at 37°C. Dyes were diluted in HBSS from a 1mM stock in anhydrous dimethyl sulfoxide. The coverslips were rinsed for 15 minutes in HBSS at room temperature. These loading parameters were tested for maximal loading without redistribution.

Experiments were performed at room temperature on two light microscope-based imaging systems with 40x quartz objective. Cells were illuminated using a Xenon lamp-based monochromator (Photonics, Germany) and light detected using a CCD camera. Data acquisition was controlled using Simple PCI software (Compix, Cranberry, PA). Cells were illuminated with a 490nm, 550nm or 575nm light depending on the dye and incidence light was attenuated with neutral density filters (Omega Optical, Brattleboro, VT). Emitted fluorescence from MitoTracker Green was passed through a 500 or 515 long pass (LP) dichroic mirror and a 535, 25 band pass (BP) or 535, 40BP emission filter (depending on the imaging system used). For MitoTracker Orange, a 570 or 575LP dichroic and a 590, 35BP or 605, 35BP emission filter was used. For MitoTracker Red, a

590LP dichroic with a 600LP emission filter was used. Coverslips were placed on the microscope stage, a field of cells (with at least 10 viable neurons or 5 viable astrocytes in the field) was chosen and a bright field image was captured. From this image, cell bodies were circled and used as regions of interest from which cellular fluorescence intensity was measured. Three small cell-free regions on the coverslip were also chosen to assess background fluorescence intensity. Images were collected once every 15 seconds for baseline and once every 5 seconds for the remainder of the experiment. Data were collected as background subtracted fluorescence intensity. All experiments were performed on at least 3 different culture dates and data were averaged. For most experiments, data were converted to percent baseline or percent of untreated control. Where pertinent, data were statistically analyzed using a two-tailed t-test or a one-way ANOVA and a Dunnett post-hoc test (when $p<0.05$).

FCCP experiments

To determine the effect of $\Delta\Psi_m$ depolarization on MitoTracker-loaded cells, individual coverslips were loaded with 10 – 500nM concentrations of MitoTracker dye (Green, Orange or Red) and imaged to observe changes in the intensity and/or pattern of fluorescence. Coverslips were perfused with HBSS for 5 minutes, with FCCP (750nM) for 5 minutes, and then with HBSS again for 5 minutes. The effect of $\Delta\Psi_m$ on loading was assessed by comparing fluorescence intensity (over 5 minutes, 1 frame/15 seconds) from coverslips incubated with 50nM MitoTracker alone to coverslips incubated in 750nM FCCP + 50nM MitoTracker.

H_2O_2 experiments

As with the FCCP experiments, the effect of an oxidant burden on pre-loaded cells was tested by loading coverslips with 50nM MitoTracker dye and imaging. Coverslips were perfused with HBSS, H_2O_2 (500μM in neurons, 3mM in astrocytes) and HBSS again. The effect of an oxidant burden on loading was assessed by incubating coverslips in H_2O_2 (10μM – 500μM in

neurons, 500μM – 3mM in astrocytes) for 15 minutes, then immediately loading 50nM MitoTracker dye (Green, Orange or Red) and imaging for 5 minutes.

Isolated brain mitochondria preparation

Rat brain mitochondria were isolated according to Rosenthal et al. (23). Briefly, a rat forebrain was removed, homogenized and suspended in 10mls of isolation buffer (pH 7.4, containing 225mM mannitol, 75mM sucrose, 1 mg/ml BSA, 1mM EDTA, 5mM HEPES-KOH). The brain homogenates were subjected to differential centrifugation and the final suspensions contained a heterogeneous population of synaptosomal and non-synaptosomal mitochondria. Protein concentration in the mitochondrial suspensions was determined according to Bradford (5). Only mitochondria that had a respiration ratio of 6 or higher (phosphylating state 3 to resting state 4 with glutamate and malate as substrates) were used.

Respiratory experiments

Mitochondrial respiration rates were measured polarographically at 37°C with a Clark oxygen electrode (Yellow Springs Instrument Co., Yellow Springs, OH) in a buffer containing 125mM KCl, 2mM K_2HPO_4, 4 mM $MgCl_2$, 3mM ATP, 5mM glutamate, 5mM malate, 5mM HEPES-KOH (pH 7.0). This buffer exhibits similarities to the intracellular environment and is believed to decrease the probability of PT (1, 2). Energized brain mitochondria (0.25mg protein/ml), oligomycin (2μM) and the MitoTracker dyes (at concentrations of 50nM (low) or 3.12μM (high) concentrations) were incubated in a 1.6ml water-jacketed glass chamber (Gilson, Middletown, WI). The experiment was initiated in an open chamber (to maintain oxygen concentration close to saturation) and mitochondrial suspension was stirred at 37°C for 10 minutes. The chamber was then sealed, state 4 (resting) respiration was measured and 1 minute later the uncoupling agent, FCCP (200nM) was added and the rate of uncoupled (maximal) respiration was determined.

Data were collected as nanograms of oxygen atoms consumed per minute per milligram of protein. Data were then transformed into percent of control respiration (in the absence of MitoTracker dye) and three separate one-way ANOVAs (for each MitoTracker dye), comparing respiration in control mitochondria to that in mitochondria incubated with the low and high concentration of dye. A Bonferroni post-hoc test was performed when $p < 0.05$.

RESULTS

FCCP-induced changes in dye labeling

All three MitoTrackers labeled neurons and astrocytes in a punctate fashion anticipated for a mitochondrion-specific dye. Staining was typically observed in perinuclear regions and processes, while the nucleus was typically devoid of staining (Fig. 1A & B, top panels). The fluorescence intensity of the MitoTrackers was concentration dependent with maximal staining seen with 200-500nM (data not shown). To determine the effect of $\Delta\Psi_m$ on fluorescence intensity, we loaded cells with different dye concentrations and then exposed the cells to FCCP. At high concentrations, the MitoTracker dyes showed an increase in fluorescence intensity upon loss of $\Delta\Psi_m$, suggesting that they become so tightly packed within mitochondria at these concentrations that fluorescence intensity is underestimated due to the phenomenon of quenching (see discussion). MitoTracker Green showed the smallest increase in fluorescence intensity during treatment with FCCP, however, in both neurons and astrocytes, no return to baseline was observed during a 5-minute wash period (Fig. 2A, D). MitoTracker Orange showed the most robust increase in fluorescence intensity in neurons and this was observed at concentrations of 50nM-500nM. A slow, delayed decrease in fluorescence was observed during the wash period, suggesting re-sequestration as mitochondria repolarize (Fig. 2B, E). MitoTracker Red showed variability in the time course of the FCCP-induced increases in fluorescence, however every concentration of MitoTracker Red tested was

influenced by mitochondrial depolarization. In addition, a rapid return to basal fluorescence was observed during the recovery period (Fig. 2C, F). All three MitoTrackers showed a diffusion of fluorescence upon mitochondrial depolarization (Fig. 1A & B, bottom panels). Interestingly, the redistribution of dye was apparent even when there was no overall change in fluorescence intensity. Taken together these data suggest that MitoTrackers are membrane-permeable and diffuse out of mitochondria during a depolarizing stimulus. It also appears that MitoTrackers, at concentrations as low as 25nM (in MitoTracker Red), are quenched in mitochondria as evidenced by the increase in fluorescence signal seen when the dyes are released from mitochondria and by the decrease when they are re-sequestered.

FCCP-induced changes in dye loading

A concentration of 50nM, the lowest concentration that reliably gave a good signal:noise ratio, was used for all MitoTrackers in this experiment. Neurons or astrocytes were loaded with MitoTracker dyes alone or in the presence of 750nM FCCP. This concentration of FCCP has been shown to result in a profound, but reversible depolarization of the $\Delta\Psi_m$ (26). In neurons, MitoTracker Green appeared to load equally well into polarized or depolarized mitochondria, however MitoTracker Orange and Red showed considerably lower fluorescence intensity when loaded into neurons treated with FCCP (Fig. 3A). In astrocytes, MitoTracker Green loading appeared to depend on the $\Delta\Psi_m$, with lower fluorescence intensity observed in the presence of FCCP. Similarly, MitoTracker Orange loading into astrocytes was compromised when mitochondria were depolarized. In contrast, MitoTracker Red appeared to load into astrocytic mitochondria regardless of $\Delta\Psi_m$ (Fig. 3B). A less punctate label (vs. Fig. 1A & B, upper panels) was observed under these loading conditions, except with MitoTracker Red in astrocytes (Fig. 4). These data reflect the different loading behaviors of the MitoTrackers and point to the significance of cell model for the appropriate use of these dyes.

H_2O_2-induced changes in dye loading

Cells were incubated with H_2O_2 for 15 minutes prior to loading with 50nM MitoTracker in order to induce an oxidant stress. The chloromethyl moieties of the MitoTracker dyes have been suggested to react with free sulfhydryls (11). Thus, we expected an oxidative stress to change the loading and stability of the MitoTrackers labeling. However, comparison of the means and standard deviations of fluorescence intensity following pretreatment showed that MitoTracker Green in neurons (Fig. 5A), MitoTracker Orange and Red in astrocytes (Fig. 5E, F) were insensitive to oxidative stress. The large variability seen with several concentrations of H_2O_2 tested typically resulted from single outlying points. Small, but reliable increases in fluorescence intensity were observed with MitoTracker Green in astrocytes (1-3mM H_2O_2, Fig. 5D) and MitoTracker Orange and Red in neurons (all concentrations, Fig. 5B, C). The changes in fluorescence intensity did not correlate with a relocalization of the dyes (Fig. 6), in that H_2O_2 increased fluorescence intensity without the migration of the dye into parts of the cell not normally labeled. This may be consistent with an alteration of the interaction of the dyes with cellular sulfhydryl moieties.

H_2O_2-induced changes in dye labeling

Neurons and astrocytes were loaded with 50nM MitoTracker dye and imaged for 5 minutes to achieve stable baseline fluorescence. Neurons were then treated with 500μM H_2O_2 for 5 minutes and the intensity of fluorescence was measured. MitoTracker Green was unaffected by treatment with H_2O_2 and MitoTracker Orange and Red fluorescence were only very modestly increased by this short-term oxidative stress, with no return to baseline observed. In astrocytes treated with 3mM H_2O_2, only MitoTracker Red fluorescence was increased (Fig. 7). No apparent relocalization of the dyes was observed (*data not shown*). These data suggest that once MitoTrackers, especially MitoTracker Green, are loaded into primary neuronal or astrocytic cultures, they are only mildly influenced by a change in the production of ROS and/or oxidation of sulfhydryl groups. However,

the effect of a longer exposure to H_2O_2 (i.e. 15 minutes) may be necessary to see the more profound effect seen during pretreatment with H_2O_2.

Respiration in isolated brain mitochondria

Isolated rat brain mitochondria were incubated in the presence of 50nM or 3.12μM MitoTracker Green, Orange or Red and state 4 (resting) and uncoupled (maximal) respiration were recorded. Since dye distribution in the mitochondrial suspensions is not in equilibrium, MitoTracker concentrations were determined based on μM of dye per mg of mitochondrial protein (50nM = 0.8μM/mg protein and 3.12μM = 12.5μM/mg protein). Initially mitochondria and the fluorescent dyes were incubated for 2-4 minutes prior to uncoupling, however there was no inhibition seen at either concentration tested (*data not shown*). Because the MitoTrackers contain sulfhydryl -reactive moieties they may bind more slowly, therefore we extended the incubation time to 10 minutes. Under these conditions, high concentrations of MitoTracker Green (3.12μM) significantly increased both resting and maximal respiration rates (Fig. 8), suggesting its ability to uncouple respiratory chain activity from ATP synthesis. MitoTracker Orange did not significantly impact respiration rate, however it exhibited trends towards increased state 4 respiration rate ($p = 0.07$) and decreased maximal respiration rate ($p=0.13$) (Fig. 8). MitoTracker Red exhibited a trend towards increased resting respiration rate ($p=0.09$) and significantly decreased the rate of maximal respiration rate (at 3.12μM, but not at 50nM). Taken together, these data suggest that all of the MitoTracker dyes are capable of inhibiting normal mitochondrial respiration at μM concentrations.

DISCUSSION

The MitoTracker dyes are being used with increasing frequency for morphological and functional measurements of mitochondria. While the pattern of their fluorescence strongly suggests mitochondrial specificity, parameters that influence their loading and/or labeling are still

controversial and have not been fully explored in neural cells. For example, reports that during apoptosis the release of cytochrome c can occur independent of changes in mitochondrial membrane potential have been partially based on the lack of change in MitoTracker Orange fluorescence (which was being used as a $\Delta\Psi_m$ sensor) during cytochrome c release (3, 8, 14). However, the present experiments suggest that there are numerous factors to consider prior to using the MitoTracker dyes and, in agreement with Scorrano et al. (24), that these aforementioned data must be interpreted with caution. We have noted that not only are MitoTracker Green, Orange and Red different from one another, but also that each MitoTracker behaves differently in neurons and astrocytes.

For all three MitoTrackers, in both neurons and astrocytes, a concentration of 50nM was sufficient to produce a bright, punctate label that appears to be associated with mitochondria. However, at this concentration, neurons and astrocytes treated with FCCP during or after loading showed a diffusion of the dye into the cytoplasm, nucleus and/or other organelles. In human osteosarcoma cells, a redistribution of MitoTracker Green was observed following a 30-minute treatment with another uncoupler, CCCP (18). However, these authors used high-resolution confocal microscopy and the observed redistribution appeared to coincide with mitochondrial swelling, not diffusion into cytoplasm (18). Whether this observation is associated with confocal versus light microscopy or osteosarcomas versus primary neurons and astrocytes is unclear.

In addition to a relocalization of fluorescence observed in association with mitochondrial depolarization, an increase in fluorescence intensity was frequently seen, especially at higher concentrations and most intensely with MitoTracker Orange (Fig. 2). We have interpreted this increased fluorescence as an unquenching of dye. Quenching occurs as the result of molecular interactions that inhibit the ability of a fluorophore to emit a photon. For example, rhodamine dyes aggregate based on $\Delta\Psi_m$ but these aggregates are non-fluorescent due to quenching. Quenching

becomes most apparent with these rhodamine dyes when the mitochondria are depolarized and the intensity of fluorescence dramatically increases (6). It is possible that MitoTrackers aggregate within mitochondria without truly quenching, however due to the similarities of the current observations with those seen with rhodamine derivatives we are tentatively referring to this phenomenon as quenching.

MitoTracker Green: MitoTracker Green is now commonly being used for measurement of mitochondrial shape changes, mass or swelling (4, 9, 13, 18, 19). At low concentrations (≤ 50nM), MitoTracker Green may be useful for these measures, however several features of this dye must be acknowledged prior to use. There are cell type- and concentration-specific differences in MitoTracker Green labeling. At 50nM, MitoTracker Green loading appeared $\Delta\Psi_m$- and oxidation-sensitive in astrocytes, but not neurons. At concentrations greater than 50nM, MitoTracker Green exhibits a tendency to quench and, upon depolarization, exhibits an irreversible increase in fluorescence. Moreover, in isolated brain mitochondria, μM concentrations of MitoTracker Green appeared capable of acting as an uncoupler and inhibiting respiration. Taken together, the present data support the use of MitoTracker Green at low concentrations for assessing mitochondrial size, localization and structure. However, determination of the appropriate concentration of MitoTracker in individual cell models will be necessary for interpretable results.

MitoTracker Orange: MitoTracker Orange has been used as a marker for $\Delta\Psi_m$ (16) and, in its reduced form, as a marker for ROS generation (12). Recently, Scorrano et al. (24) characterized this dye in MH1C1 rat hepatoma cells and in agreement with the present findings, found that the fluorescence was punctate and stable. However, in their cell model, a redistribution of the dye was observed following pretreatment with agents that decrease free sulfhydryls, but not with FCCP. In the present paper, pretreatment with FCCP, but not H_2O_2, caused a redistribution of MitoTracker Orange into neuronal and astrocytic cultures. H_2O_2 pretreatment, however, did appear to increase

MitoTracker Orange fluorescence in neurons, but not astrocytes. Moreover, Scorrano et al. (24) did not observe quenching or relocalization of MitoTracker Orange when cells were treated with FCCP following loading. In our experiments, neurons and astrocytes treated with FCCP following loading showed increased fluorescence intensity (suggestive of quenching) as well as a relocalization of fluorescence. In isolated rat liver mitochondria, MitoTracker Orange inhibited complex I of the respiratory chain, induced PT and caused depolarization, swelling and the release of cytochrome c in liver mitochondria (24). However, in isolated brain mitochondria, we did not observe inhibition of complex I by MitoTracker Orange, even at concentrations exceeding 3μM. Again, these observed differences suggest that care must be taken in extrapolating MitoTracker data obtained in different cell models. In addition, MitoTracker Orange should be used with caution and that the interpretation of data with MitoTracker Orange must consider their effects on mitochondrial function and their sensitivity to $\Delta\Psi_m$ and free sulfhydryls.

MitoTracker Red: MitoTracker Red has been utilized as a $\Delta\Psi_m$-sensitive dye, since being reported as one by Macho et al. (15). The linearity between $\Delta\Psi_m$ and MitoTracker Red fluorescence has been brought into question due to thiol binding of MitoTracker Red (7, 20). It seems unlikely that this dye would offer advantages over JC-1, TMRE or rhodamine 123 for assessing $\Delta\Psi_m$. However, MitoTracker Red can be fixed and maintain a mitochondrial-specific localization, as observed in double labeling experiments with cytochrome c oxidase (22). Gilmore et al. (10) used flow cytometry to show that MitoTracker Red was $\Delta\Psi_m$-sensitive because it decreased with depolarizing stimuli, but it could not reliably indicate $\Delta\Psi_m$ at the time of fixation. Moreover, MitoTracker Red has been implicated as a mitochondrial-specific photosensitiser, due to the laser-induced mitochondrial damage observed in osteosarcomas (18). In light of these observations, clear understanding of how MitoTracker Red influences neuronal and astrocytic mitochondria is necessary. In the present experiments, the loading of MitoTracker Red appeared

$\Delta\Psi_m$- and oxidant-dependent in neurons, but not astrocytes. Following loading, MitoTracker Red fluorescence relocalized during mitochondrial depolarization and increased following treatment with FCCP and H_2O_2 in astrocytes, and to a lesser degree, neurons. It also appears to inhibit normal respiratory activity through complex I. These data illustrate that MitoTracker Red loading, stability and mitochondrial localization is contingent on cell type, $\Delta\Psi_m$, ROS and/or free sulfhydryl groups. Therefore, in addition to being less than ideal as a $\Delta\Psi_m$ marker, MitoTracker Red seems incapable of functionally characterizing mitochondria in intact cells and should be used only as a marker for the localization of normal, energized mitochondria.

To determine whether MitoTracker dyes directly influenced bioenergetics, isolated rat brain mitochondria were examined for resting and uncoupled (maximal) respiration rates through complex I in the presence of the different MitoTrackers. We observed that MitoTracker Green acted as both a weak uncoupler and inhibitor of respiration and MitoTracker Red significantly decreased the rate of maximal respiration. MitoTracker Orange showed similar trends. These data suggest that the MitoTracker dyes are capable of inhibiting normal mitochondrial respiration at μM concentrations. Previously, MitoTracker Orange was found to inhibit complex I in isolated liver mitochondria and was observed to induce PT and swelling and release cytochrome c (24). In the present experiments, a respiration buffer containing physiological concentrations of Mg^{2+} and ATP and an acidic pH (7.0) was used to minimize the likelihood of PT. The opening of the PTP can lead to the loss of respiratory substrates, such as NADH, as well as cytochrome c, thereby confounding the assessment of the MitoTracker dyes on respiratory chain activity. Moreover, since the MitoTracker dyes are sulfhydryl agents, they may increase the probability of opening the PTP (27). We therefore designed the respiration experiments to enhance a straightforward assessment of respiratory chain activity through complex I and did not test the MitoTracker dyes' ability to induce transition. In keeping with Scorrano et al. (24), however, we performed preliminary experiments in isolated liver mitochondria

and observed inhibition of respiration with MitoTracker Red, and to a lesser extent with MitoTracker Orange (*data not shown*).

There are clearly some potential limitations to the present studies. The resolution obtainable with wide-field microscopy precludes the ready assessment of the fluorescence signal at the single mitochondrion level, so that relocalization of dye is difficult to quantitatively measure. Indeed, it is even difficult to conclusively establish that the punctate staining that we have observed is associated with mitochondria, because any correlative co-staining approach would also require assumptions about the localization of the co-stain. We are also unable to monitor the impact of permeability transition on the localization of the dyes because of the lack of an unequivocal method for inducing robust and measurable transition in intact neurons or astrocytes. Nevertheless, the characterization provided by this study will help to establish suitable methods for the use of these dyes, and suggests caution when using the MitoTrackers for even a semi-quantitative determination of $\Delta\Psi_m$.

Acknowledgment: The authors gratefully acknowledge Teresa Hastings for her collaboration with the respiration experiments. This work was supported by USAMRMC grant DAMD-17-98-1-8627 (IJR) , the Scaife Family Foundation (IJR) and an NIH grant T32NS07391 (JFB).

REFERENCES

1. Andreyev, A., and Fiskum, G. 1999. Calcium induced release of mitochondrial cytochrome c by different mechanisms selective for brain versus liver. *Cell Death Differentiation* **6:** 825-32.
2. Andreyev, A. Y., Fahy, B., and Fiskum, G. 1998. Cytochrome c release from brain mitochondria is independent of the mitochondrial permeability transition. *FEBS Letters* **439:** 373-6.

3. Bossy-Wetzel, E., Newmeyer, D. D., and Green, D. R. 1998. Mitochondrial cytochrome c release in apoptosis occurs upstream of DEVD-specific caspase activation and independently of mitochondrial transmembrane depolarization. *EMBO J* **17:** 37-49.

4. Bowser, D. N., Minamikawa, T., Nagley, P., and Williams, D. A. 1998. Role of mitochondria in calcium regulation of spontaneously contracting cardiac muscle cells. *Biophys J* **75:** 2004-14.

5. Bradford, M. M. 1976. A rapid and sensitive method for the quantitation of microgram quantities of protein utilizing the principle of protein-dye binding. *Analy Biochem* **72:** 248-54.

6. Chen, L. B., and Smiley, S. T. 1993. Probing mitochondrial membrane potential in living cells by a J-aggregate-forming dye. Pages 124-131 in W. T. Mason, Ed., *Fluorescent and Luminescent Probes for Biological Activity.* Academic Press Limited, London.

7. Ferlini, C., Scambia, G., and Fattorossi, A. 1998. Is chloromethyl-X-rosamine useful in measuring mitochondrial transmembrane potential? [letter; comment]. *Cytometry* **31:** 74-5.

8. Finucane, D. M., Bossy-Wetzel, E., Waterhouse, N. J., Cotter, T. G., and Green, D. R. 1999. Bax-induced caspase activation and apoptosis via cytochrome c release from mitochondria is inhibitable by Bcl-xL. *J Biol Chem* **274:** 2225-33.

9. Funk, R. H., Nagel, F., Wonka, F., Krinke, H. E., Golfert, F., and Hofer, A. 1999. Effects of heat shock on the functional morphology of cell organelles observed by video-enhanced microscopy. *Anat Record* **255:** 458-64.

10. Gilmore, K., and Wilson, M. 1999. The use of chloromethyl-X-rosamine (Mitotracker red) to measure loss of mitochondrial membrane potential in apoptotic cells is incompatible with cell fixation. *Cytometry* **36:** 355-8.

11. Haugland, R. P. 1996. *Handbook of Fluorescent Probes and Research Chemicals.* Molecular Probes, Eugene, OR.

12. Karbowski, M., Kurono, C., Wozniak, M., Ostrowski, M., Teranishi, M., Soji, T., and Wakabayashi, T. 1999. Cycloheximide and 4-OH-TEMPO suppress chloramphenicol-induced apoptosis in RL-34 cells via the suppression of the formation of megamitochondria. *Biochim Biophys Acta* **1449:** 25-40.

13. Krohn, A. J., Wahlbrink, T., and Prehn, J. H. 1999. Mitochondrial depolarization is not required for neuronal apoptosis. *J Neurosci* **19:** 7394-404.

14. Li, N., Oberley, T. D., Oberley, L. W., and Zhong, W. 1998. Inhibition of cell growth in NIH/3T3 fibroblasts by overexpression of manganese superoxide dismutase: mechanistic studies. *J Cell Physiol* **175:** 359-69.

15. Macho, A., Decaudin, D., Castedo, M., Hirsch, T., Susin, S. A., Zamzami, N., and Kroemer, G. 1996. Chloromethyl-X-Rosamine is an aldehyde-fixable potential-sensitive fluorochrome for the detection of early apoptosis [see comments]. *Cytometry* **25:** 333-40.

16. Matylevitch, N. P., Schuschereba, S. T., Mata, J. R., Gilligan, G. R., Lawlor, D. F., Goodwin, C. W., and Bowman, P. D. 1998. Apoptosis and accidental cell death in cultured human keratinocytes after thermal injury. *Am J Pathol* **153:** 567-77.

17. McCarthy, K. D., and de Vellis, J. 1980. Preparation of separate astroglial and oligodendroglial cell cultures from rat cerebral tissue. *J Cell Biol* **85:** 890-902.

18. Minamikawa, T., Williams, D. A., Bowser, D. N., and Nagley, P. 1999. Mitochondrial permeability transition and swelling can occur reversibly without inducing cell death in intact human cells. *Exp Cell Res* **246:** 26-37.

19. Monteith, G. R., and Blaustein, M. P. 1999. Heterogeneity of mitochondrial matrix free Ca2+: resolution of Ca2+ dynamics in individual mitochondria in situ. *Am J Physiol* **276:** C1193-204.

20. Poot, M., and Pierce, R. C. 1999. Detection of apoptosis and changes in mitochondrial membrane potential with chloromethyl-X-rosamine [letter]. *Cytometry* **36:** 359-60.

21. Poot, M., and Pierce, R. H. 1999. Detection of changes in mitochondrial function during apoptosis by simultaneous staining with multiple fluorescent dyes and correlated multiparameter flow cytometry. *Cytometry* **35:** 311-7.

22. Poot, M., Zhang, Y. Z., Kramer, J. A., Wells, K. S., Jones, L. J., Hanzel, D. K., Lugade, A. G., Singer, V. L., and Haugland, R. P. 1996. Analysis of mitochondrial morphology and function with novel fixable fluorescent stains. *J Histochem Cytochem* **44:** 1363-72.

23. Rosenthal, R. E., Hamud, F., Fiskum, G., Varghese, P. J., and Sharpe, S. 1987. Cerebral ischemia and reperfusion: prevention of brain mitochondrial injury by lidoflazine. *J Cereb Blood Flow Metab* **7:** 752-8.

24. Scorrano, L., Petronilli, V., Colonna, R., Di Lisa, F., and Bernardi, P. 1999. Chloromethyltetramethylrosamine (Mitotracker Orange) induces the mitochondrial permeability transition and inhibits respiratory complex I. Implications for the mechanism of cytochrome c release. *J Biol Chem* **274:** 24657-63.

25. White, R. J., and Reynolds, I. J. 1995. Mitochondria and Na+/Ca2+ exchange buffer glutamate-induced calcium loads in cultured cortical neurons. *J Neurosci* **15:** 1318-28.

26. White, R. J., and Reynolds, I. J. 1996. Mitochondrial depolarization in glutamate-stimulated neurons: an early signal specific to excitotoxin exposure. *J Neurosci* **16:** 5688-97.

27. Zoratti, M., and Szabo, I. 1995. The mitochondrial permeability transition. *Biochim Biophys Acta* **1241:** 139-76.

FIG. 1: Representative micrographs of fluorescence intensity and distribution of the MitoTracker dyes prior to and during treatment with FCCP in (A) primary neurons and (B) astrocytes. In both (A) and (B), the upper row of images shows baseline fluorescence in cells loaded with 50nM MitoTracker Green, Orange and Red (from left to right). The lower row of images shows fluorescence in cells treated with a mitochondrial depolarizing stimulus (images collected after approximately 3 minutes of FCCP treatment).

FIG. 2: Intensity of MitoTracker fluorescence during mitochondrial depolarization. **(A-C)** Primary neurons and **(D-F)** astrocytes were loaded with 50nM MitoTracker **(A, D)** Green, **(B, E)** Orange or **(C, F)** Red and the fluorescence intensity was measured. Baseline fluorescent images were recorded for 5 minutes, then the MitoTracker response to a depolarizing concentration (750nM) of the uncoupling agent, FCCP was measured for 5 minutes. Following treatment, cells were allowed to recover for 5 minutes. Data are presented as percent of baseline fluorescence intensity.

FIG. 3: Effect of mitochondrial depolarization on MitoTracker loading. **(A)** Neurons and **(B)** astrocytes were loaded with 50nM MitoTracker dye in the presence of 750nM FCCP and the fluorescence intensity (averaged over 5 minutes) was compared to cells loaded without FCCP. The loading of MitoTracker Green (MTG) in astrocytes, MitoTracker Orange (MTO) in neurons and astrocytes and Red (MTR) in neurons was sensitive to $\Delta\psi_m$, as evidenced by the significant decrease in fluorescence intensity when FCCP was present. Unpaired t test revealed that in neurons: MTG did not differ from baseline ($t= 0.1$, $df = 5$, $p > 0.05$), but MTO ($t= 10.45$, $df = 4$, $p < 0.001$) and MTR ($t= 8.0$, $df = 4$, $p < 0.01$) did. In astrocytes: MTG was different ($t=6.66$, $df = 6$, $p < 0.001$) as was MTO ($t= 3.1$, $df = 9$, $p < 0.02$),but MTR was not ($t= 0.3$, $df = 4$, $p > 0.05$).

FIG. 4: Representative micrographs of distribution of the MitoTracker fluorescence when loaded in the presence of a mitochondrial depolarizing stimulus. (**A-C**) Primary neurons and (**D-F**) astrocytes were loaded with 50nM MitoTracker (**A, D**) Green, (**B, E**) Orange or (**C, F**) Red in the presence of 750nM FCCP.

FIG. 5: Effect of H_2O_2 pretreatment on MitoTracker loading. (**A-C**) Neurons were incubated with 10μM -500μM of H_2O_2 for 15 minutes, then loaded with 50nM MitoTracker (**A, D**) Green, (**B, E**) Orange or (**C, F**) Red. The intensity of fluorescence was measured (over 5 minutes) and the mean ± standard deviation was calculated. Data are expressed as percent of untreated control.

FIG. 6: Representative micrographs of distribution of the MitoTracker loading in cells pretreated with H_2O_2. (**A, B**) The upper rows of images show neurons loaded with 50nM MitoTracker Green, Orange and Red (from left to right) without any pretreatment. In the lower rows, (**A**) neurons were preincubated with 500μM H_2O_2 and then loaded with 50nM MitoTracker (**B**) astrocytes were preincubated with 3mM H_2O_2 and then loaded with 50nM MitoTracker.

FIG. 7: Intensity of MitoTracker fluorescence in response to H_2O_2. (**A**) Neurons and (**B**) astrocytes were loaded with 50nM MitoTracker and their response to 500μM (neurons) or 3mM (astrocytes) H_2O_2 was measured. Baseline fluorescent images were recorded for 5 minutes, followed by a 5-minute H_2O_2 treatment and a 5-minute recovery period. Data are expressed as percent of basal fluorescence (± SEM).

FIG. 8: Respiration of isolated rat brain mitochondria. (**A**) State 4 (resting) respiration rate was determined following a 10 minute preincubation of isolated mitochondria with 2μM oligomycin and

50nM or 3.12μM MitoTracker Green (MTG), Orange (MTO) or Red (MTR). The mean (± SEM) respiration rates were computed and data were transformed into percent of respiration rate of control (without MitoTracker dyes). Statistical analysis using a one-way ANOVA and a Bonferroni's post-hoc test showed the following: MTG: $F_{(2, 10)} = 7.5$, $p < 0.05$ with the high concentration being significantly different from both the control and 50nM group ($p < 0.05$). MTO: $F_{(2, 8)} = 3.7$, $p > 0.05$. MTR: $F_{(2, 8)} = 3.3$, $p > 0.05$. (**B**) Following assessment of resting respiration, 200nM FCCP was added and the maximal respiration rate was determine in the same isolated mitochondria. The mean (± SEM) respiration rate was computed and data were transformed into percent of respiration rate of control (without MitoTracker dyes). Statistical analysis showed the following: MTG: $F_{(2, 8)} = 16.2$, $p < 0.05$ with the high concentration being significantly different from both the control and 50nM group ($p < 0.05$). MTO: $F_{(2, 6)} = 2.9$, $p > 0.05$. MTR: $F_{(2, 6)} = 130.1$, $p < 0.05$ with the high concentration being significantly different from both the control and 50nM group ($p < 0.05$).

Fig. 1

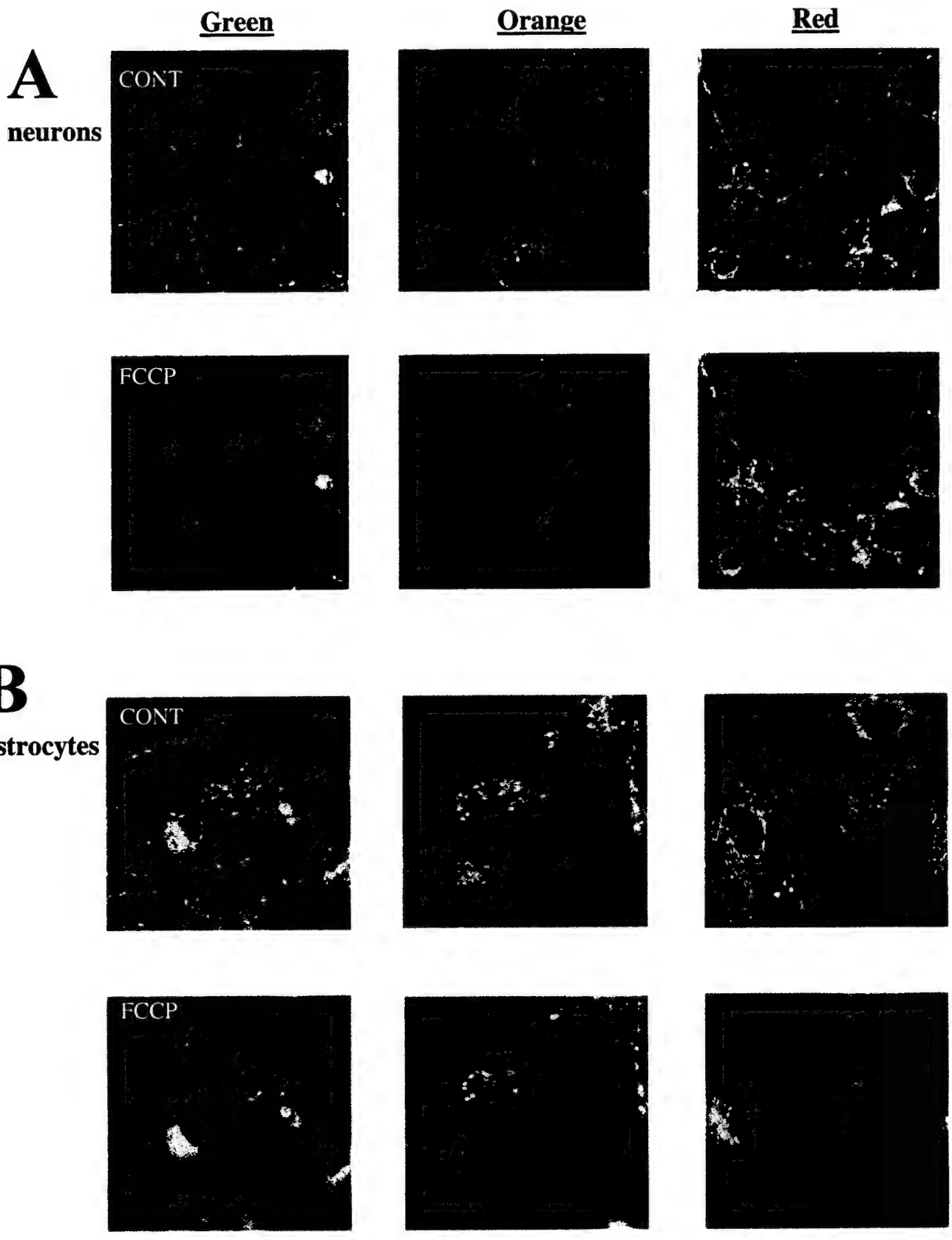

Fig. 2

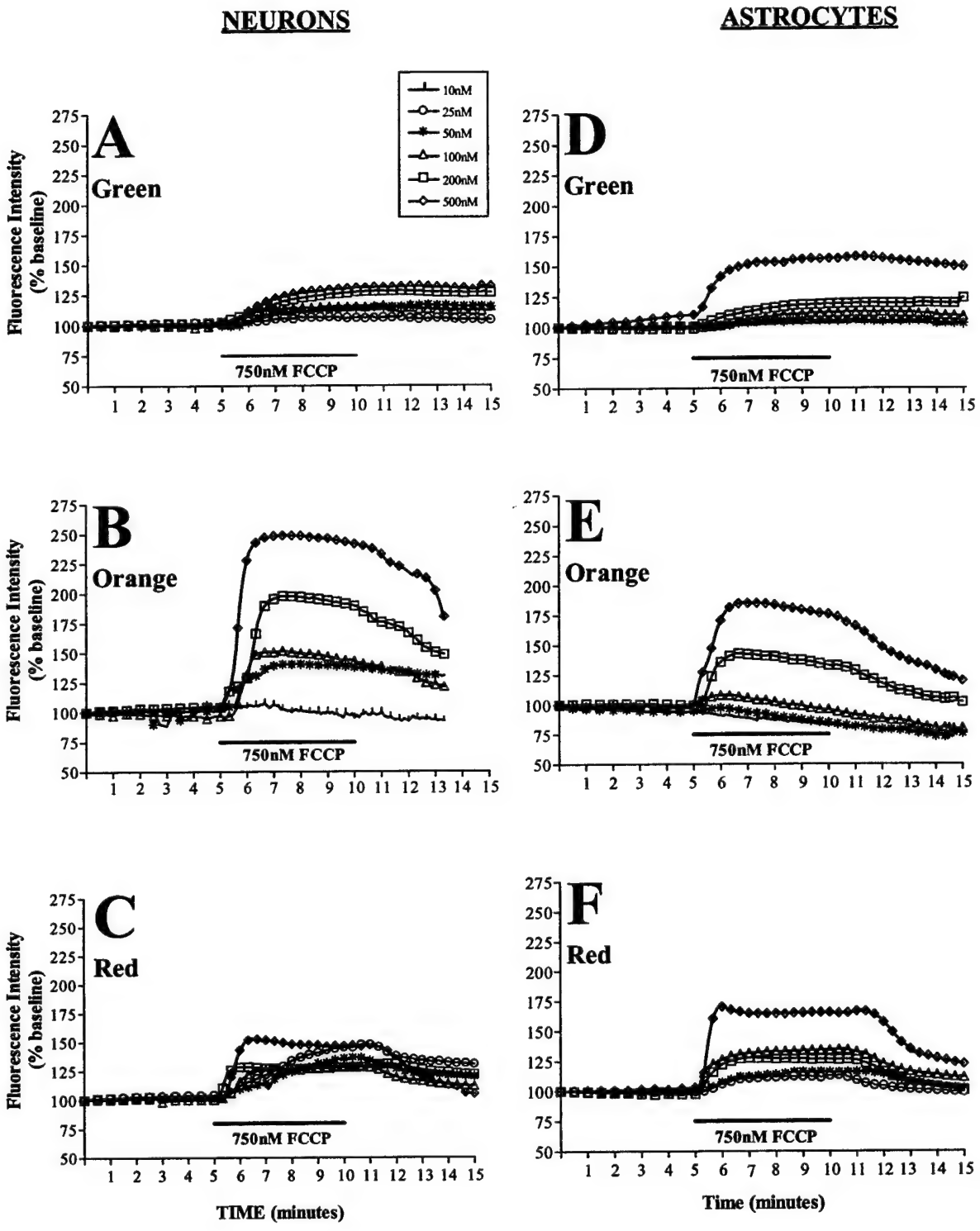
NEURONS
ASTROCYTES
10nM
25nM
50nM
100nM
200nM
500nM
A
Green
B
Orange
C
Red
D
Green
E
Orange
F
Red
Fluorescence Intensity (% baseline)
750nM FCCP
TIME (minutes)
Time (minutes)

Fig. 3

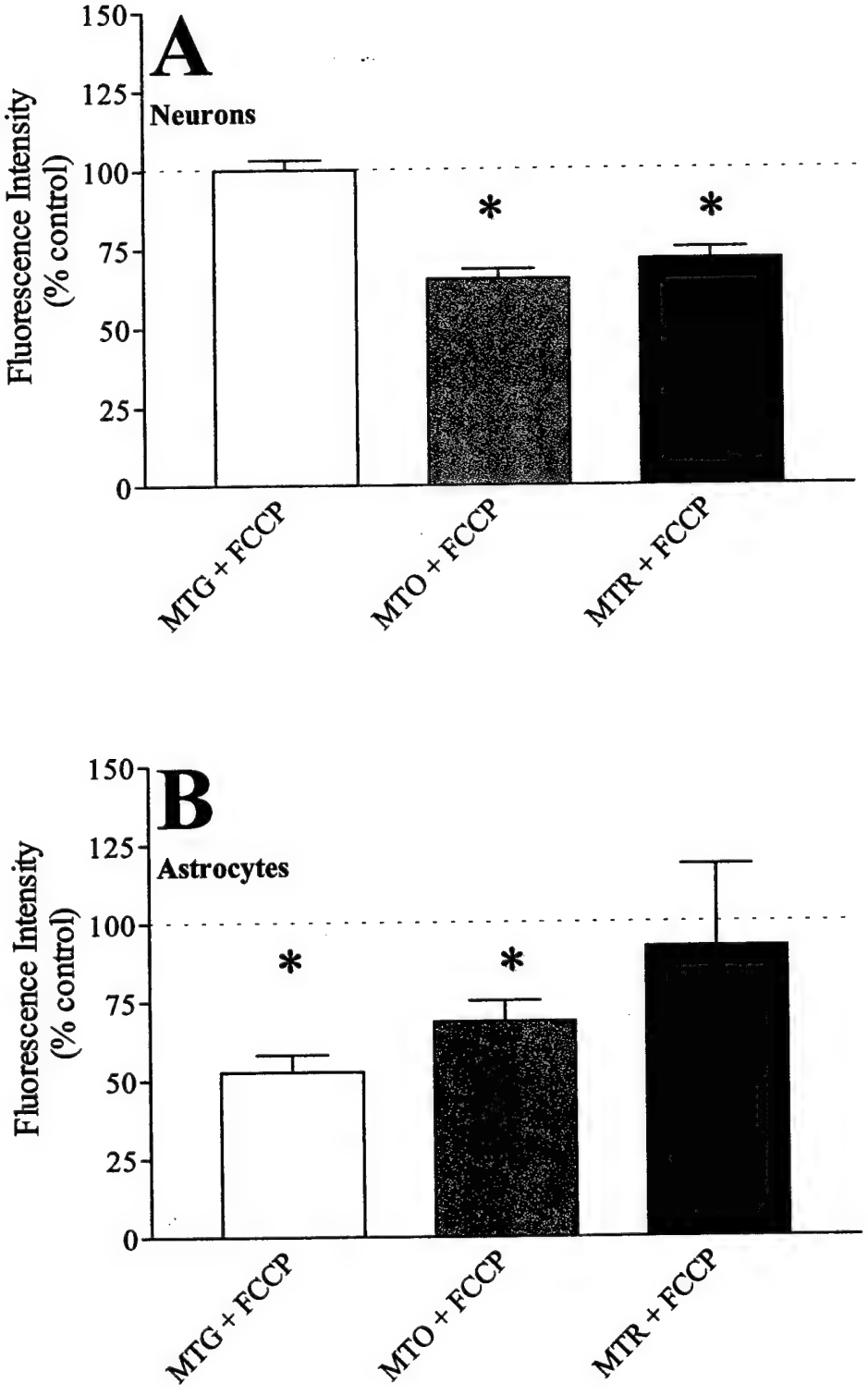
A
Neurons
Fluorescence Intensity
(% control)
150
125
100
75
50
25
0
*
*
MTG + FCCP
MTO + FCCP
MTR + FCCP
B
Astrocytes
Fluorescence Intensity
(% control)
150
125
100
75
50
25
0
*
*
MTG + FCCP
MTO + FCCP
MTR + FCCP

Fig. 4

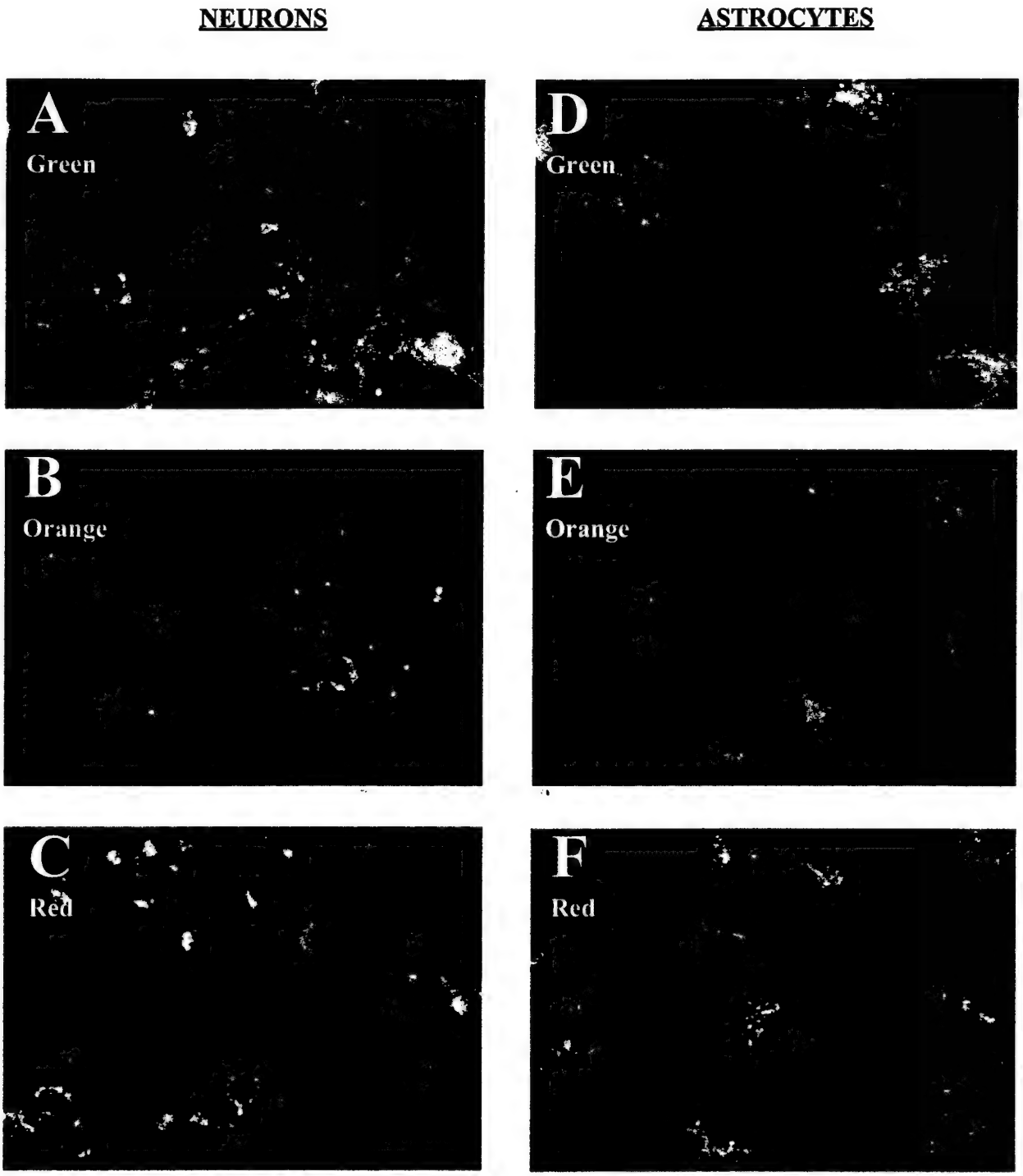
NEURONS
ASTROCYTES
A
Green
D
Green
B
Orange
E
Orange
C
Red
F
Red

Fig. 5

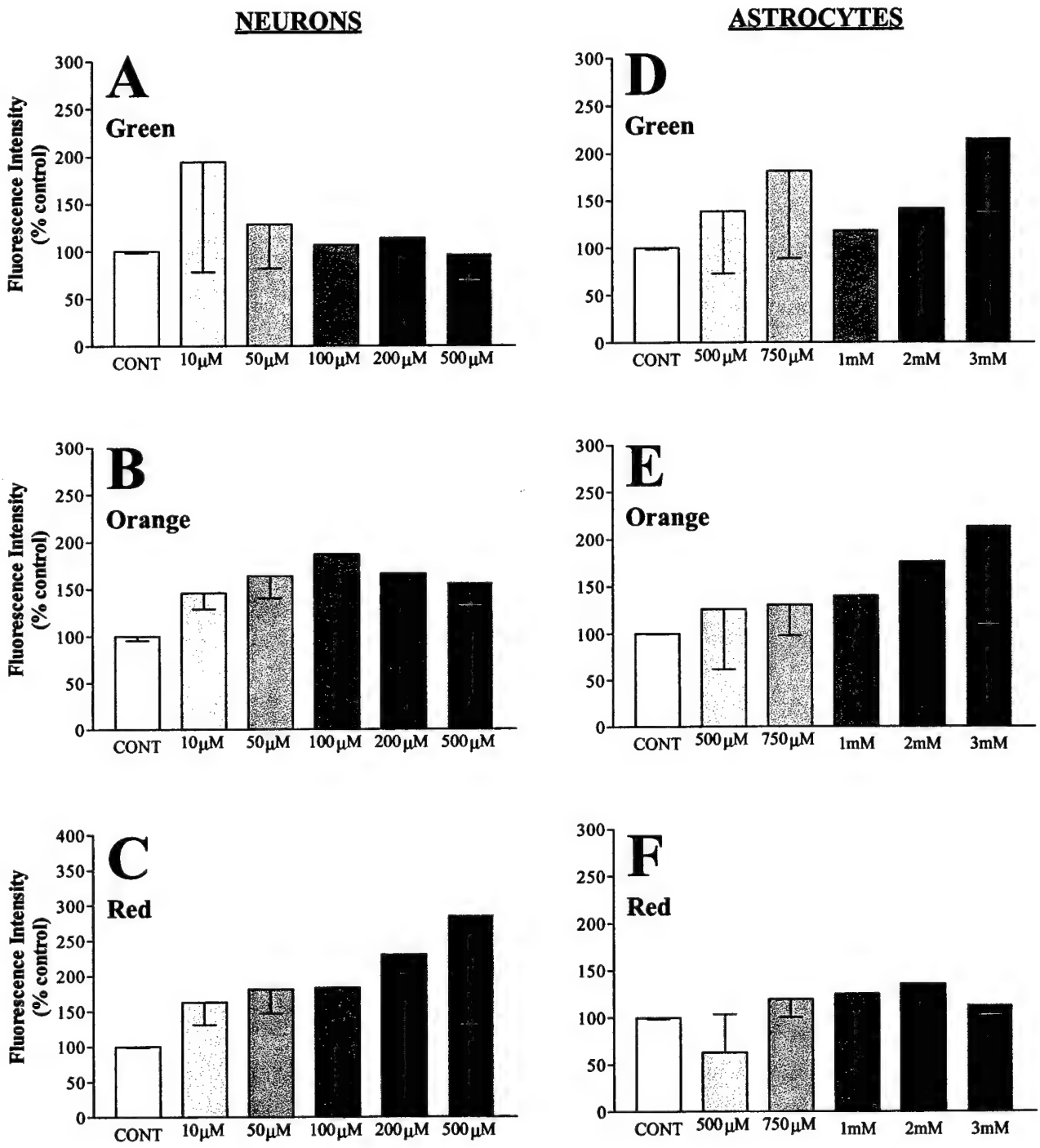
NEURONS
ASTROCYTES
A
Green
B
Orange
C
Red
D
Green
E
Orange
F
Red
Fluorescence Intensity (% control)
CONT
10μM
50μM
100μM
200μM
500μM
500μM
750μM
1mM
2mM
3mM

Fig. 6

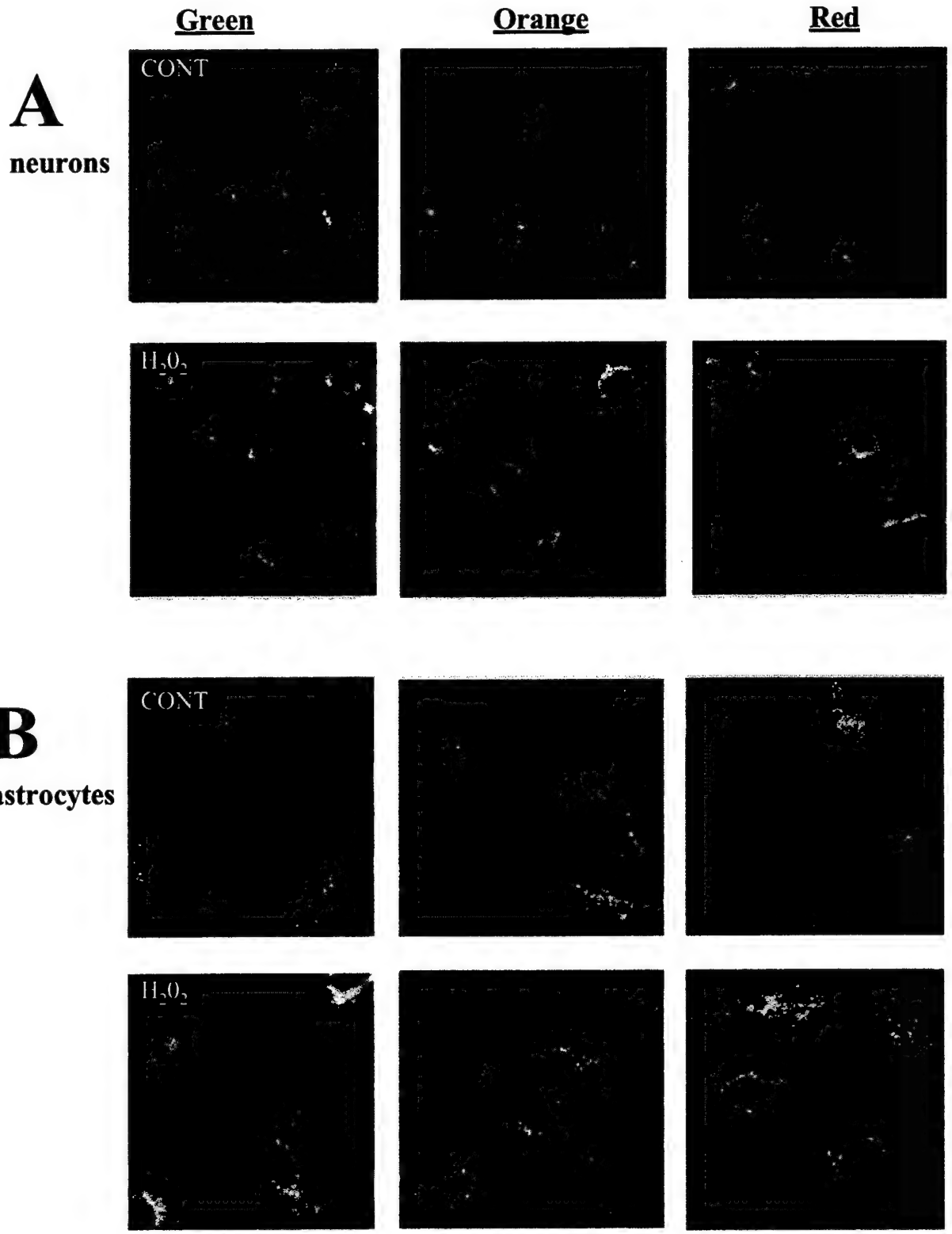

Fig. 7

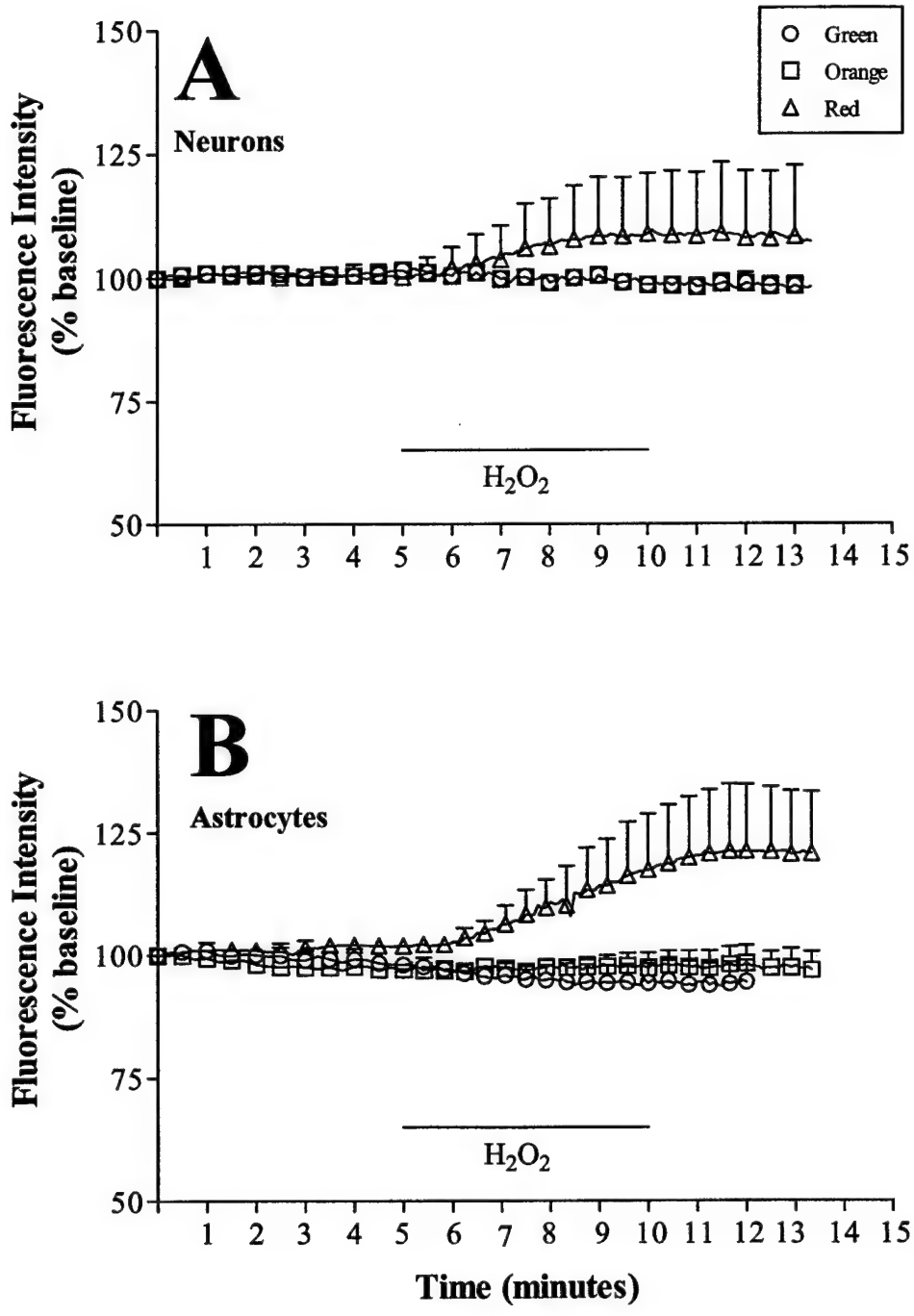
A
Neurons
Green
Orange
Red
Fluorescence Intensity
(% baseline)
150
125
100
75
50
H_2O_2
1 2 3 4 5 6 7 8 9 10 11 12 13 14 15
B
Astrocytes
Fluorescence Intensity
(% baseline)
150
125
100
75
50
H_2O_2
1 2 3 4 5 6 7 8 9 10 11 12 13 14 15
Time (minutes)

Fig. 8

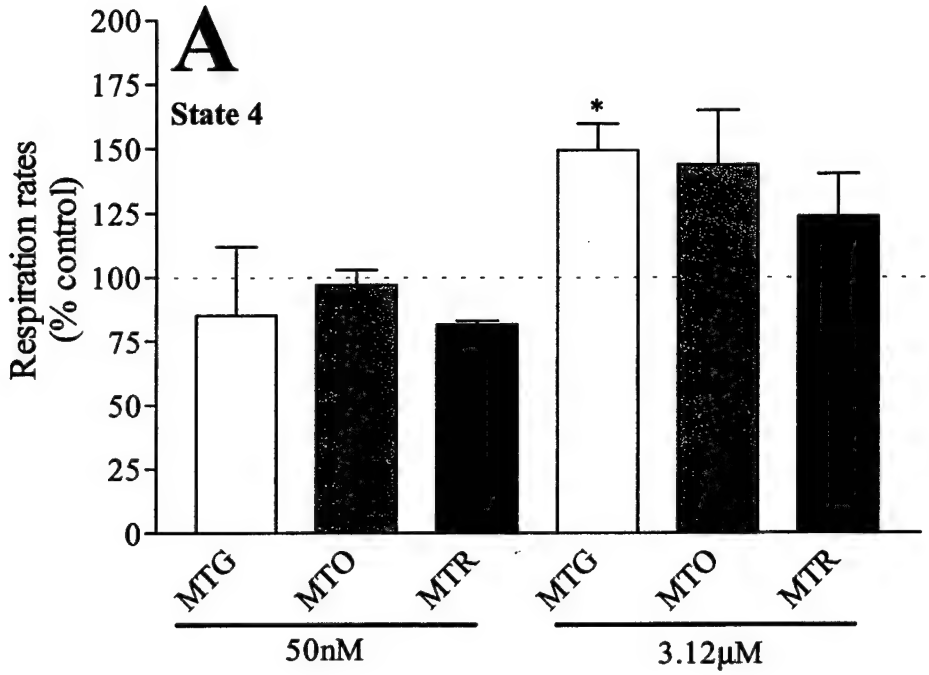
A
State 4
Respiration rates
(% control)
200
175
150
125
100
75
50
25
0
*
MTG
MTO
MTR
MTG
MTO
MTR
50nM
3.12µM

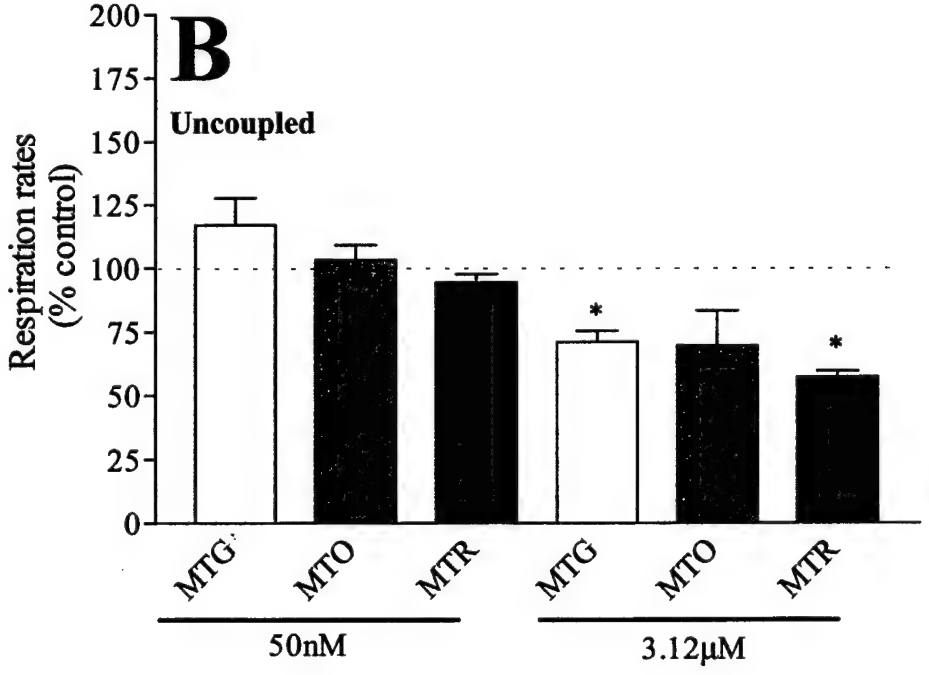
B
Uncoupled
Respiration rates
(% control)
200
175
150
125
100
75
50
25
0
*
*
MTG
MTO
MTR
MTG
MTO
MTR
50nM
3.12µM

Pharmacological Investigation of Mitochondrial Ca^{2+} Transport in Central Neurons: Studies With CGP-37157, An Inhibitor of the Mitochondrial Na^{+}/Ca^{2+} Exchanger

by: Joelle M. Scanlon, Jacques B. Brocard, Amy K. Stout, and Ian J. Reynolds

University of Pittsburgh

School of Medicine

Department of Pharmacology

Pittsburgh, PA 15261

Address for correspondence:

Dr. Ian J. Reynolds, Department of Pharmacology, W1351 Biomedical Science Tower, University of Pittsburgh, School of Medicine, Pittsburgh, PA 15261, U.S.A.

Voice: 412-648-2134, Fax: 412-624-0794, e-mail: iannmda+@pitt.edu

Joelle Scanlon, UPMC Health Systems, PET Facility, B-938 PUH, 200 Lothrop Street, Pittsburgh, PA 15213, U.S.A. Voice:412-647-0736, e-mail: joelle+@pitt.edu

Jacques Brocard, Department of Pharmacology, W1351 Biomedical Science Tower, University of Pittsburgh, School of Medicine, Pittsburgh, PA 15261, U.S.A.

Voice: 412 683 7667, e-mail: calcium99@hotmail.com

Amy K. Stout, MitoKor Inc, 11494 Sorrento Valley Rd, San Diego, CA 92121, U.S.A.

Voice: 858-509-5623, Fax: 858-793-7805, e-mail: stouta@mitokor.com

ABSTRACT

Mitochondria buffer large changes in $[Ca^{2+}]_i$ following an excitotoxic glutamate stimulus. Mitochondrial sequestration of $[Ca^{2+}]_i$ can beneficially stimulate oxidative metabolism and ATP production. However, Ca^{2+} overload may have deleterious effects on mitochondrial function and cell survival, particularly Ca^{2+}-dependent production of reactive oxygen species (ROS) by the mitochondria. We recently demonstrated that the mitochondrial Na^+/Ca^{2+} exchanger in neurons is selectively inhibited by CGP-37157, a benzothiazepine analogue of diltiazem. In the present series of experiments we investigated the effects of CGP-37157 on mitochondrial functions regulated by Ca^{2+}. Our data showed that 25μM CGP-37157 quenches DCF fluorescence similar to 100μM glutamate and this effect was enhanced when the two stimuli were applied together. CGP-37157 did not increase ROS generation and did not alter glutamate or 3mM hydrogen peroxide induced increases in ROS as measured by DHE fluorescence. CGP-37157 induces a slight decrease in intracellular pH, much less than that of glutamate. In addition, CGP-37157 does not enhance intracellular acidification induced by glutamate. Although it is possible that CGP-37157 can enhance mitochondrial respiration both by blocking Ca^{2+} cycling and by elevating intramitochondrial Ca^{2+}, we did not observe any changes in ATP levels or toxicity either in the presence or absence of glutamate. Finally, mitochondrial Ca^{2+} uptake during an excitotoxic glutamate stimulus was only slightly enhanced by inhibition of mitochondrial Ca^{2+} efflux. Thus, although CGP-37157 alters mitochondrial Ca^{2+} efflux in neurons, the inhibition of Na^+/Ca^{2+} exchange does not profoundly alter glutamate mediated changes in mitochondrial function or mitochondrial Ca^{2+} content.

INTRODUCTION

Of the many ways in which neurons can die perhaps the most extensively studied are the processes collectively referred to as "excitotoxicity" [1;2]. This phenomenon is associated with the release of glutamate from neuronal and non-neuronal stores and subsequently the excessive activation of ionotropic glutamate receptors. Excitotoxic glutamate injury probably reflects a collection of neurotoxic mechanisms depending on the duration and intensity of the glutamate exposure and the type of receptors activated. This is most readily appreciated, and well studied, in primary cell culture. In cortical neurons, for example, a brief exposure (approximately 5 minutes) to a high concentration of glutamate results in activation of the N-methyl-D-aspartate (NMDA) subtype of glutamate receptor, allows massive Ca^{2+} entry and results in predominantly necrotic cell injury [3;4]. Lower concentrations of glutamate can also be toxic via the activation of NMDA receptors, but it has been suggested that this results in apoptotic injury [5]. If non-NMDA glutamate receptors are activated a form of injury is triggered that depends less on extracellular calcium, and requires several hours of stimulation to commit neurons to die, but is expressed as necrotic cell death [6]. Evidence for all of these forms of injury have been found *in vivo* [2;7;8]. Thus, excitotoxicity should not be considered as a single homogenous phenomenon.

In this laboratory we have focused on the acute, necrotic injury that results from NMDA receptor activation and depends on Ca^{2+} entry [4]. This form of injury is likely to be a consequence of the particular effectiveness with which NMDA receptors permit neuronal Ca^{2+} accumulation, because they form a Ca^{2+} permeable channel that only partially inactivates during prolonged exposure to agonists (unlike, for example, voltage gated Ca^{2+} channels). Thus,

excitotoxic NMDA receptor activation results in very high cytoplasmic free Ca^{2+} concentrations [9;10] in addition to potentially allowing Ca^{2+} entry into specific sites in neurons poised to cause injury [11]. As has been reported in several types of excitable cells [12-14], neuronal mitochondria buffer these glutamate-induced large Ca^{2+} loads particularly well [15-24]. However, it appears that the consequence of this mitochondrial Ca^{2+} buffering is lethal. Thus, if mitochondrial Ca^{2+} accumulation is prevented by eliminating the mitochondrial membrane potential (and thus abrogating the driving force for mitochondrial Ca^{2+} uptake) neurons are protected from NMDA receptor-mediated injury [25;26].

It remains unclear what links mitochondrial Ca^{2+} accumulation to injury. Studies in isolated mitochondria and intact neurons have suggested that glutamate stimulated mitochondrial Ca^{2+} accumulation results in the production of reactive oxygen species (ROS) that may originate from mitochondria [27-31]. The activation of the permeability transition pore has also been suggested [32-34], although evidence supporting this mechanism is incomplete.

The finding that excitotoxicity requires mitochondrial Ca^{2+} accumulation is an exciting development because it suggests novel targets at which to aim neuroprotective drug strategies. However, at this stage the pharmacology of mitochondrial transport is rather poorly developed. The major Ca^{2+} uptake pathway is likely to be the Ca^{2+} uniporter [12], which may be complemented by a rapid uptake mode of the kind described in liver mitochondria [35;36]. There are several inhibitors of the Ca^{2+} uniporter, including ruthenium red and the related Ru360 [37], as well as some cobaltammine agents [38]. However, most of these agents penetrate cells very poorly, as exemplified by the 10,000-fold decrease in potency of Ru360 in intact cardiac myocytes compared to cardiac mitochondria [37]. Indeed, even applying relatively high

concentrations of Ru360 (~10μM) for several tens of minutes to intact neurons has very little effect on glutamate-induced cytosolic Ca^{2+} transients (JBB and IJR, unpublished observations). It was also recently suggested that mitochondrial Ca^{2+} accumulation can occur if the mitochondrial Na^{+}-Ca^{2+} exchanger reverses [39], although it is not known if this occurs in neurons.

An alternative approach to modifying mitochondrial Ca^{2+} loading is to manipulate the primary efflux pathways. In excitable cells mitochondrial Ca^{2+} efflux may be mediated by several different pathways. Under normal circumstances the mitochondrial Na^{+}-Ca^{2+} exchanger may be the primary mechanism for efflux [40]. In principle, it is also possible that the uniporter could reverse if the mitochondrial membrane potential is lost [41] , and activation of permeability transition should also result in massive Ca^{2+} release [42]. Both of these latter situations would be associated with catastrophic alterations in mitochondrial membrane potential that might occur in relation to pathophysiological states, and we have seen little evidence for either process in intact neurons even following prolonged exposure to glutamate. However, using pharmacological approaches we have been able to demonstrate the presence of the mitochondrial Na^{+}-Ca^{2+} exchanger and the impact of mitochondrial Ca^{2+} release on cytosolic Ca^{2+} concentrations. For example, when mitochondria are loaded with Ca^{2+} following the exposure of neurons to a relatively high glutamate concentration the resulting recovery of $[Ca^{2+}]_i$ to baseline levels is rather slow. This slow recovery is evidently due to the persistent efflux of mitochondrial Ca^{2+} stores through the Na^{+}-Ca^{2+} exchanger, because inhibiting this process with the diltiazem analogue CGP-37157 rapidly restores $[Ca^{2+}]_i$ to basal values, while removing the inhibitor is associated with a resumption of mitochondrial Ca^{2+} release [43;44]. Similar effects

are also observed in peripheral neurons that show a particularly prominent mitochondrial Ca^{2+} release component following the activation of voltage-gated Ca^{2+} channels [45]. Although CGP-37157 does have other pharmacological effects, such as the inhibition of voltage-gated Ca^{2+} channels [45], it rapidly and reversibly inhibits mitochondrial Ca^{2+} efflux in intact neurons and as such appears to be one of the more useful agents currently available to manipulate mitochondrial Ca^{2+} signaling.

In the experiments reported here we investigated the notion that by blocking what may be the major mitochondrial Ca^{2+} efflux pathway we could potentiate glutamate-stimulated, Ca^{2+}-mediated alterations in mitochondrial function. We examined the effects of CGP-37157 on several different aspects of mitochondrial physiology, including ROS generation, intracellular acidification, and excitotoxic neuronal injury, anticipating that CGP-37157 would increase mitochondrial Ca^{2+} accumulation and thereby potentiate glutamate-induced neuronal death.

MATERIALS AND METHODS

Cell Culture- Primary neuronal cultures were obtained from the forebrains of embryonic day 17 Sprague-Dawley rats and dissociated as previously described [46]. Animals were handled in accordance with the National Institutes of Health Guide for the Care and Use of Laboratory Animals and with the Institutional Animal Care and Use Committee of the University of Pittsburgh. Briefly, the cortical lobes were incubated in 0.005-0.01% trypsin in Ca^{2+}-free, Mg^{2+}-free media (in mM: 116 NaCl, 5.4 KCl, 26.2 $NaHCO_3$, 11.7 NaH_2PO_4, 5 glucose, 0.001% Phenol Red, and minimum essential media amino acids; pH adjusted to 7.4 with NaOH) for 30 minutes at 37°C. Viability determinations were made with the trypan blue (0.08%) exclusion method. The plating suspension was diluted to 300,000 cell/ml using plating medium (v/v solution of 90% Dulbecco's modified Eagle's medium, 10% heat-inactivated fetal bovine serum, 24 U/ml penicillin, 24 μg/ml streptomycin; final glutamine concentration 3.1 mM). Cells were plated onto poly-L-lysine-coated (40 μg/ml) 31mm glass coverslips that were inverted one day later in a maintenance medium (horse serum substituted for fetal calf serum, all other constituents identical). Inversion of the coverslips prevents glial proliferation. Cells were maintained under 95% air, 5% CO_2 until use two weeks later. Only those coverslips containing healthy neurons (rounded-oval, smooth, and bright cell bodies when viewed using phase-contrast optics) were used. On the day of experimentation, culture medium was removed and replaced with HEPES-buffered salt solution (HBSS) of the following composition (mM): 137 NaCl, 5 KCl, 0.9 $MgSO_4$, 1.4 $CaCl_2$, 3 $NaHCO_3$, 0.6 Na_2HPO_4, 0.4 KH_2PO_4, 5.6 glucose, and 20 HEPES; adjusted to pH 7.4 with NaOH.

Intracellular ROS Production- ROS production was measured by fluorescence

microscopy using the oxidation sensitive dyes, 2,7-dichlorodihydrofluorescein ($DCFH_2$) or dihydroethidium (DHE) [29;31] as previously described [47]. Fluorescence was recorded using a Meridian ACAS 570c laser scanning confocal imaging system. A 488 nm excitation line from an argon laser was used in conjunction with a 510 nm dichroic mirror and focused through a 225 μm pinhole and a 40x phase-contrast objective to yield an optical slice of about 2.5 μm through the middle of the neurons (≈20 μm in diameter).

Forebrain neurons that were two weeks in culture were loaded with 10 μM $DCFH_2$ or 2 μM DHE for 15 min. at 37°C in HBSS supplemented with 5 mg/ml bovine serum albumin. 4 mM stocks of $DCFH_2$ or DHE were made in methanol or anhydrous DMSO, respectively. $DCFH_2$ was removed just prior to imaging whereas DHE was maintained in solution throughout the experiment. Fluorescence was recorded at room temperature from a single field of cells (180 x 180 μm) per coverslip typically containing 5-15 neurons. Cells were imaged over a period of 15 min. at 1 scan per min. After obtaining 2 min. of basal fluorescence, cells were exposed to various treatments for a period of 10-15 min. Fluorescence was normalized to the intensity measured in the first scan to account for problems in equal dye loading. Data was presented for each test condition as the change in normalized fluorescence (mean ± SEM) over time (minutes). All experiments were performed on at least two coverslips from no less than two different culture dates. Cells displaying localized increases in DCF fluorescence were determined visually by an observer blinded to the treatment.

Measurement of Intracellular pH- Fluorescence imaging, as previously described [26], was performed on a Nikon Diaphot 300 microscope fitted with a 40x quartz objective, a Dage-MTI cooled-CCD camera with 640 x 480-pixel resolution in combination with a Dage-MTI Gen

II Sys image intensifier and a 75 watt Xenon lamp-based monochromator light source. Attenuation of incident light was achieved with a 0.1% neutral density filter and passed through a 515nm dichroic mirror. Emitted fluorescence was measured with a 535 ± 12.5nm band-pass filter after alternate excitation at 498nm and 450nm. Data acquisition analysis was controlled using Simple PCI software (Compix, Cranberry, PA). Forebrain neurons (2 weeks in culture) were incubated for 15 min. at 37°C with 2',7'-bis-(2-carboxyethyl)-5(and 6)-carboxyfluorescein (BCECF) (5 μM) in HBSS supplemented with 5mg/ml BSA. After loading, coverslips were rinsed with HBSS, mounted in a recording chamber and perfused with HBSS at a rate of 20 ml/min. Cells were exposed to various treatments for a period of 5min. After approximately 10 min of recovery in normal HBSS, cells were exposed to 25 mM NH_4Cl for 1 min as a positive control. Fluorescence was recorded at room temperature and background fluorescence values (determined from cell-free regions of each coverslip) were subtracted from all signals.

Toxicity Assay- Forebrain neurons (2 weeks in culture) were rinsed twice with HBSS, and coverslips were inverted to orient the cultured neurons face-up. Neurons were exposed to various treatments for a period of 5 min and then rinsed with HBSS. Cells were placed in Minimum Essential Medium containing penicillin(24 U/ml) and streptomycin (24 μg/ml) and allowed to incubate for 20-24hr at 37°C. Neuronal viability was then assessed with a trypan blue (0.4%) exclusion method as previously described [26]. Data is presented as the mean number of live cells from three experiments in which three fields, from each of three coverslips, were counted by an observer blinded to the treatment condition.

Determination of Intracellular ATP- Forebrain neurons (2 weeks in culture) were rinsed twice with HBSS and coverslips were inverted to orient the cultured neurons face-up. Neurons

were exposed to various treatments for a period of 10min and then rinsed with ice-cold PBS. Cellular ATP was extracted from 3 coverslips per condition in 400μL of 0.5% TCA/125 μM EDTA using a disposable cell scraper. Extracts were centrifuged at 13,800 g for 5min at 37°C. For each condition, 300μL of supernatant was added to 120μL of 0.1 M Tris and kept on ice throughout the experiment. ATP content was measured using a Luciferin-Luciferase Assay (Molecular Probes, Eugene, Oregon) with a scintillation counter (Beckman LS 1801) to detect luminescence. Sample [ATP] was determined using nonlinear regression analysis of the ATP Standard Curve. Data is presented as the percent of controls (mean ± SEM) from 3 separate experiments using two different cell culture dates.

Measurement of $[Ca^{2+}]_i$ - The acetoxy methyl ester form of Magfura-2 (Molecular Probes, Oregon) was diluted to 1 mM in anhydrous DMSO. Coverslips were incubated in HBSS containing 5μM of Magfura-2, 0.5% of DMSO and 5mg/ml of bovine serum albumin for 20 minutes at 37°C. Cells were then rinsed with HBSS, mounted on a record chamber and perfused with HBSS at a rate of 20ml/min. All recordings were made at room temperature.

The imaging system consisted of a Nikon Diaphot 300 inverted microscope fitted with a 40x objective, a digital Orca camera (Hamamatsu Corporation, New Jersey) and a 75 Watt Xenon lamp-based monochromator light source as previously described [10]. Cells were alternately illuminated with 335 nm and 375 nm beams. Incident light was attenuated with neutral density filters (typically by about 90%; Omega Optical, Vermont) and emitted fluorescence passed through a 515-nm dichroic mirror and a 535 ± 12.5 nm band-pass filter (Omega Optical, Vermont). Background fluorescence, determined from three cell-free regions of the coverslips, was subtracted from all the signals prior to calculating the ratios as described.

Materials- CGP-37157 (7-chloro-3,5-dihydro-5-phenyl-1H-4,1-benzothiazepine-2-on) was a generous gift from Ciba-Geigy Pharmaceuticals (Basel, Switzerland) and was also purchased from Tocris Cookson Inc. (Missouri). Stock solutions of CGP-37157 were prepared using anhydrous dimethyl sulfoxide and further diluted in HBSS. All fluorescent indicators were purchased from Molecular Probes (Eugene, Oregon).

Statistical Analysis- Statistical significance between groups of three or more experimental conditions was determined by One-way analysis of variance (ANOVA) followed with a Bonferroni post-hoc analysis using Prism v3.0 (GraphPad Software, San Diego CA). Statistical significance between two groups was determined using a two-tailed, unpaired t-test.

RESULTS

Effects of CGP-37157 on Production of ROS. Several studies have demonstrated a Ca^{2+}-dependent production of ROS via the mitochondria following a glutamate stimulus [29-31]. If one can speculate that blocking Ca^{2+} entry into the mitochondria may potentially inhibit glutamate-induced ROS production, then along the same line of reasoning blocking Ca^{2+} efflux may enhance mitochondrial ROS generation. Thus, we studied the impact of the Na^{+}/Ca^{2+} exchange inhibitor on the fluorescence of two oxidation sensitive indicators in the presence or absence of glutamate or an exogenous oxidant.

In this model system glutamate induced a 3-fold increase in DHE fluorescence (Fig. 1A). Interestingly, hydrogen peroxide produced a somewhat smaller oxidation of DHE compared to glutamate (Fig. 1B). DHE fluorescence after exposure to CGP-37157 was similar to controls (Fig. 1A&B). In addition, CGP-37157 did not alter glutamate or hydrogen peroxide induced increases in DHE fluorescence (Fig. 1A&B).

Both CGP-37157 and glutamate decreased DCF fluorescence to a similar extent (Fig. 1C). This effect was enhanced when the two stimuli were applied together (Fig. 1C). Glutamate but not CGP-37157 produces localized increases in intracellular DCF fluorescence (Fig. 2). We used a cell counting method to assess DCF oxidation responses, as we have previously described [29]. The number of cells displaying glutamate-induced increases in localized fluorescence was reduced by 73% when CGP-37157 is applied with glutamate ($t=5.23$; $p<0.0008$; Fig. 2). In these experiments we used hydrogen peroxide (3mM) as a positive control, and this stimulus induced a 2-2.5-fold increase in DCF fluorescence which was not affected by the addition of CGP-37157 (Fig. 1D).

CGP-37157 Produces Decreases in Intracellular pH. Glutamate will quench DCF fluorescence due to intracellular acidification [29]. Thus we wanted to determine if CGP-37157 decreases DCF fluorescence due to a similar mechanism using the pH sensitive indicator BCECF, which is not sensitive to ROS. CGP-37157 produces a slight and reversible decrease in intracellular pH (Fig. 3). The intracellular acidification induced by glutamate is much greater than the effect of CGP-37157. However, the intracellular acidification produced by glutamate is not altered by the addition of CGP-37157 (Fig. 3).

Blocking Mitochondrial Na^+/Ca^{2+} exchange Does Not Affect Cellular ATP Content. Ca^{2+} may act as a second messenger to stimulate ATP production. Mitochondrial Ca^{2+} can stimulate several key enzymes involved in cellular respiration [48]. Previous studies have shown that CGP-37157 will increase the $\Delta\psi_m$ possibly as a result of enhanced mitochondrial activity [32]. Mitochondrial Ca^{2+} cycling following glutamate exposure uncouples oxidative respiration from ATP production. Thus, inhibition of mitochondrial Ca^{2+} cycling and enhancement of the mitochondrial Ca^{2+} load with CGP-37157 may enhance ATP production or inhibit decreases due to glutamate. A 5min exposure to 100 μM glutamate and 1 μM glycine did not significantly decrease the ATP levels compared to controls (Fig 4) similar to a 5min exposure to 750 nM FCCP (Fig. 4). CGP-37157 in the presence or absence of glutamate did not alter cellular ATP content (Fig. 4).

Effects of CGP-37157 on Glutamate-Induced Neuronal Viability. Excessive mitochondrial Ca^{2+} cycling following glutamate exposure can lead to mitochondrial depolarization and bioenergetic failure and may contribute to neuronal death. As a result of inhibiting Ca^{2+} cycling CGP-37157 may be neuroprotective following an excitotoxic glutamate

stimulus. However, recent studies have demonstrated that inhibition of mitochondrial Ca^{2+} uptake is neuroprotective against glutamate excitotoxicity [25;26]. Also, mitochondrial Ca^{2+} can stimulate opening of the PTP. It is possible that enhancing mitochondrial Ca^{2+} loads with CGP-37157 could increase toxicity following a glutamate stimulus. Thus, we examined the effects of the Na^{+}/Ca^{2+} exchange inhibitor on glutamate-induced neurotoxicity. Our results show that a 5min exposure to 100μM glutamate/ 1μM glycine typically produces a 40% loss in viable neurons as compared to cells exposed to buffer changes alone (Fig 5). CGP-37157 does not alter neuronal viability. Glutamate and the combination of glutamate and CGP-37157 significantly decrease cell viability compared to controls ($P<0.01$). However, these two conditions are not significantly different from each other.

Effects of CGP-37157 on glutamate-induced changes in $[Ca^{2+}]_i$ and mitochondrial Ca^{2+}. The relative lack of effect of CGP-37157 on mitochondrial function and glutamate-induced changes in mitochondrial function led us to examine the effects of Na^{+}/Ca^{2+}-exchange inhibition on glutamate-induced changes in $[Ca^{2+}]_i$ and mitochondrial Ca^{2+} loads. We have recently demonstrated the feasibility of estimating matrix Ca^{2+} by using FCCP to release mitochondrial Ca^{2+} and MagFura-2 to measure the $[Ca^{2+}]_i$ after this procedure (Figure 6A, [49]).

A 5min exposure to 100 μM glutamate and 1 μM glycine increases $[Ca^{2+}]_i$ as measured with Magfura-2 (Fig. 6D grey bar; glutamate). However, this may not indicate the full extent of Ca^{2+} influx following glutamate-receptor activation as the mitochondria are simultaneously buffering $[Ca^{2+}]_i$ (Figure 6A). Thus, we used 750 nM FCCP to release accumulated mitochondrial Ca^{2+} following glutamate stimulation (Fig. 6D grey bar; FCCP). FCCP is applied in Ca^{2+}-free HBSS to ensure that Ca^{2+} entry is not occurring via voltage-sensitive Ca^{2+} channels

as a result of FCCP-induced depolarization of the plasma membrane. The application of CGP-37157 during the 5min glutamate stimulus had no significant effect on measurable $[Ca^{2+}]_i$ levels (Fig. 6D black bar; Glutamate). Surprisingly, inhibition of the Na^+/Ca^{2+} exchanger only produced a slight enhancement of accumulated mitochondrial Ca^{2+} (Fig. 6D black bar; FCCP). Although the use of the low affinity Ca^{2+} indicator MagFura-2 in these experiments makes it unlikely that dye saturation occurred during these experiments, this is a possible explanation for the failure of CGP-37157 to enhance glutamate-induced mitochondrial Ca^{2+} accumulation. To exclude this possibility we also monitored the effects of CGP-37157 using the same paradigm but with lower glutamate concentrations which result in reduced cytoplasmic and mitochondrial Ca^{2+} accumulation (Figures 6B,C). However, although an increase in mitochondrial Ca^{2+} might be expected in the presence of CGP-37157 we actually observed a decrease in cytosolic and mitochondrial Ca^{2+} under these conditions..

DISCUSSION

In this study we have explored the effect of the mitochondrial Na^+/Ca^{2+}-exchange inhibitor CGP-37157 on glutamate-stimulated, NMDA receptor-mediated changes in mitochondrial function in central neurons. Our anticipation in approaching these experiments was that CGP-37157 would increase matrix Ca^{2+} concentrations and thereby potentiate the glutamate stimulated changes in function. What is quite obvious from the present experiments is that this is not at all the case.

The oxidation sensitive dyes DCF and DHE are able to report several phenomena associated with glutamate receptor activation. DHE is preferentially oxidized by superoxide [31] but may also report alterations in mitochondrial membrane potential [50]. However, CGP-37157 did not potentiate the DHE signal. That it did not alter the effects of peroxide on DHE fluorescence argues that the apparent lack of effect is not due to some non-specific effect on the dye or that it has antioxidant properties (Figure 1B). DCF is sensitive to the formation of ROS and is also quenched by intracellular acidification [29]. The CGP-37157-induced decrease in DCF may be consistent with intracellular acidification, as is the potentiation of the effects of glutamate (although see below). Detecting an increase in oxidation of DCF can be somewhat problematic with the marked decrease in signal that occurs with acidification. However counting the cells that show the characteristic localized increases in fluorescence circumvents this problem [29]. Once again, these results are not consistent with enhancement of the accumulation of matrix calcium.

Increases in matrix Ca^{2+} stimulates Ca^{2+}-sensitive, rate-limiting dehydrogenases involved

in metabolism, and thus couples increased energy demand signaled by an elevation in $[Ca^{2+}]_i$ to the aerobic production of ATP [48]. This should have several consequences for the neurons stimulated by glutamate. Enhanced metabolic activation has been proposed to account for the well-documented intracellular acidification associated with NMDA receptor activation and Ca^{2+} influx [51-53], and this would be consistent with the increased quenching of DCF shown in figure 1B. However, an authentic pH indicator, BCECF, showed relatively little effect either of CGP-37157 alone or in combination with glutamate (Figure 3). In addition, mitochondrial Na^+/Ca^{2+} exchange occurs at the expense of ATP generation [40;53], so that inhibition of this process should at least prevent ATP loss. However, increases in the $\Delta\psi_m$ can also result from ATP hydrolysis in an effort to maintain or restore $\Delta\psi_m$ [19;54] and may alternatively explain the hyperpolarization induced by CGP-37157 our neuronal cultures. Surprisingly, CGP-37157 had no effect on cellular ATP levels, compared to controls, in the presence or absence of glutamate (Fig. 4). One could speculate that the lack of change in cellular ATP levels in our culture system is because of a greater dependence on glycolytic ATP production than on oxidative phosphorylation as seen in cultured cerebellar granule cells [19;25], but again it is difficult to relate these observations simply to enhanced matrix Ca^{2+} accumulation. The ultimate question with respect to glutamate-induced alterations in mitochondrial function is the impact of CGP-37157 on neuronal viability, and CGP-37157 evidently has no beneficial or detrimental effect (Figure 5) on the viability of neurons in the absence or presence of glutamate. Thus, although mitochondrial uptake of Ca^{2+} during excitotoxicity is clearly detrimental to cell viability [25;26], CGP-37157 clearly does not have a substantial impact on this process.

This raises the question of whether CGP-37157 has any effect on matrix Ca^{2+} content at

all. This has been a difficult question to address experimentally for a variety of reasons. In the kinds of experimental approach used here, several laboratories have used the Ca^{2+} indicator rhod-2 to estimate matrix Ca^{2+} changes [55-60]. This is clearly an effective approach provided that the dye can be localized to the mitochondrial matrix rather than any other cellular compartment, and also provided that the matrix Ca^{2+} concentrations do not exceed the dynamic range of the dye. Indeed, some of the other reports in this volume elegantly demonstrate the use of this approach. However, under conditions of excitotoxicity it is likely that matrix Ca^{2+} greatly exceeds the limit of sensitivity of this dye (~5μM, based on an affinity of about 500nM). Thus, although it is possible to load the dye into mitochondria in neurons and to monitor changes in matrix Ca^{2+} [59-61] it is not clear that the dye faithfully reports the full extent of the Ca^{2+} change.

We recently developed an alternative approach to determining mitochondrial Ca^{2+} content following glutamate exposure [49]. This approach takes advantage of the reversibility of the Ca^{2+} uniporter [13]. Thus, following exposure of neurons to glutamate the cells are exposed to FCCP which collapses the mitochondrial membrane potential and releases Ca^{2+} into the matrix, presumably by the reversal of the uniporter. A low affinity Ca^{2+} indicator (MagFura-2 in this case) can then be used to report the Ca^{2+} changes, and provide a semiquantitative insight into the Ca^{2+} contents of the mitochondria.

Using this approach we were thus able to monitor the Ca^{2+} loading of mitochondria following glutamate exposure in the absence or presence of CGP-37157 (Figure 6). Rather surprisingly, CGP-37157 had little effect on the matrix Ca^{2+} content under the conditions employed for most of the studies reported here (i.e. 100μM glutamate for 5 minutes). To ensure that the failure to observe an effect of CGP-37157 was not due to dye saturation, or to the

possibility that mitochondria are overwhelmed with the Ca^{2+} load caused by this toxic stimulus we also tried lower glutamate concentration, but also failed to see an effect of CGP-37157 beyond a small inhibition of the glutamate triggered Ca^{2+} entry, which may be a consequence of the Ca^{2+} channel inhibition produced by this drug.

It is not at all clear how to account for the lack of effect of a drug that, under some circumstances at least, has a substantial effect on the egress of Ca^{2+} from neuronal mitochondria [43;45;62]. Although the failure to increase matrix Ca^{2+} accounts for the lack of effect of CGP-37157 on ROS generation, ATP depletion or synthesis and neuronal viability, it is not obvious why Ca^{2+} was not increased. Perhaps the most obvious suggestion is that the major Ca^{2+} efflux pathway in effect during glutamate exposure is not, in fact, the Na^+-Ca^{2+} exchanger. Based on the observations of the effects of FCCP it is clear that a loss of $\Delta\psi_m$ can result in release of Ca^{2+} from mitochondria, presumably via reversal of the uniporter. We know that at least some of the neurons will exhibit mitochondrial depolarization during glutamate exposure [32] which might result in Ca^{2+} release. Activation of the permeability transition pore would also result in Ca^{2+} release that is insensitive to CGP-37157, although evidence for the activation of this process during glutamate stimulation is less than robust. Most tissues also have a Na^+-independent mitochondrial Ca^{2+} efflux pathway [40]. Although the Na^+-Ca^{2+} exchanger is considered to be the dominant mechanism in brain, it is perhaps possible that the Na^+-independent pathway is more active in our neurons under the circumstances of Na^+-Ca^{2+} exchanger inhibition. A more trivial explanation of such observations would be that CGP-37157 blocks NMDA receptors at the concentrations used. We have no evidence for such an effect at this point (and this would certainly not account for its ability to alter mitochondrial Ca^{2+} efflux previously reported) but this

remains an issue with all pharmacological approaches to studying physiological function.

More broadly, the difficulties in interpreting what should be a straightforward set of results illustrate the problems encountered with the pharmacological manipulation of mitochondrial Ca^{2+} transport. The drugs that inhibit the main mitochondrial influx pathways do not penetrate cells well (Ru360), are not very specific for the uniporter (ruthenium red) and do not very clearly distinguish between the different modes of Ca^{2+} uptake [36]. Assuming that the Na^{+}-Ca^{2+} exchanger is the main efflux pathway, an apparently specific and effective inhibitor does not at all have the anticipated effect, as reported here. This leaves one with the option of manipulating these processes indirectly, such as by the use of FCCP or by inhibition of electron transport to manipulate membrane potential. However, these approaches cannot be considered specific either, and the other actions of FCCP, for example, are well recognized [63]. Thus, investigating mitochondrial Ca^{2+} transport in intact cells using pharmacological approaches remains quite problematic.

Acknowledgments.

These studies were supported by USAMRMC grant DAMD17-98-1-8627 and by NIH grant NS 34138 (IJR). JBB was supported by a Long-Term Fellowship from the Human Frontiers Science Program (LT0500/1999B).

REFERENCES

1. Mayer ML, Westbrook GL. Cellular mechanisms underlying excitotoxicity. *Trends Neurosci* 1987; **10:** 59-61.

2. Choi DW. Glutamate neurotoxicity and diseases of the nervous system. *Neuron* 1988; **1:** 623-634.

3. Choi DW, Maulucci-Gedde M, Kriegstein AR. Glutamate neurotoxicity in cortical cell culture. *J Neurosci* 1987; **7:** 357-368.

4. Choi DW. Ionic dependence of glutamate neurotoxicity. *J Neurosci* 1987; **7:** 369-379.

5. Ankarcrona M, Dypbukt JM, Bonfoco E et al. Glutamate-induced neuronal death: a succession of necrosis or apoptosis depending on mitochondrial function. *Neuron* 1995; **15:** 961-973.

6. Koh JY, Goldberg MP, Hartley DM, Choi DW. Non-NMDA receptor mediated neurotoxicity in cortical culture. *J Neurosci* 1990; **10:** 693-705.

7. Kristián T, Ouyang Y, Siesjö BK. Calcium-induced neuronal cell death in vivo and in vitro: Are the pathophysiologic mechanisms different? *Adv Neurol* 1996; **71:** 107-118.

8. Doble A. The role of excitotoxicity in neurodegenerative disease: Implications for therapy. *Pharmacol Ther* 1999; **81:** 163-221.

9. Hyrc K, Handran SD, Rothman SM, Goldberg MP. Ionized intracellular calcium concentration predicts excitotoxic neuronal death: observations with low affinity fluorescent calcium indicators. *J Neurosci* 1997; **17:** 6669-6677.

10. Stout AK, Reynolds IJ. High-affinity calcium indicators underestimate increases in intracellular calcium concentrations associated with excitotoxic glutamate stimulations. *Neuroscience* 1999; **89:** 91-100.

11. Sattler R, Xiong Z, Lu WY, Hafner M, MacDonald JF, Tymianski M. Specific coupling of NMDA receptor activation to nitric oxide neurotoxicity by PSD-95 protein. *Science* 1999; **284:** 1845-1848.

12. Nicholls DG, Akerman KEO. Mitochondrial calcium transport. *Biochim Biophys Acta* 1982; **683:** 57-88.

13. Gunter TE, Pfeiffer DR. Mechanisms by which mitochondria transport calcium. *Am J Physiol Cell Physiol* 1990; **258:** C755-C786.

14. Babcock DF, Hille B. Mitochondrial oversight of cellular Ca^{2+} signaling. *Curr Opin Neurobiol* 1998; **8:** 398-404.

15. Duchen MR. Ca^{2+}-dependent changes in the mitochondrial energetics in single dissociated mouse sensory neurons. *Biochem J* 1992; **283:** 41-50.

16. Friel DD, Tsien RW. An FCCP-sensitive Ca^{2+} store in bullfrog sympathetic neurons and its participation in stimulus-evoked changes in $[Ca^{2+}]_i$. *J Neurosci* 1994; **14:** 4007-4024.

17. Werth JL, Thayer SA. Mitochondria buffer physiological calcium loads in cultured rat dorsal root ganglion neurons. *J Neurosci* 1994; **14:** 348-356.

18. Kiedrowski L, Costa E. Glutamate-induced destabilization of intracellular calcium concentration homeostasis in cultured cerebellar granule cells: role of mitochondria in calcium buffering. *Mol Pharmacol* 1995; **47:** 140-147.

19. Budd SL, Nicholls DG. A reevaluation of the role of mitochondria in neuronal Ca^{2+} homeostasis. *J Neurochem* 1996; **66:** 403-411.

20. Khodorov B, Pinelis V, Storozhevykh T, Vergun O, Vinskaya N. Dominant role of mitochondria in protection against a delayed neuronal Ca^{2+} overload induced by endogenous excitatory amino acids following a glutamate pulse. *FEBS Lett* 1996; **393:** 135-138.

21. Wang GJ, Thayer SA. Sequestration of glutamate-induced Ca^{2+} loads by mitochondria in cultured rat hippocampal neurons. *J Neurophysiol* 1996; **76:** 1611-1621.

22. Brorson JR, Sulit RA, Zhang H. Nitric oxide disrupts Ca^{2+} homeostasis in hippocampal neurons. *J Neurochem* 1997; **68:** 95-105.

23. Murchison D, Griffith WH. Age-related alterations in caffeine-sensitive calcium stores and mitochondrial buffering in rat basal forebrain. *Cell Calcium* 1999; **25:** 439-452.

24. Pivovarova NB, Hongpaisan J, Andrews SB, Friel DD. Depolarization-induced mitochondrial Ca accumulation in sympathetic neurons: spatial and temporal

characteristics. *J Neurosci* 1999; **19:** 6372-6384.

25. Budd SL, Nicholls DG. Mitochondria, calcium regulation and acute glutamate excitotoxicity in cultured cerebellar granule cells. *J Neurochem* 1996; **67:** 2282-2291.

26. Stout AK, Raphael HM, Kanterewicz BI, Klann E, Reynolds IJ. Glutamate-induced neuron death requires mitochondrial calcium uptake. *Nature Neurosci* 1998; **1:** 366-373.

27. Lafon-Cazal M, Pietri S, Culcasi M, Bockaert J. NMDA-dependent superoxide production and neurotoxicity. *Nature* 1993; **364:** 535-537.

28. Dykens JA. Isolated cerebral and cerebellar mitochondria produce free radicals when exposed to elevated Ca^{2+} and Na^{+}: implications for neurodegeneration. *J Neurochem* 1994; **63:** 584-591.

29. Reynolds IJ, Hastings TG. Glutamate induces the production of reactive oxygen species in cultured forebrain neurons following NMDA receptor activation. *J Neurosci* 1995; **15:** 3318-3327.

30. Dugan LL, Sensi SL, Canzoniero LMT et al. Mitochondrial production of reactive oxygen species in cortical neurons following exposure to N-methyl-D-aspartate. *J Neurosci* 1995; **15:** 6377-6388.

31. Bindokas VP, Jordan J, Lee CC, Miller RJ. Superoxide production in rat hippocampal neurons: selective imaging with hydroethidine. *J Neurosci* 1996; **16:** 1324-1336.

32. White RJ, Reynolds IJ. Mitochondrial depolarization in glutamate-stimulated neurons: An early signal specific to excitotoxin exposure. *J Neurosci* 1996; **16:** 5688-5697.

33. Schinder AF, Olson EC, Spitzer NC, Montal M. Mitochondrial dysfunction is a primary event in glutamate neurotoxicity. *J Neurosci* 1996; **16:** 6125-6133.

34. Nieminen A-L, Petrie TG, Lemasters JJ, Selman WR. Cyclosporin A delays mitochondrial depolarization induced by N-methyl-D-aspartate in cortical neurons: evidence of the mitochodrial permeability transition. *Neuroscience* 1996; **75:** 993-997.

35. Sparagna GC, Gunter KK, Sheu S-S, Gunter TE. Mitochondrial calcium uptake from physiological-type pulses of calcium. A description of the rapid uptake mode. *J Biol Chem* 1996; **270:** 27510-27515.

36. Gunter TE, Buntinas L, Sparagna GC, Gunter KK. The Ca^{2+} transport mechanisms of mitochondria and Ca^{2+} uptake from physiological type calcium transients. *Biochim Biophys Acta* 1998; **1366:** 5-15.

37. Matlib MA, Zhou Z, Knight S et al. Oxygen-bridged dinuclear ruthenium amine complex specifically inhibits Ca^{2+} uptake into mitochondria *in vitro* and *in situ* in single cardiac myocytes. *J Biol Chem* 1998; **273:** 10223-10231.

38. Crompton M, Andreeva L. On the interactions of Ca^{2+} and cyclosporin A with a mitochondrial inner membrane pore: a study using cobaltammine complex inhibitors of the Ca^{2+} uniporter. *Biochem J* 1994; **302:** 181-185.

39. Griffiths EJ. Reversal of mitochondrial Na Ca exchange during metabolic inhibition in rat cardiomyocytes. *FEBS Lett* 1999; **453:** 400-404.

40. Gunter TE, Gunter KK, Sheu S-S, Gavin CE. Mitochondrial calcium transport: Physiological and pathological relevance. *Am J Physiol Cell Physiol* 1994; **267:** C313-C339.

41. Fiskum G, Cockrell RS. Uncoupler-stimulated release of Ca^{2+} from Ehrlich ascites tumor cell mitochondria. *Arch Biochem Biophys* 1985; **240:** 723-733.

42. Zoratti M, Szabo I. The mitochondrial permeability transition. *Biochim Biophys Acta* 1995; **1241:** 139-176.

43. White RJ, Reynolds IJ. Mitochondria accumulate Ca^{2+} following intense glutamate stimulation of cultured rat forebrain neurones. *J Physiol (Lond)* 1997; **498:** 31-47.

44. Hoyt KR, Stout AK, Cardman JM, Reynolds IJ. An evaluation of intracellular sodium and mitochondria in the buffering of kainate-induced intracellular free calcium changes in rat forebrain neurons. *J Physiol (Lond)* 1998; **509:** 103-116.

45. Baron KT, Thayer SA. CGP 37157 modulates mitochondrial Ca^{2+} homeostasis in cultured rat dorsal root ganglion neurons. *Eur J Pharmacol* 1997; **340:** 295-300.

46. White RJ, Reynolds IJ. Mitochondria and Na^{+}/Ca^{2+} exchange buffer glutamate-induced calcium loads in cultured cortical neurons. *J Neurosci* 1995; **15:** 1318-1328.

47. Scanlon JM, Reynolds IJ. Effects of oxidants and glutamate receptor activation on mitochondrial membrane potential in rat forebrain neurons. *J Neurochem* 1998; **71:** 2392-2401.

48. McCormack JG, Halestrap AP, Denton RM. Role of calcium ions in regulation of mammalian intramitochondrial metabolism. *Physiol Rev* 1990; **70:** 391-425.

49. Brocard JB, Tassetto M, Reynolds IJ. Quantitative evaluation of mitochondrial calcium content following glutamate receptor stimulation in rat cortical neurones. *J. Physiol (Lond)* 2000; under revision.

50. Budd SL, Castilho RF, Nicholls DG. Mitochondrial membrane potential and hydroethidine-monitored superoxide generation in cultured cerebellar granule cells. *FEBS Lett* 1997; **415:** 21-24.

51. Hartley Z, Dubinsky JM. Changes in intracellular pH associated with glutamate excitotoxicity. *J Neurosci* 1993; **13:** 4690-4699.

52. Irwin RP, Lin S-Z, Long RT, Paul SM. N-methyl-D-aspartate induces a rapid, reversible and calcium dependent intracellular acidosis in cultured fetal rat hippocampal neurons. *J Neurosci* 1994; **14:** 1352-1357.

53. Wang GJ, Randall RD, Thayer SA. Glutamate-induced intracellular acidification of cultured hippocampal neurons demonstrates altered energy metabolism resulting from Ca^{2+} loads. *J Neurophysiol* 1994; **72:** 2563-2569.

54. Di Lisa F, Blank PS, Colonna R et al. Mitochondrial membrane potential in single living adult rat cardiac myocytes exposed to anoxia or metabolic inhibition. *J Physiol (Lond)* 1995; **486:** 1-13.

55. Burnier M, Centeno G, Burki E, Brunner HR. Confocal microscopy to analyze cytosolic and nuclear calcium in cultured vascular cells. *Am J Physiol* 1994; **266:** C1118-C1127.

56. Simpson PB, Russell JT. Mitochondria support inositol 1,4,5-trisphosphate-mediated Ca^{2+} waves in cultured oligodendrocytes. *J Biol Chem* 1996; **271:** 33493-33501.

57. Babcock DF, Herrington J, Goodwin PC, Park YB, Hille B. Mitochondrial participation in the intracellular Ca^{2+} network. *J Cell Biol* 1997; **136:** 833-844.

58. Trollinger DR, Cascio WE, Lemasters JJ. Selective loading of Rhod 2 into mitochondria shows mitochondrial Ca^{2+} transients during the contractile cycle in adult rabbit cardiac myocytes. *Biochem Biophys Res Commun* 1997; **236:** 738-742.

59. David G, Barrett JN, Barrett EF. Evidence that mitochondria buffer physiological Ca^{2+} loads in lizard motor nerve terminals. *J Physiol (Lond)* 1998; **509:** 59-65.

60. Peng TI, Jou MJ, Sheu S-S, Greenamyre JT. Vizualization of NMDA receptor-induced mitochondrial calcium accumulation in striatal neurons. *Exp Neurol* 1998; **149:** 1-12.

61. Peng TI, Greenamyre JT. Privileged access to mitochondria of calcium influx through *N*-methyl-D-aspartate receptors. *Mol Pharmacol* 1998; **53:** 974-980.

62. Zhang YL, Lipton P. Cytosolic Ca^{2+} changes during *in vitro* ischemia in rat hippocampal slices: Major roles for glutamate and Na^{+}-dependent Ca^{2+} release from mitochondria. *J Neurosci* 1999; **19:** 3307-3315.

63. Tretter L, Chinopoulos C, Adam-Vizi V. Plasma membrane depolarization and disturbed Na^{+} homeostasis induced by the protonophore carbonyl cyanide-p-trifluoromethoxyphenyl-hydrazone in isolated nerve terminals. *Mol Pharmacol* 1998; **53:** 734-741.

Figure Legends.

Fig. 1. CGP-37157 Does Not Stimulate Intracellular ROS Generation

Neurons were loaded with 2μM DHE (A & B) or 10μM DCF (C & D) for 15 min at 37°C. After obtaining 2 min. of basal fluorescence, neurons were exposed to various treatments for a period of 10-15 min. (A & C) Data shows the effects of HBSS, 25μM CGP-37157, 100μM glutamate with 1μM glycine, or both. (B & D) Data shows the effects of HBSS, 25μM CGP-37157, 3mM hydrogen peroxide, or both. Points represent the mean ± SEM from 20 to 100 neurons obtained from 2-6 coverslips from no less than 2 culture dates.

Fig.2. CGP-37157 Inhibits Localized ROS Production By Glutamate

Representative images display the effects of 25 μM CGP-37157, 100 μM glutamate with 1 μM glycine, or both on intracellular DCF fluorescence. For each condition neurons are shown at the start of the experiment (3 min prior to exposure), 6 min (3 min after exposure), or 12 min (9 min after exposure) The color scale represents arbitrary fluorescent units. Experiments were repeated on five different coverslips from four different culture dates typically yielding 50-100 cells (N=5). Glutamate produced localized increases in DCF fluorescence in 70.8 % of the cells, whereas CGP-37157 plus glutamate only displayed localized increases in fluorescence in 18.8 % of the cells. Examples of cells that would be scored as positive by the counting approach are identified by white arrows in the panels on the right. These effects were significantly different ($t=5.23$; $p<0.0008$, two-tailed, unpaired t-test).

Fig.3. Effects Of CGP-37157 And Glutamate On Intracellular pH

Neurons were stimulated with 25 μM CGP-37157, 100 μM glutamate with 10 μM glycine, or both for 5min (indicated by the bar). After approximately 10min of recovery in normal HBSS, neurons were exposed to 25mM NH_4Cl for 1 min as a positive control to display the dynamic range of dye response. A decrease in the BCECF ratio indicates a decrease in intracellular pH. Traces represent the mean data from separate coverslips containing 17-25 neurons. Similar results were obtained in cells from two additional culture dates.

Fig. 4. Effects Of CGP-37157 & Glutamate On Cellular ATP Levels.

Neuronal ATP levels are presented as the percent ATP of control values. Neurons were exposed to either HBSS, 750nM FCCP, 25 μM CGP-37157, 100 μM glutamate with 1 μM glycine, or both CGP-37157 and glutamate for 10min prior to extraction of cell lysate. Cell extracts were harvested from 3 coverslips per condition. ATP levels were determined by a luciferase assay system. Data is presented as the percent of control (mean ± SEM) of 3 separate experiments from two different culture dates. None of the conditions were significantly different from control as determined by ANOVA followed by a Bonferroni post-hoc analysis.

Fig. 5. CGP-37157 Does Not Alter Neuronal Death.

Bars represent the mean results from three experiments in which three fields from each of three coverslips were counted for each treatment condition in a blinded manner. On each experimental day coverslips were exposed (in triplicate) for 5min to the following conditions: HBSS, 25 μM CGP-37157, 100 μM glutamate plus 1 μM glycine, or glutamate and CGP-37157. Cells excluding trypan blue were counted. Statistical significance was determined using a one-way ANOVA test followed by Bonferroni post-hoc analysis. *Significantly different ($p<0.01$) compared to control.

Fig. 6. Effects of CGP-37157 on Glutamate-Induced Mitochondrial Ca^{2+} Loading

(A) A representative trace is included to display the experimental paradigm. After 4 minutes of baseline monitoring of MagFura-2 loaded cells, glutamate (30μM) and glycine (1μM), were applied for 5 minutes. Cells were then rinsed with HBSS for 5 min and perfused with FCCP (750nM) for 5 more minutes . The baseline was taken as the ratio preceding the introduction of glutamate in the buffer. The solid line represents the mean of 15 neurons from a single cover slip, while the broken line shows the S.E.M. for these cells. (B-D) Mean data obtained using this paradigm while varying the concentration of glutamate between 3 and 100μM as indicated. Note that the experiments depicted in B and C were performed with 10μM CGP-37157 while the experiment in D used 25μM. Data represents the integrated area under the curve of baseline-subtracted values obtained during exposure to glutamate or to FCCP. Bars represents the mean results from 5-7 coverslips over two or more culture dates. CGP-37157 significantly *decreased* the glutamate-induced cytosolic and mitochondrial Ca^{2+} changes determined using ANOVA (*

indicates significantly different from control, $p < 0.05$).

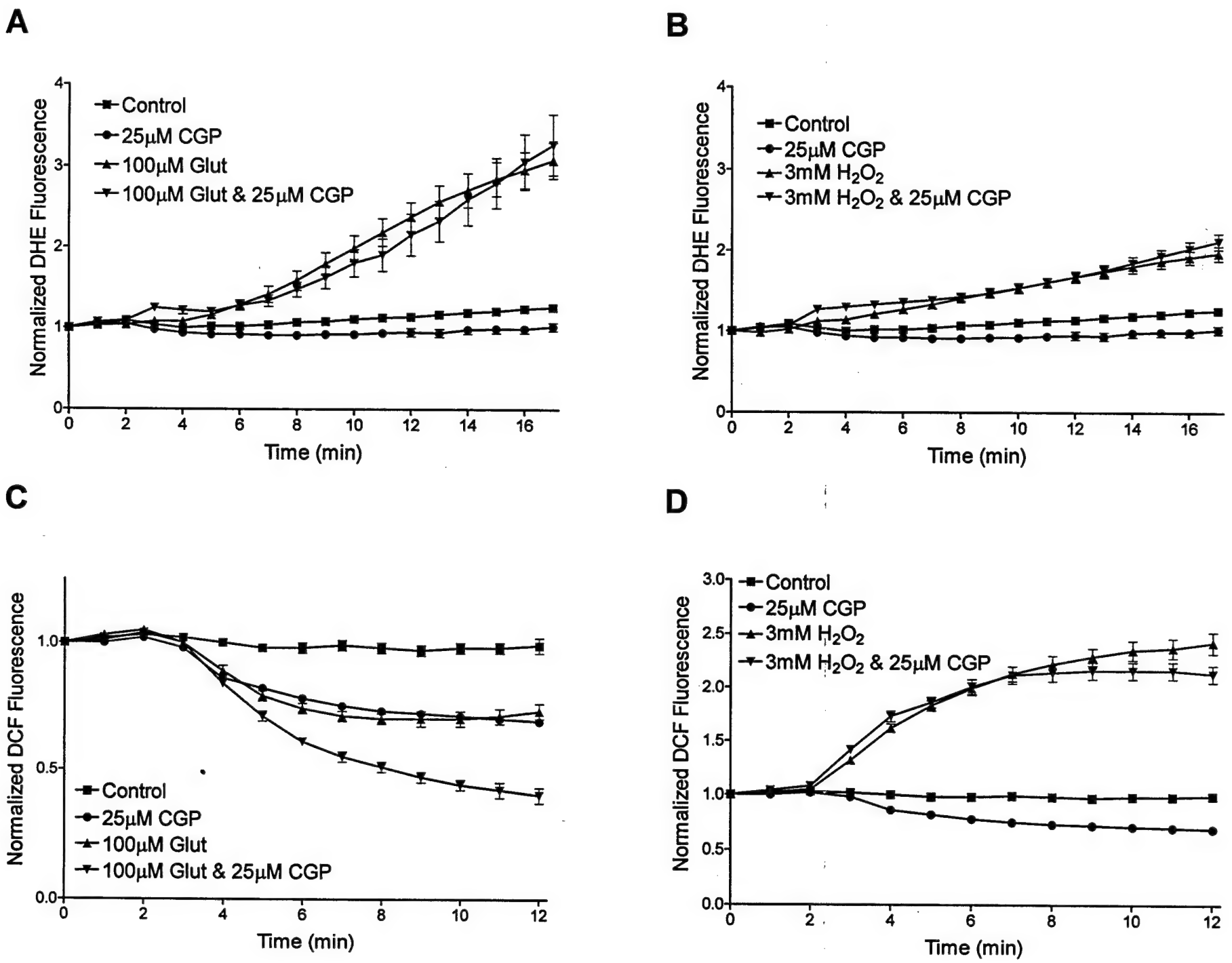
A
Normalized DHE Fluorescence
Control
25μM CGP
100μM Glut
100μM Glut & 25μM CGP
Time (min)
B
Normalized DHE Fluorescence
Control
25μM CGP
3mM H2O2
3mM H2O2 & 25μM CGP
Time (min)
C
Normalized DCF Fluorescence
Control
25μM CGP
100μM Glut
100μM Glut & 25μM CGP
Time (min)
D
Normalized DCF Fluorescence
Control
25μM CGP
3mM H2O2
3mM H2O2 & 25μM CGP
Time (min)

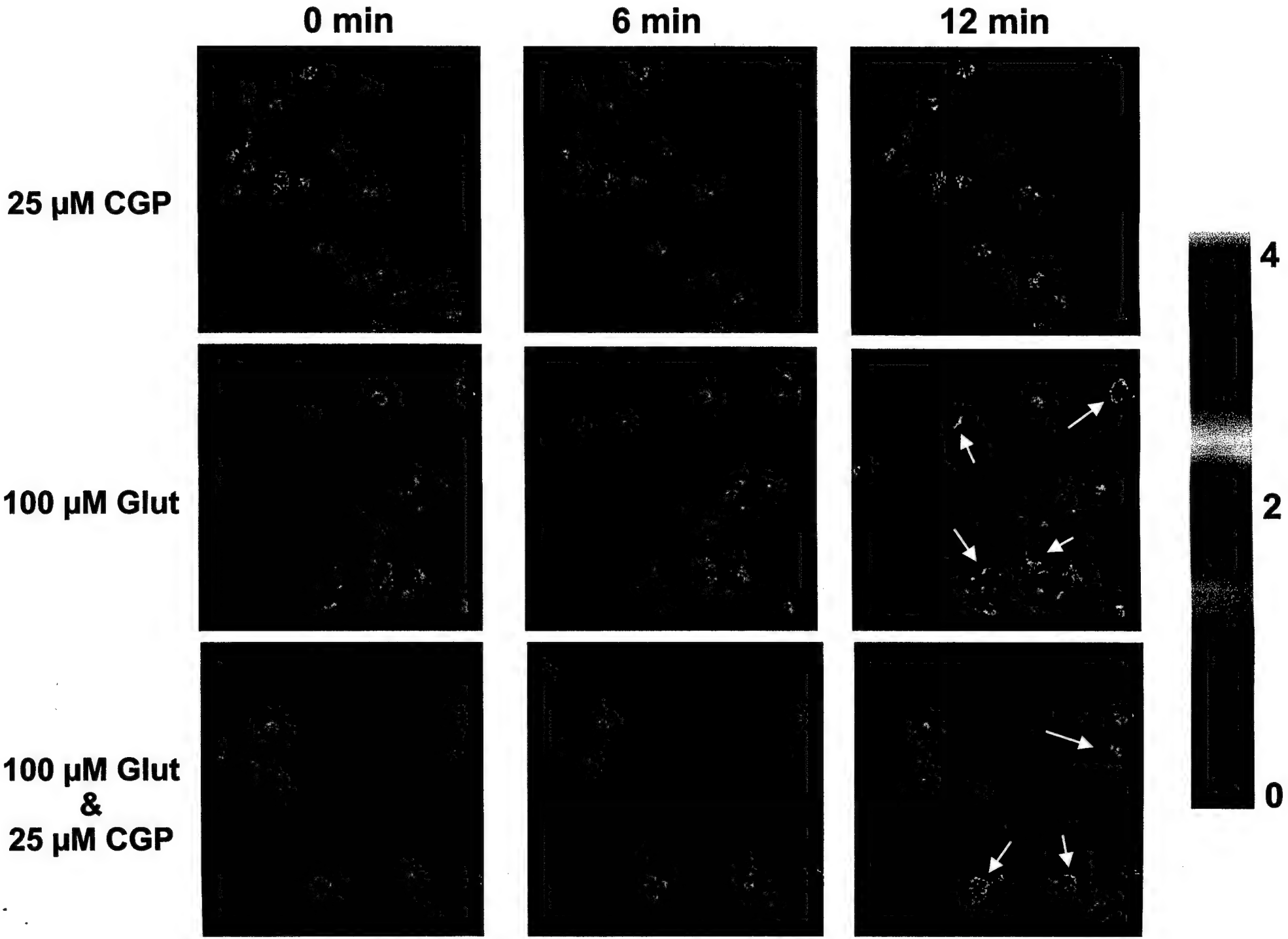
0 min
6 min
12 min
25 µM CGP
100 µM Glut
100 µM Glut
&
25 µM CGP
4
2
0

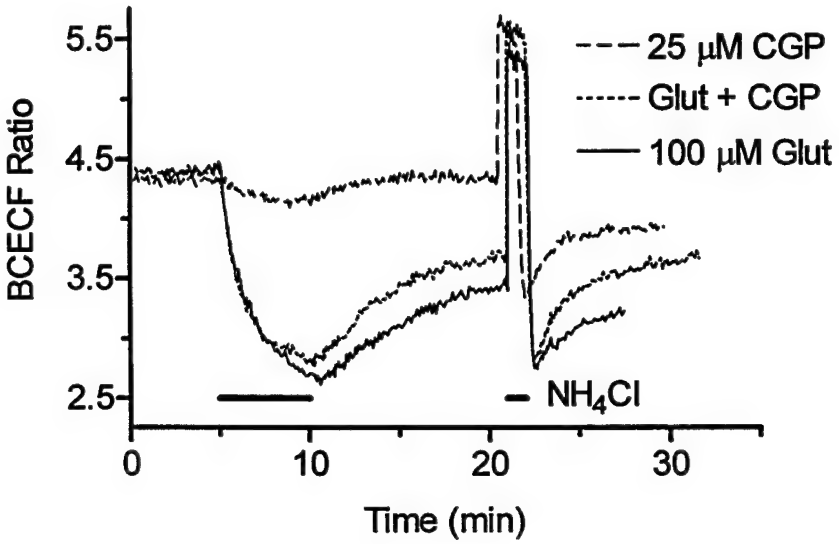
5.5
4.5
3.5
2.5
BCECF Ratio
0
10
20
30
Time (min)
25 μM CGP
Glut + CGP
100 μM Glut
NH4Cl

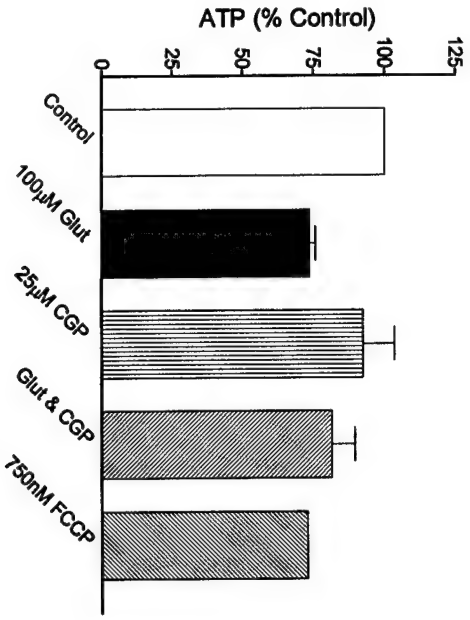
ATP (% Control)
0
25
50
75
100
125
Control
100μM Glut
25μM CGP
Glut & CGP
750nM FCCP

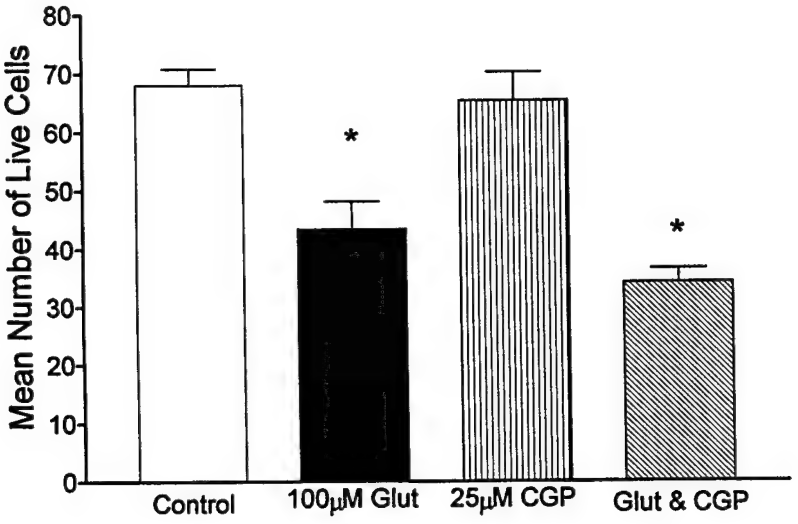
Mean Number of Live Cells
80
70
60
50
40
30
20
10
0
*
*
Control
100μM Glut
25μM CGP
Glut & CGP

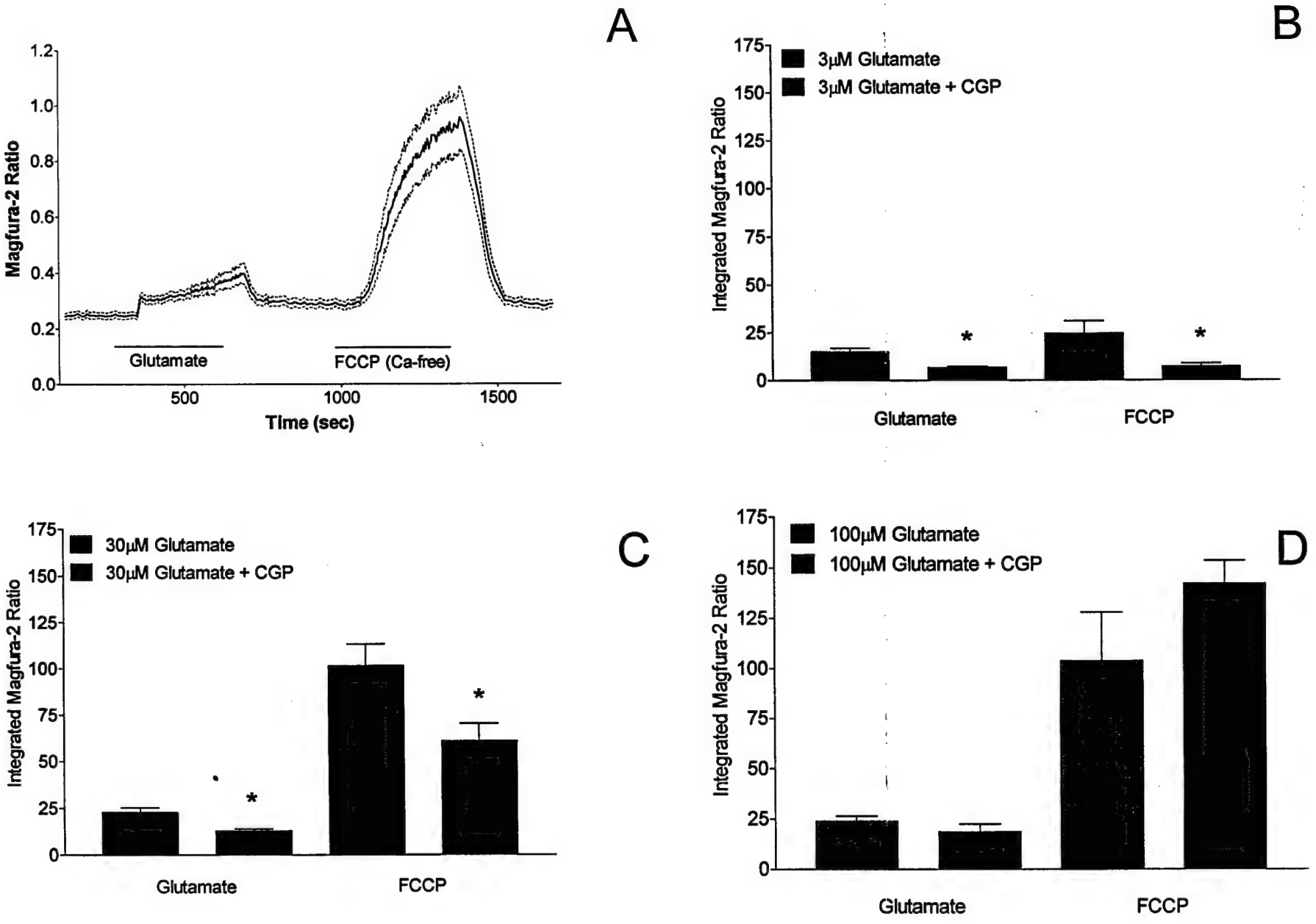
A
Magfura-2 Ratio
1.2
1.0
0.8
0.6
0.4
0.2
0.0
Glutamate
FCCP (Ca-free)
500
1000
1500
Time (sec)
B
Integrated Magfura-2 Ratio
175
150
125
100
75
50
25
0
3μM Glutamate
3μM Glutamate + CGP
*
*
Glutamate
FCCP
C
Integrated Magfura-2 Ratio
175
150
125
100
75
50
25
0
30μM Glutamate
30μM Glutamate + CGP
*
*
Glutamate
FCCP
D
Integrated Magfura-2 Ratio
175
150
125
100
75
50
25
0
100μM Glutamate
100μM Glutamate + CGP
Glutamate
FCCP

Title page

Quantitative evaluation of mitochondrial calcium content following a glutamate stimulation in rat cortical neurones

Jacques B. Brocard, Michel Tassetto[*,†] & Ian J. Reynolds[‡]

Department of Pharmacology - University of Pittsburgh - School of Medicine - Pittsburgh PA 15261 USA

[*] Ecole Normale Supérieure - Département de Neurobiologie - 46, rue d'Ulm - 75005 Paris, France

[†] Present address: Ecole Normale Supérieure - ACI Biologie Cellulaire des Homéoprotéines (UMR 8542) – 46, rue d'Ulm - 75005 Paris, France

Running title: Evaluation of mitochondrial calcium content

[‡] To whom correspondence should be addressed at the Department of Pharmacology, W1351 Biomedical Science Tower, Pittsburgh PA 15261, USA. Phone: 1.412.648.2134. Fax: 1.412.624.0794. E-mail: iannmda@pop.pitt.edu

Summary

1. Recent observations showed that a mitochondrial Ca^{2+} increase is necessary for an N-Methyl-D-Aspartate (NMDA) receptor stimulus to be toxic to cortical neurones. In an attempt to determine the magnitude of the Ca^{2+} fluxes involved in this phenomenon, we used carbonyl cyanide *p*- (trifluoromethoxy) phenyl-hydrazone (FCCP), a mitochondrial proton gradient uncoupler, to release mitochondrial free calcium ($[Ca^{2+}]_m$) during and following a glutamate stimulus, and Magfura-2 to monitor cytoplasmic free calcium ($[Ca^{2+}]_c$).

2. FCCP added after a glutamate stimulus elevated $[Ca^{2+}]_c$ to a much greater extent than did glutamate exposure, suggesting a very large accumulation of Ca^{2+} in the mitochondria.

3. Mitochondrial Ca^{2+} uptake was dependent on glutamate concentration whereas the changes in the overall quantity of Ca^{2+} entering the cell, obtained by simultaneously treating neurones with glutamate and FCCP, showed a response that was essentially all-or-none.

4. Mitochondrial Ca^{2+} uptake was also dependent on the nature and duration of a given stimulus as shown by comparing $[Ca^{2+}]_m$ associated with depolarization, kainate, NMDA and glutamate stimulations. Large mitochondrial Ca^{2+} accumulation only occured after a glutamate or NMDA stimulation.

5. These studies provide an approach to estimating $[Ca^{2+}]_m$ in neurones, and suggest that it may reach millimolar concentrations following intense glutamate stimulation.

Introduction

Glutamate is a predominant excitatory neurotransmitter in mammalian brain (Headley & Grillner, 1990). However, an excess of glutamate can be toxic to various populations of neuronal cells (Rothman & Olney, 1986; Choi *et al.*, 1987; Manev *et al.*, 1989). Delayed glutamatergic excitotoxicity has been identified as a consequence of NMDA receptor activation which requires an intracellular calcium ($[Ca^{2+}]_i$) increase (Choi, 1987; Randall & Thayer, 1992; Hartley *et al.*, 1993). Although mitochondria were known to accumulate Ca^{2+} following cytosolic free calcium ($[Ca^{2+}]_c$) increases in neurones (Nicholls & Åkerman, 1982; White & Reynolds, 1995), it was thought for a long time that this process was not involved in cell death but in preventing toxicity associated with elevated $[Ca^{2+}]_i$. However, recent studies showed opposite results: when mitochondrial calcium Ca^{2+} uptake is prevented during glutamate stimulation, neuronal cells survive toxic doses (Dessi *et al.*, 1995; Budd & Nicholls, 1996b; Stout *et al.*, 1998).

Ca^{2+} entry in mitochondria may be linked to cell death in many ways. These include changes in the polarization state of the mitochondria which jeopardizes the energy balance maintained by the metabolic functions of the mitochondria and also leads to production of reactive oxygen species (See Duchen, 1999 and Nicholls & Budd, 2000 for review). Several studies have monitored alterations in mitochondrial free calcium ($[Ca^{2+}]_m$) using fluorescent indicators such as Rhod-2 (Peng & Greenamyre, 1998; Peng *et al.*, 1998). However, Rhod-2 has a relatively high affinity for Ca^{2+} and it is not clear that it can accurately report $[Ca^{2+}]_m$ under conditions involving large fluxes of Ca^{2+} which may lead to the saturation of the dye.

We used the protonophore carbonyl cyanide *p*- (trifluoromethoxy) phenyl-hydrazone (FCCP) to release mitochondrial Ca^{2+} into the cytoplasm (Duchen *et al.*, 1990; Thayer & Miller, 1990;

Kiedrowski & Costa, 1995) where it is measured with the low affinity Ca^{2+}-sensitive fluorescent dye Magfura-2 (Raju *et al.*, 1989; Stout & Reynolds, 1999). We were able to demonstrate that mitochondrial Ca^{2+} accumulation is large compared to what is seen in the cytoplasm during a given stimulus and to establish the kinetics of Ca^{2+} fluxes during and after different stimuli.

Methods

Cell culture

Pregnant Sprague-Dawley female rats were anesthetized with diethyl ether inhalation until complete loss of responsiveness to tail and foot pinch was achieved. Embryonic day 17 fetuses were released from the uterus and decapitated. The mother was also decapitated without being allowed to regain consciousness. The forebrains were then removed from the fetuses and dissociated as follows. The lobes were incubated in 0.005-0.01 % trypsin in 2 ml of Ca^{2+} / Mg^{2+} –free medium (in mM: 115 NaCl, 5.4 KCl, 26.2 NaHCO3, 9.9 NaH2PO4, 5.5 glucose, 0.001% phenol red, and minimum essential medium amino acids; pH adjusted to 7.4 with NaOH) for 30 min at 37°C. The tissue was triturated an average of 12 times before the volume was brought to 10 ml and viability determinations were made with trypan blue (0.08 %) exclusion. The plating suspension was diluted to 450,000 cells.ml^{-1} using plating medium (v/v solution of 90% Dulbecco's modified Eagle's medium, 10 % heat-inactivated fetal bovine serum, 24 U.ml^{-1} penicillin, 24 μg.ml^{-1} streptomycin; final glutamine concentration, 3.9 mM). Cells were plated onto poly-D-lysine-coated (MW = 120,400; 40 mg.ml^{-1}) 31-mm glass coverslips that were inverted 1 day later into maintenance medium (horse serum substituted for fetal bovine serum, all other constituents identical). Neurones were used after 13-16 days in culture, with no further medium changes. These culture conditions provide the sparse, glia-poor neuronal cultures that are optimal for fluorescence microscopy measurements. Each experiment described was performed on 8 to 25 neurones per coverslip and 5 to 15 coverslips from two or more different culture dates. All procedures using animals were in accordance with the National Institutes of

Health Guide for the Care and Use of Laboratory Animals and were approved by the University of Pittsburgh's Institutional Animal Care and Use Committee.

Solutions and drugs

For perfusion of coverslips in the fluorescence microscopy experiments, we used a HEPES-buffered salt solution (HBSS, adjusted to pH 7.4 with NaOH) of the following composition (in mM): NaCl 137, KCl 5, $NaHCO_3$ 10, HEPES 20, glucose 5.5, KH_2PO_4 0.6, Na_2HPO_4 0.6, $CaCl_2$ 1.4, $MgSO_4$ 0.9. Ca^{2+} was omitted in the Ca^{2+} free HBSS buffer; High KCl buffer contains 50 mM of KCl and 92 mM of NaCl. The drugs used in the present experiments were purchased from Sigma® (Missouri, USA) and prepared from the following stock solutions:
1-100 μM glutamate from 10 mM in water, 1 μM glycine from 10 mM in water, 750 nM carbonyl cyanide *p*- (trifluoromethoxy) phenyl-hydrazone (FCCP) from 750 μM in methanol, 100 μM kainate from 10 mM in water and 300 μM N-Methyl-D-Aspartic acid (NMDA) from 10 mM in water. 1 μM glycine was always added in the glutamate- and NMDA-containing solutions. For treatments with FCCP alone, the drug was diluted in Ca^{2+} free buffer to avoid external Ca^{2+} entry in the cells.

$[Ca^{2+}]_c$ measurements

A 1 mM stock solution for the acetoxy methyl ester form of Magfura-2 (Molecular Probes, Oregon, USA) was prepared in anhydrous DMSO. Coverslips were incubated in HBSS containing 5 μM of Magfura-2, 0.5 % of DMSO and 5 $mg.ml^{-1}$ of bovine serum albumin for 10-15 minutes at 37°C. Cells were then rinsed with HBSS, mounted on a record chamber and perfused with HBSS at a rate of 20 $ml.min^{-1}$. All recordings were made at room temperature (20-

25°C). The imaging system used in this study consisted of a Nikon Diaphot 300 inverted microscope fitted with a 40x objective, a digital camera (Hamamatsu Corporation, New Jersey, USA) and a 75 Watt Xenon lamp-based monochromator light source (Applied Scientific Instrumentation Inc., Oregon, USA) as specified (Stout *et al.*, 1998). Cells were alternately illuminated with 335 nm and 375 nm wavelengths. Incident light was attenuated with neutral density filters (ND 0.5 and 0.3 for 16% transmittance; Omega Optical, Vermont, USA) and emitted fluorescence passed through a 515 nm dichroic mirror and a 535 / 25 nm band pass filter (Omega Optical, Vermont, USA). Background fluorescence, determined from three cell free regions of the coverslips, was subtracted from all the signals prior to calculating the ratios. The baseline ratio corresponds to the last ratio before the first stimulus (usually, glutamate; see the arrows in Fig. 1A-D). The areas under curve (AUCs) are calculated from baseline-subtracted Magfura-2 ratios during the first five minutes of a given stimulus as described (see Fig. 1F & G).

Statistics

Unpaired t-tests and one-way analyses of variances (ANOVAs) coupled with Bonferroni multi comparison post-hoc tests were performed using Prism 3.0 software (GraphPad Software Inc., San Diego, USA).

Results

Ca^{2+} uptake and Ca^{2+} release in neuronal cells

We have previously shown that Ca^{2+} that enters cells during glutamate application is largely due to NMDA receptor activation, and that a substantial fraction of the Ca^{2+} load is buffered by mitochondria (White & Reynolds, 1997). In this study, we used the low affinity Ca^{2+} indicator Magfura-2 to estimate $[Ca^{2+}]_c$ (Raju *et al.*, 1989; Stout & Reynolds, 1999). We ruled out the possibility that Magfura-2 was measuring large cytoplasmic Mg^{2+} changes, because Calcium Green-5N, a low affinity Ca^{2+} dye that is insensitive to Mg^{2+} (Rajdev and Reynolds, 1993) produced qualitatively similar results in the paradigms described below (J. B. Brocard & I. J. Reynolds, unpublished observations). Magfura-2 is almost exclusively found in the cytoplasm of neurones under the loading conditions used here because all of the dye could be released (as indicated by a decrease of cell-associated fluorescence) by a low concentration of digitonin (≤ 5 μM) that selectively removed the plasma membrane (Ishijima *et al.*, 1991); magfura-2 loaded into the cells could be quenched by the addition of Mn^{2+} in a depolarizing solution to the outside of the cell; and dye released from neurones by 5 μM digitonin displayed a peak excitation wavelength of 340 nm when incubated with saturating Ca^{2+} concentrations and could also be completely quenched by Mn^{2+} which does not bind to the uncleaved Magfura-2AM (Brocard *et al.*, 1993). To evaluate $[Ca^{2+}]_m$ following a glutamate stimulation we used the protonophore FCCP, which rapidly and reversibly collapses the mitochondrial membrane potential. This results in the release of Ca^{2+} from the mitochondria, probably by the reversed operation of the Ca^{2+} uniporter (Budd & Nicholls, 1996a). Thus, assessing $[Ca^{2+}]_c$ during an FCCP application corresponds to measuring $[Ca^{2+}]_m$.

Concentration-dependent increase of $[Ca^{2+}]_m$

Representative curves of Magfura-2 ratios (background subtracted) obtained for 1 μM, 3 μM, 10 μM and 30 μM glutamate are shown in Fig. 1A-D. The arrows indicate the ratio taken as the baseline for further studies. They show a concentration-dependent increase of $[Ca^{2+}]_c$ with both glutamate and FCCP. These curves represent the mean of 8 to 25 neurones from a single coverslip, and the mean response is considered to be a single experiment. The average Magfura-2 ratios obtained from 5 to 15 experiments with each concentration of glutamate were baseline-subtracted and plotted in Fig. 1E. Due to the variability in the characteristics of the Ca^{2+} responses in single cells (as exemplified in Fig. 2A & B) , we calculated the area under the curve (AUC), defined as the sum of the baseline-subtracted ratios for the duration of the treatment (Fig. 1F), as a measure of the overall Ca^{2+} fluxes occurring during a specific treatment (Fig. 1G). Average AUCs ± SEM for glutamate -induced and FCCP -induced Ca^{2+} responses are shown in Fig. 3A. At all concentrations, the FCCP-induced Ca^{2+} release is greater than what is observed during the glutamate treatment. Thus, most of the Ca^{2+} entering the neurones is not measured by the fluorescent dye during the glutamate treatment (Thayer & Miller, 1990). At a very high glutamate concentration (300μM), the corresponding $[Ca^{2+}]_c$ increase is smaller than that observed with lower glutamate concentrations. The ratio of FCCP-induced divided by the glutamate-induced $[Ca^{2+}]_c$ changes (F/G ratio) is also concentration-dependent and increases with the concentration of glutamate used during the stimulus (Fig. 3D). However, the increase in the rate of Ca^{2+} uptake seems to reach a maximum at high concentrations of glutamate. Taken together, these data indicate that the higher the glutamate concentration, the more Ca^{2+} is taken up by the mitochondria until the limit of their capacity is reached.

Overall cellular Ca^{2+} uptake during a glutamate stimulus

By inactivating the predominant Ca^{2+} buffering mechanism with FCCP during glutamate stimulations, it is possible to evaluate the overall quantity of Ca^{2+} being taken up by the neurones (Stout *et al.*, 1998). Representative curves of Magfura-2 ratios (background subtracted) obtained for glutamate (0 μM, 1 μM, 3 μM, 30 μM and 300 μM) + FCCP are shown in Fig. 4A-E. AUCs obtained for those treatments are shown in Fig. 4F. Although the concentration at which glutamate started to produce a sizeable response was similar in the absence or presence of FCCP, there appeared to be an all or none characteristic to the concentration response relationship for glutamate in the presence of FCCP. However, at most concentrations, the AUCs shown in Fig. 4F appear to reflect the sum of the glutamate-induced transient and the subsequent FCCP-induced release (with the notable exception of the measurements made with 3 μM) suggesting that this approach does provide a reasonable estimate of the total Ca^{2+} load during glutamate exposure.

Duration-dependent increase of $[Ca^{2+}]_m$ after a glutamate stimulus

We next sought to determine the time-dependence of the mitochondrial Ca^{2+} accumulation in the neurones. Representative curves of Magfura-2 ratios (background subtracted) obtained for 0, 1, 3, 5, 10 and 20 min of 30 μM glutamate stimulation are shown in Fig. 5A-F. AUCs obtained for the FCCP treatment correspond to significantly bigger Ca^{2+} fluxes than that measured in the cytoplasm during any glutamate stimulus shorter than 10 min (Fig. 6A). However, after 20 min of 30 μM glutamate activation, the AUC obtained after the FCCP treatment is significantly smaller than the Ca^{2+} flux measured during the stimulus (Fig. 6A). Thus, the F/G ratio is stable

for 1-5 min of glutamate treatment then drops for 10 min and 20 min to a value significantly smaller than what is observed for 1, 3 or 5 min (Fig. 6B).

Recovery-dependent decrease of $[Ca^{2+}]_m$

We also estimated the rate of Ca^{2+} extrusion from the mitochondria by varying the duration of the washout following a 30 μM glutamate stimulus. Representative curves of Magfura-2 ratios (background subtracted) obtained for 0, 5, 10 and 20 min after the exposure when the cells are washed in the absence of external Ca, are shown in Fig. 7A-D. As a comparison, the response obtained when using FCCP in naïve cells is shown in Fig. 7E. AUCs obtained for the FCCP treatment 0-5 min after the glutamate correspond to higher $[Ca^{2+}]_m$ than 10 or 20 min after the stimulus or in naïve cells (Fig. 7F). The absence of Ca^{2+} in the medium during glutamate washout did not significantly alter Ca^{2+} extrusion from the neurones. However, after a $[Ca^{2+}]_m$ decrease of 3-fold within the first 10 min of Ca^{2+} free buffer washout, it stays stable over the next 10 min period. Thus, $[Ca^{2+}]_m$ is still higher after 20 min of washout compared to naïve cells (Fig. 7F).

Stimulus-dependent increase of $[Ca^{2+}]_m$

Previous studies have suggested that the magnitude of $[Ca^{2+}]_m$ increase depends on the route of Ca^{2+} entry *per se* (Sattler *et al.*, 1998) whereas others showed that only NMDA receptor activation would lead to large $[Ca^{2+}]_c$ followed by high $[Ca^{2+}]_m$ increases (Hyrc *et al.*, 1997; Stout & Reynolds, 1999; Keelan *et al.*, 1999). Moreover, as Magfura-2 is sensitive to physiological $[Mg^{2+}]_i$ (Raju *et al.*, 1989), it was important to determine whether there were dye changes in the absence of Ca^{2+} in the buffer. We further investigated these principles by

exposing neurones to other stimuli that elevate Ca^{2+} to a varying extent (Stout & Reynolds, 1999). Representative curves of Magfura-2 ratios (background subtracted) obtained for 30 μM glutamate in Ca^{2+} free buffer, high KCl buffer, 100 μM kainate and 300 μM NMDA are shown in Fig. 8. AUCs obtained using glutamate in Ca^{2+} free buffer, high KCl or kainate correspond to significantly smaller Ca^{2+} fluxes than the $[Ca^{2+}]_c$ change obtained with 30 μM glutamate (Fig. 9A). Similarly, Ca^{2+} responses with FCCP following those stimuli are significantly smaller than the response obtained with FCCP after a 30 μM glutamate stimulation (Fig. 9B). Interestingly though, the magnitude of the $[Ca^{2+}]_c$ changes following glutamate stimulation in Ca^{2+} free buffer and kainate is significantly higher than the $[Ca^{2+}]_c$ change observed in naïve cells (see Fig. 7F and J. B. Brocard & I. J. Reynolds, unpublished observations).

Discussion

The goal of these experiments was to develop a method to measure $[Ca^{2+}]_m$ during and after a glutamate stimulation in cortical neurones. The protonophore FCCP was used to release Ca^{2+} from mitochondria, and the Ca^{2+} elevation was detected in the cytoplasm using the low affinity Ca^{2+} indicator Magfura-2. Our results demonstrate the value of this approach, as we show that mitochondrial Ca^{2+} accumulation is dependent on the glutamate concentration, the time of exposure to glutamate, and the duration of the washout following the glutamate stimulation. The only exception seems to be the Ca^{2+} increases measured during combined FCCP and glutamate applications (Fig. 4F). This result may be explained by the inhibition of the NMDA receptor through high $[Ca^{2+}]_c$, thereby underestimating the overall Ca^{2+} entry at high glutamate concentrations (Rosemund *et al.*, 1995).

However, the most notable observation is the size of the $[Ca^{2+}]_m$ pool. The Ca^{2+} changes detected by Magfura-2 approached the maximal ratios we have obtained with this dye, suggesting that the dye is close to being saturated with Ca^{2+}. Given that the K_D of the dye for Ca^{2+} is ~10-20 μM (Raju *et al.*, 1989; Stout and Reynolds, 1999), this suggests that $[Ca^{2+}]_c$ following FCCP-induced release may significantly exceed 100 μM. When one considers that the usual estimate of the fractional volume of the cytoplasm occupied by mitochondria is < 5% (Scott & Nicholls, 1980) this implies that $[Ca^{2+}]_m$ following glutamate exposure approaches several millimolar.

This study reveals some interesting characteristics of the relationship between $[Ca^{2+}]_c$ and $[Ca^{2+}]_m$ after NMDA receptor activation. The threshold glutamate concentration for producing $[Ca^{2+}]_m$ increase in this study is approximately 1 μM, and this led to similar small increases in

Magfura-2 fluorescence during the stimulus and the FCCP application. Higher glutamate concentrations produced an elevation in $[Ca^{2+}]_c$ that exceeds the set point with the result that there is a progressive accumulation of Ca^{2+} in the matrix (Nicholls, 1978). There was a clear relationship between the magnitude of the $[Ca^{2+}]_c$ response to glutamate and the subsequent FCCP-induced Ca^{2+} release from the mitochondrial Ca^{2+} stores between 1 and 100 μM glutamate following a five minute glutamate exposure. This suggests that the approach provides a reasonable, semi quantitative estimate of $[Ca^{2+}]_m$ under these conditions. A similar relationship was observed when the time of glutamate exposure was varied between one and five minutes, again suggesting that the method can report mitochondrial Ca^{2+} accumulation under the conditions of these experiments. It is worth noting though, that the relationship between $[Ca^{2+}]_m$ and $[Ca^{2+}]_c$ is not linear under these circumstances, as revealed by the variation in the F/G ratio obtained with increasing concentrations of glutamate (Fig. 3D). This non-linear relationship could be due to the inherent properties of the low-affinity dye Magfura-2 itself as described elsewhere (Hyrc et al., 2000) or, alternatively, be a consequence of the activation of the mitochondrial Ca^{2+} uniporter by high $[Ca^{2+}]_c$ as reported previously (Colegrove *et al.*, 2000). Furthermore, mitochondrial Ca^{2+} buffering capacity is limited as becomes evident when stimulating cells with concentrations of glutamate greater than 100 μM or for periods of time beyond 5 min. With these more extreme stimulation paradigms we observed that the F/G ratio decreased, reflecting a limitation in the accumulation of Ca^{2+} by mitochondria. This could reflect a saturation phenomenon, where the limit of the ability of mitochondria to accumulate Ca^{2+} is reached. Alternatively, the limitation could reflect the dissipation of the gradient that drives Ca^{2+} into the mitochondria ($\Delta\Psi_m$; Zoccarato & Nicholls, 1982), the glutamate-induced Ca^{2+} - dependent decrease of $\Delta\Psi_m$ being a well characterized property of neuronal mitochondria

(Schinder *et al.*, 1996; White and Reynolds, 1996; Vergun *et al.*, 1999). It is also possible that the later failure of Ca^{2+} accumulation and/or release of matrix Ca^{2+} in these long exposures reflects activation of permeability transition (Hunter & Haworth, 1979; Al Nasser & Crompton, 1986). However, recent studies argued against the induction of transition in a similar paradigm (Castilho *et al.*, 1998; Hüser *et al.*, 1998). Interestingly, $[Ca^{2+}]_c$ always stayed high for the whole duration of the FCCP treatment, probably reflecting a continuous release of Ca^{2+} from the mitochondria and/or a slow rate of Ca^{2+} extrusion from the cytoplasm. Given that the subsequent decline in $[Ca^{2+}]_c$ appeared to be the consequence of FCCP removal this observation suggests that the FCCP treatment was not of sufficient duration to empty the mitochondria of calcium. It is not clear wether this is due to the relatively slow mobilization of intramitochondrial calcium, or whether the efflux pathway is rate-limiting in this process.

For smaller concentrations of glutamate (1 μM) and non-NMDA stimulations, the stimulus- and FCCP -induced increases in Magfura-2 fluorescence are not necessarily related to mitochondrial Ca^{2+} accumulation. We first confirmed that the initial $[Ca^{2+}]_m$ in naïve cells is very small by monitoring Magfura-2 fluoresence increase during an FCCP application on untreated cells (see Fig. 7E). This content was estimated to be $<< 1$ μM (J. B. Brocard & I. J. Reynolds, unpublished observations) when using Fura-2, a fluorescent dye more sensitive to Ca^{2+} (Grynkiewicz *et al.*, 1985; Stout & Reynolds, 1999). The Magfura-2 fluorescence increases obtained when using 0 μM glutamate (+1 μM glycine; see Methods) followed by FCCP were identical to what was observed in naïve cells, thus confirming the absence of any intrisic ability of glycine to active the NMDA receptors (Johnson & Ascher, 1987).

Using 1 μM glutamate led to similar small increases in Magfura-2 fluorescence during the stimulus and the FCCP application. If there is any Ca^{2+} entry, it does not lead to $[Ca^{2+}]_c$ changes large enough to trigger the process of mitochondrial buffering (Nicholls, 1978; see above). Identical results were obtained when using depolarization as a stimulus. In contrast, increases in Magfura-2 fluorescence observed during a 30 μM glutamate stimulus followed by an FCCP application, all in Ca^{2+} free buffer, are unlikely to be due to Ca^{2+} variations. However, we previously demonstrated that glutamate can stimulate the influx of Mg^{2+} in Ca^{2+} free buffer, and this may be the source of Magfura-2 fluorescence changes in the absence of Ca^{2+} (Brocard *et al.*, 1993; Stout *et al.*, 1996). Interestingly, the AUC obtained during FCCP application in this experiment is higher than what was obtained when the drug was applied on naïve cells. Therefore, this signal could be due to either Mg^{2+} initially taken up, then extruded by the mitochondria or to Mg^{2+} released from ATP during the FCCP application (Leyssens *et al.*, 1996). Interestingly, similar observations were made with kainate stimuli (in the presence of Ca^{2+} in the buffer): in this case, it is difficult to decide between a Ca^{2+}- or a Mg^{2+}-specific increase or both.

Several previous studies have reported the determination of $[Ca^{2+}]_m$ in neurones. Perhaps the most direct approach involves electron microprobe x-ray analysis to determine the mitochondrial ion content (Pivovarova *et al.*, 1999; Taylor *et al.*, 1999). However, as of yet it has not proved possible to apply this method to monolayer cultures of neurones, and it is also rather more difficult to establish time courses with this technique. Others have reported the use of fluorescent indicators that report Ca^{2+} and preferentially accumulate in mitochondria. The major limitation in this approach would appear to be the problem of dye saturation. For example, Rhod-2 has an affinity for Ca^{2+} of ~0.5 μM, and can selectively accumulate in mitochondria because the

acetoxymethyl ester is a partially charged cation (Peng & Greenamyre, 1998; Peng *et al.*, 1998). However, as noted above, the estimate of $[Ca^{2+}]_m$ suggests that millimolar Ca^{2+} might be expected, which is far beyond the capacity of these dyes to report accurately. Alternatively, it is also possible that a substantial majority of the Ca^{2+} that enters mitochondria is not actually free in solution, and is instead precipitated as Ca^{2+} phosphate or sequestered in any other form in the matrix (Lehninger, 1974; Zoccarato & Nicholls, 1982). In this way, the actual free Ca^{2+} concentration may still be in the low micromolar range.

We have not directly investigated the efflux mechanisms triggered by FCCP. It has previously been reported that dissipation of $\Delta\Psi_m$ results in reverse operation of the Ca^{2+} uniporter in isolated mitochondria (Budd & Nicholls, 1996a). Other potential efflux mechanisms are the mitochondrial Na^+ / Ca^{2+} exchanger (White & Reynolds, 1995 and references therein) and the activation of permeability transition (see Duchen, 1999 and Nicholls & Budd, 2000 for review). As already noted, it is likely that some fraction of the Ca^{2+} that accumulates into mitochondria is taken out of solution in the form of Ca^{2+} phosphate or other insoluble form in the matrix (Lehninger, 1974; Zoccarato & Nicholls, 1982). It is difficult to establish the extent to which this alters the characteristics of the efflux that we observed. We might tentatively infer, based on the experiments shown in Fig. 7, that there are two pools of releasable Ca. The first and larger pool leaves the mitochondria within 10 minutes, while the second pool remains stable prior to the addition of FCCP. One might speculate that these pools represent soluble and insoluble forms of Ca^{2+} in the mitochondrion, recognizing that there is yet little direct evidence to support this supposition. Alternatively, the activation of the Ca^{2+} efflux routes may be less sensitive to $[Ca^{2+}]_m$ than entry routes are to $[Ca^{2+}]_c$. In any case, whatever the form of Ca^{2+} that these pools

represent, both must be mobilized by the effects of FCCP, either the result of the alteration of membrane potential or by the change in the matrix pH.

References

Al Nasser, I. & Crompton, M. (1986). The reversible Ca^{2+} –induced permeabilization of rat liver mitochondria. *Biochemical Journal* **239**, 19–29.

Brocard, J. B., Rajdev, S. & Reynolds, I. J. (1993). Glutamate-induced increases in intracellular free Mg^{2+} in cultured cortical neurons. *Neuron* **11**, 751-757.

Budd, S. L. & Nicholls, D. G. (1996a). A reevaluation of the role of mitochondria in neuronal Ca^{2+} homeostasis. *Journal of Neurochemistry* **66**, 403-411.

Budd, S. L. & Nicholls, D. G. (1996b). Mitochondria, calcium regulation, and acute glutamate excitotoxicity in cultured cerebellar granule cells. *Journal of Neurochemistry* **67**, 2282-2291.

Castilho, R. F., Hansson, O., Ward, W. M., Budd, S. L. & Nicholls, D. G. (1998). Mitochondrial control of acute glutamate excitotoxicity in cultured cerebellar granule cells. *Journal of Neuroscience* **18**, 10277-10286.

Choi, D. W. (1987). Ionic dependence of glutamate neurotoxicity. *Journal of Neuroscience* **7**, 369-379.

Choi, D. W., Maulucci-Gede, M. & Kriegstein, A. R. (1987). Glutamate neurotoxicity in cortical cell culture. *Journal of Neuroscience* **7**, 357–368.

Colegrove, S. L., Albrecht, M. A. & Friel, D. D. (2000). Dissection of mitochondrial Ca(2+) uptake and release fluxes in situ after depolarization-evoked [Ca(2+)](i) elevations in sympathetic neurons. *Journal of General Physiology* **115**, 351-370.

Dessi, F., Ben-Ari, Y. & Charriaut-Marlangue, C. (1995). Ruthenium red protects against glutamate-induced neuronal death in cerebellar culture. *Neuroscience Letters* **201**, 53–56.

Duchen, M. R. (1990). Effects of metabolic inhibition on the membrane properties of isolated mouse primary sensory neurones. *Journal of Physiology* **424**, 387–409.

Duchen, M. R. (1999). Contributions of mitochondria to animal physiology: from homeostatic sensor to calcium signalling and cell death. *Journal of Physiology* **516**, 1-17.

Grynkiewicz, G., Poenie, M. & Tsien, R. Y. (1985). A new generation of Ca^{2+} indicators with greatly improved fluorescence properties. *Journal of Biological Chemistry* **260**, 3440-3450.

Hartley, D. M., Kurth, M. C., Bjerkness, L., Weiss, J. H. & Choi, D. W. (1993). Glutamate receptor -induced $^{45}Ca^{2+}$ accumulation in cortical cell culture correlated with subsequent neuronal degeneration. *Journal of Neuroscience* **13**, 1993–2000.

Headley, P. M. & Grillner, S. (1990). Excitatory amino acids and synaptic transmission: evidence for a physiological function. *Trends in Pharmacological Sciences – A special report* **1991**, 30-36.

Hunter, D. R. & Haworth, R. A. (1979). The Ca^{2+} -induced membrane transition in mitochondria. I. The protective mechanisms. *Archives in Biochemistry and Biophysics* **195**, 453–459.

Hüser, J., Rechenmacher, C. E. & Blatter, L. A. (1998). Imaging the permeability pore transition in single mitochondria. *Biophysics Journal* **74**, 2129–2137.

Hyrc, K., Handran, S. D., Rothman, S. M. & Goldberg, M. P. (1997). Ionized intracellular calcium concentration predicts excitotoxic neuronal death: observations with low-affinity fluorescent calcium indicators. *Journal of Neuroscience* **17**, 6669-6677.

Hyrc, K. L., Bownik, J. M. & Goldberg, M. P. (2000). Ionic selectivity of low-affinity ratiometric calcium indicators: mag-Fura-2, Fura-2FF and BTC. *Cell Calcium* **27**, 75-86.

Ishijima, S., Sonoda, T. & Tatibana, M. (1991). Mitogen-induced early increase in cytosolic free Mg2+ concentrations in single Swiss 3T3 fibroblasts. *American Journal of Physiology* **261**, C1074-C1080.

Johnson, J. W. & Ascher, P. (1987). Glycine potentiates the NMDA response in cultured mouse brain neurons. *Nature* **325**, 529-531.

Keelan, J., Vergun, O. & Duchen, M. R. (1999). Excitotoxic mitochondrial depolarisation requires both calcium and nitric oxide in rat hippocampal neurons. *Journal of Physiology* **520**, 797-813.

Kiedrowski, L. & Costa, E. (1995). Glutamate-induced destabilization of intracellular calcium concentration homeostasis in cultured cerebellar granule cells: role of mitochondria in calcium buffering. *Molecular Pharmacology* **47**, 140-147.

Lehninger, A. L. (1974). Role of phosphate and other proton-donating anions in respiration-coupled transport of Ca^{2+} by mitochondria. *Proceedings of the National Academy of Sciences (USA)* **71**, 1520–1524.

Leyssens, A., Nowicky, A. V., Patterson, L., Crompton, M. & Duchen. M. R. (1996). The relationship between mitochondrial state, ATP hydrolysis, $[Mg^{2+}]_i$ and $[Ca^{2+}]_i$ studied in isolated rat cardiomyocytes. *Journal of Physiology* **496**, 111-128.

Manev, H., Favaron, M., Guidotti, A. & Costa, E. (1989). Delayed increase of Ca^{2+} influx elicited by glutamate: role in neuronal death. *Molecular Pharmacology* **36**, 106–112.

Nicholls, D. G. (1978). The regulation of extra-mitochondrial free Ca^{2+} by rat liver mitochondria. *Biochemical Journal* **176**, 463–474.

Nicholls, D. G. & Åkerman, K. E. O. (1982). Mitochondrial calcium trasport. *Biochimica Biophysica Acta* **683**, 57–88.

Nicholls, D. G. & Budd, S. L. (2000). Mitochondria and neuronal survival. *Physiological Reviews* **80**, 315-360.

Peng, T. I. & Greenamyre, J. T. (1998). Privileged access to mitochondria of calcium influx through *N*-methyl-D-aspartate receptors. *Molecular Pharmacology* **53**, 974–980.

Peng, T. I., Jou, M. J., Sheu, S. S. & Greenamyre, J. T. (1998). Visualization of NMDA receptor-induced mitochondrial calcium accumulation in striatal neurons. *Experimental Neurology* **149**, 1–12.

Pivovarova, N. B., Hongpaisan, J., Andrews, S. B. & Friel, D. D. (1999). Depolarization-induced mitochondrial Ca^{2+} accumulation in sympathetic neurons : spatial and temporal characteristics. *Journal of Neuroscience* **19**, 6372-6384.

Raju, B., Murphy, E., Levy, L. A., Hall, R. D. & London, R. E. (1989). A fluorescent indicator for measuring cytosolic free magnesium. *American Journal of Physiology* **256**, C540-C548.

Randall, R. D. & Thayer, S. A. (1992). Glutamate-induced calcium transient triggers delayed calcium overload and neurotoxicity in rat hippocampal neurons. *Journal of Neuroscience* **12**, 1882–1895.

Rosemund, C., Feltz, A. & Westbrook, G. L. (1995) Calcium-dependent inactivation of synaptic NMDA receptors in hippocampal neurons. *Journal of Neurophysiology* **73**, 427-430.

Rothman, S. M. & Olney, J. W. (1986). Glutamate and the pathophysiology of hypoxic-ischaemic brain damage. *Annals of Neurology* **19**, 105–111.

Sattler, R., Charlton, M. P., Hafner, M. & Tymianski, M. (1998). Distinct influx pathways, not calcium load, determine neuronal vulnerability to calcium neurotoxicity. *Journal of Neurochemistry* **71**, 2349–2364.

Schinder, A. F., Olson, E. C., Spitzer, N. C. & Montal, M. (1996). Mitochondrial dysfunction is a primary event in glutamate excitotoxicity. *Journal of Neuroscience* **16**, 6125–6133.

Scott, I. D. & Nicholls, D. G. (1980). Energy transduction in intact synaptosomes. Influence of plasma-membrane depolarization on the respiration and membrane potential of internal mitochondria determined in situ. *Biochemical Journal* **186**, 21-33.

Stout, A. K., Li-Smerin, Y., Johnson, J. W. & Reynolds. I. J. (1996). Mechanisms of glutamate-stimulated Mg^{2+} influx and subsequent Mg^{2+} efflux in rat forebrain neurones in culture. *Journal of Physiology* **492**, 641-657.

Stout, A. K., Raphael, H. M., Kanterewicz, B. I., Klann, E. & Reynolds, I. J. (1998). Glutamate-induced neuron death requires mitochondrial calcium uptake. *Nature Neuroscience* **1**, 366-373.

Stout, A. K. & Reynolds, I. J. (1999). High-affinity calcium indicators underestimate increases in intracellular calcium concentrations associated with excitotoxic glutamate stimulations. *Neuroscience* **89**, 91–100.

Taylor, C. P., Weber, M. L., Gaughan, C. L., Lehning, E. J. & LoPachin, R. M. (1999). Oxygen/glucose deprivation in hippocampal slices: altered intraneuronal elemental composition predicts structural and functional damage. *Journal of Neuroscience* **19**, 619-629.

Thayer, S. A. & Miller, R. J. (1990). Regulation of the intracellular free calcium concentration in single rat dorsal root ganglion neurones *in vitro*. *Journal of Physiology* **425**, 85-115.

Vergun, O., Keelan, J., Khodorov, B. I. & Duchen, M. R. (1999). Glutamate-induced mitochondrial depolarisation and perturbation of calcium homeostasis in cultured rat hippocampal neurones. *Journal of Physiology* **519**, 451-466.

White, R. J., & Reynolds, I. J. (1995). Mitochondria and Na^{+} / Ca^{2+} exchange buffer glutamate-induced calcium loads in cultured cortical neurons. *Journal of Neuroscience* **15**, 1318-1328.

White, R. J., & Reynolds, I. J. (1996). Mitochondrial depolarization in glutamate-stimulated neurons: an early signal specific to excitotoxin exposure. *Journal of Neuroscience* **16**, 5688–5697.

White, R. J., & Reynolds, I. J. (1997). Mitochondria accumulate Ca^{2+} following intense glutamate stimulation of cultured rat forebrain neurones. *Journal of Physiology* **498**, 31–47.

Zoccarato, F & Nicholls, D. G. (1982). The role of phosphate in the regulation of the Ca^{2+} efflux pathway of liver mitochondria. *European Journal of Biochemistry* **127**, 333–338.

Acknowledgements

We gratefully thank G. J. Kress for excellent technical help and Dr J. F. Buckman for critically reading this manuscript. J. B. B. was supported by a long term fellowship from the European Molecular Biology Organization (ALTF – 743 – 1998). This study was also supported by NIH grant NS34138.

Figure legends

Figure 1: Evaluation of $[Ca^{2+}]_c$ and $[Ca^{2+}]_m$ during and following a glutamate stimulus. (A-D) Representative traces obtained from *n* neurones treated with 1 μM (A), 3 μM (B), 10 μM (C) or 30 μM (D) glutamate and with FCCP as indicated. The arrows point to the ratio taken as the baseline. (E) Means ± SEMs of the Magfura-2 ratios (baseline-subtracted) obtained from *n* coverslips for each glutamate treatment: 1 μM glutamate (▲; $n = 5$), 3 μM glutamate (▼; $n = 10$), 10 μM glutamate (△; $n = 10$), 30 μM glutamate (▽; $n = 15$). (F) Mean ± SEM of the Magfura-2 ratios (baseline-subtracted) obtained from 15 coverslips with 30 μM glutamate (▽; $n = 15$) and areas under the curve (AUCs) used as a measure of the Ca^{2+} fluxes after the glutamate stimulation (□) and the FCCP application (▨). The FCCP applications were performed in absence of Ca^{2+} in the buffer. (G) Mean ± SEM for AUCs as described in (F), for the 30 μM glutamate stimulus (□) and the FCCP treatment (▨).

Figure 2: Variability in single cells responses during and following a glutamate stimulus. Traces for single cells treated with 3 μM (A) or 30 μM (B) glutamate corresponding to Fig. 1B & D, respectively.

Figure 3: Dose-dependent increase of $[Ca^{2+}]_c$ and $[Ca^{2+}]_m$ during and following a glutamate stimulus. (A) *n* coverslips were treated as indicated in Fig. 1 and means ± SEMs for AUCs after the glutamate (□) and the FCCP treatments (▨) were plotted (Significant differences from the corresponding FCCP treatment, unpaired t-tests: *, $P < 0.05$). (D) Means ± SEMs of normalized ratios of FCCP- induced divided by glutamate- induced $[Ca^{2+}]_c$ changes (Significant differences

from the 1 μM and 3 μM glutamate treatments, ANOVA followed by Bonferroni tests: *, $P < 0.05$. Significant differences from the 10 μM glutamate treatment, ANOVA followed by Bonferroni tests: †, $P < 0.05$).

Figure 4: Evaluation of $[Ca^{2+}]_c$ and $[Ca^{2+}]_m$ during a simultaneous glutamate + FCCP stimulus. (A-E) Representative traces obtained from *n* neurones treated with 0 μM (A), 1 μM (B), 3 μM (C), 30 μM (D) or 300 μM (E) glutamate + FCCP as indicated. (F) *n* coverslips were treated as indicated above and means ± SEM for AUCs after the glutamate + FCCP treatments were plotted (Significant differences from 0 μM and 1 μM glutamate treatments, ANOVA followed by Bonferroni tests: *, $P < 0.05$)

Figure 5: Evaluation of $[Ca^{2+}]_c$ and $[Ca^{2+}]_m$ during and following a glutamate stimulus. (A-F) Representative traces obtained from *n* neurones treated with 30 μM glutamate for 0 (A), 1 (B), 3 (C), 5 (D), 10 (E) or 20 min (F) and FCCP as indicated. The FCCP applications were performed in absence of Ca^{2+} in the buffer. Neurones treated for 0 min were subjected to the same experimental procedure but not to the glutamate exposure.

Figure 6: Duration-dependent increase of $[Ca^{2+}]_c$ and $[Ca^{2+}]_m$ during and following a glutamate stimulus. (A) *n* coverslips were treated as indicated in Fig. 5 and means ± SEMs for AUCs after the glutamate (□) and the FCCP treatments (▨) were plotted (Significant differences from the corresponding FCCP treatment, unpaired t-tests: *, $P < 0.05$). (B) Means ± SEMs of normalized ratios of FCCP- induced divided by glutamate- induced cytoplasmic Ca^{2+} changes (Significant differences from the 20 min glutamate treatment, ANOVA followed by Bonferroni tests: *, P <

0.05. Significant differences from the 10 min glutamate treatment, ANOVA followed by Bonferroni tests: †, $P < 0.05$).

Figure 7: Recovery-dependent decrease of $[Ca^{2+}]_m$ following a glutamate stimulus. (A-D) Representative traces obtained from *n* neurones treated with 30 μM glutamate, rinsed for 0 (A), 5 (B), 10 (C) or 20 min (D) in Ca^{2+} free buffer and treated with FCCP as indicated. (E) *n* naïve cells were treated with FCCP only, as indicated. The FCCP applications were performed in absence of Ca^{2+} in the buffer. (F) *n* coverslips were treated as indicated above and means ± SEMs for AUCs obtained after the glutamate and the FCCP treatments were plotted (Significant differences from 10 min and 20 min recovery, ANOVA followed by Bonferroni tests: *, $P < 0.05$. Significant differences from naïve cells, ANOVA followed by Bonferroni tests: †, $P < 0.05$).

Figure 8: Evaluation of $[Ca^{2+}]_c$ and $[Ca^{2+}]_m$ during and following various stimuli. (A-D) Representative traces obtained from *n* neurones treated with 30 μM glutamate in Ca^{2+} free buffer (A), KCl 50 mM (B), kainate 100 μM (C) or NMDA 300 μM (D) and FCCP as indicated. The FCCP applications were performed in absence of Ca^{2+} in the buffer.

Figure 9: Stimulus-dependent increase of $[Ca^{2+}]_c$ and $[Ca^{2+}]_m$. *n* coverslips were treated as indicated in Fig. 8 and means ± SEMs for AUCs obtained after the stimuli (A) and the FCCP (B) treatments were plotted (Significant differences from the 30 μM glutamate treatment, ANOVA followed by Bonferroni tests: *, $P < 0.05$).

Figure 1

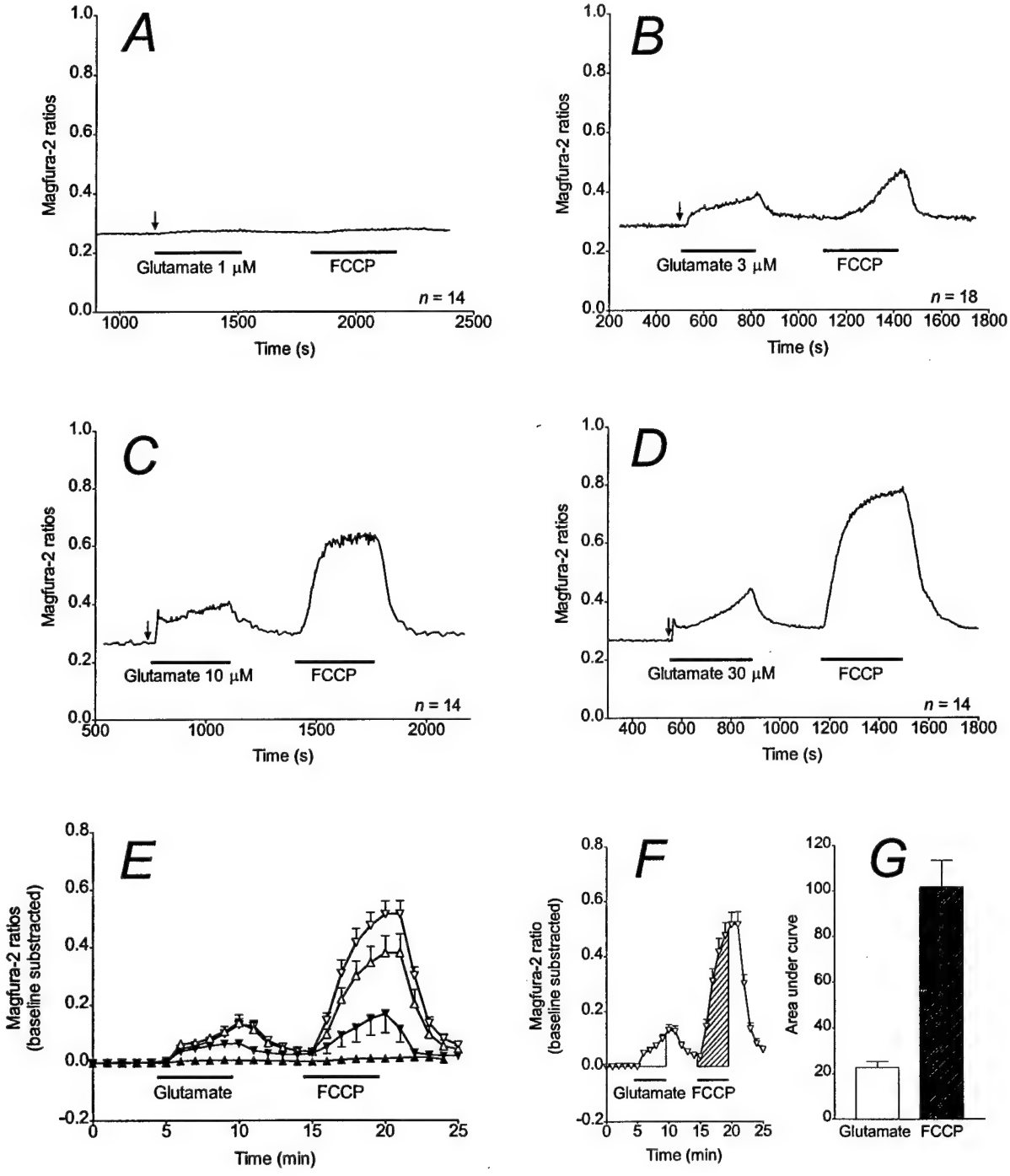
A
Magfura-2 ratios
Glutamate 1 μM
FCCP
n = 14
Time (s)
B
Magfura-2 ratios
Glutamate 3 μM
FCCP
n = 18
Time (s)
C
Magfura-2 ratios
Glutamate 10 μM
FCCP
n = 14
Time (s)
D
Magfura-2 ratios
Glutamate 30 μM
FCCP
n = 14
Time (s)
E
Magfura-2 ratios (baseline substracted)
Glutamate
FCCP
Time (min)
F
Magfura-2 ratio (baseline substracted)
Glutamate FCCP
Time (min)
G
Area under curve
Glutamate FCCP

Figure 2

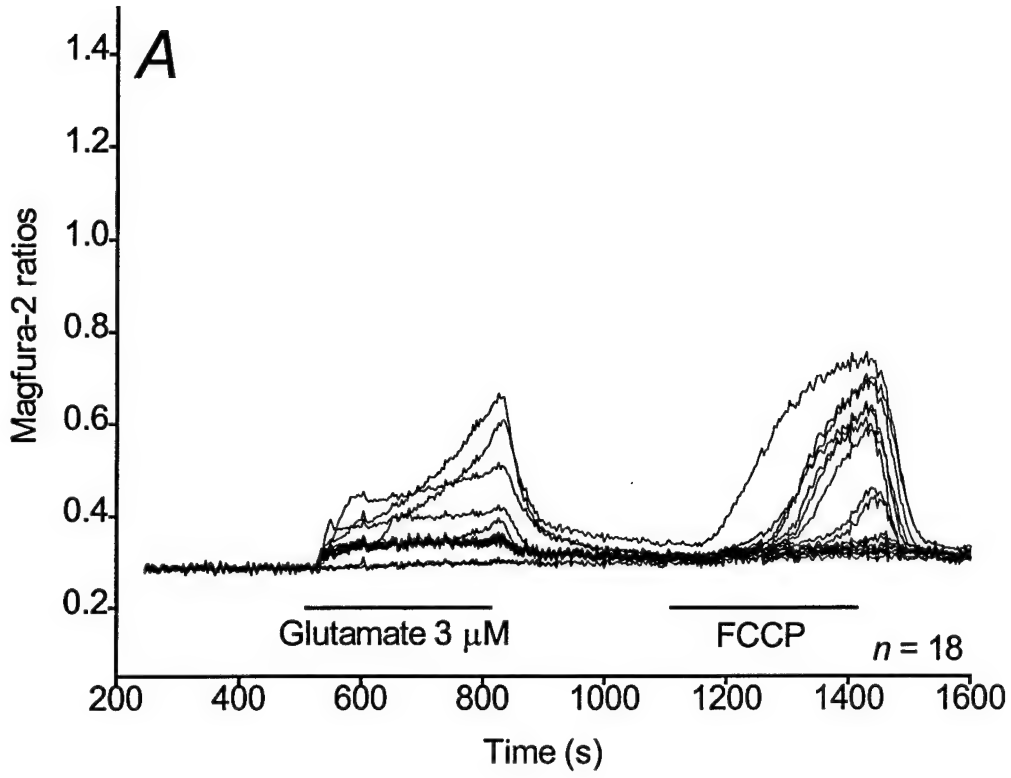
A
Magfura-2 ratios
1.4
1.2
1.0
0.8
0.6
0.4
0.2
Glutamate 3 μM
FCCP
n = 18
200
400
600
800
1000
1200
1400
1600
Time (s)

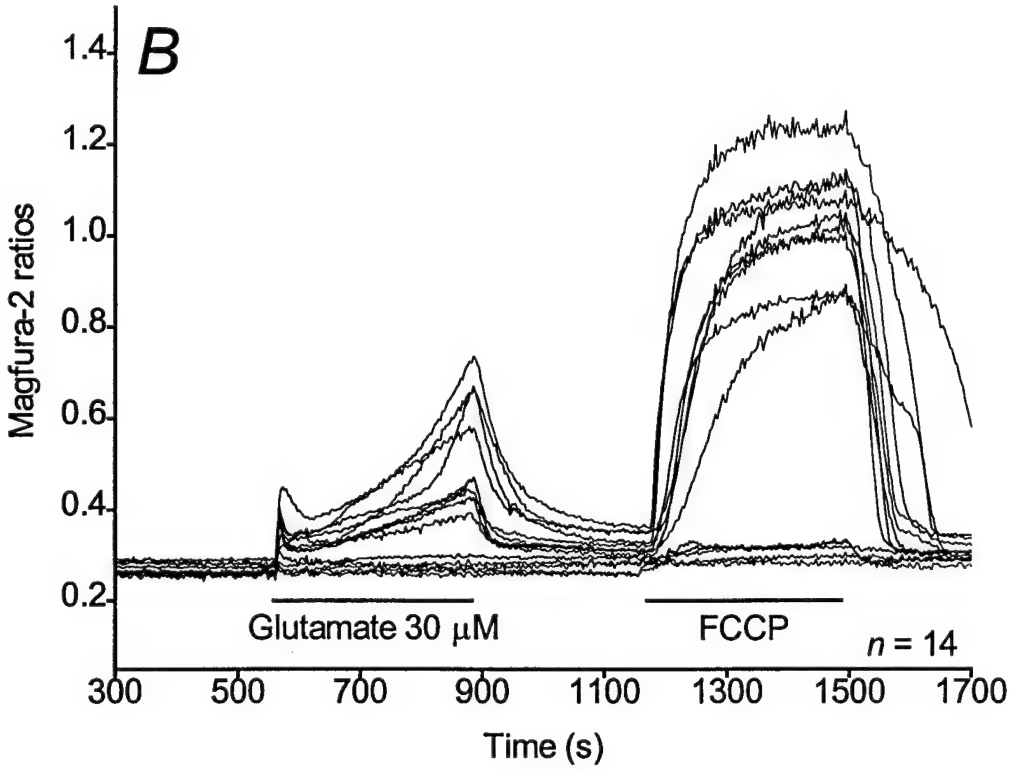
B
Magfura-2 ratios
1.4
1.2
1.0
0.8
0.6
0.4
0.2
Glutamate 30 μM
FCCP
n = 14
300
500
700
900
1100
1300
1500
1700
Time (s)

Figure 3

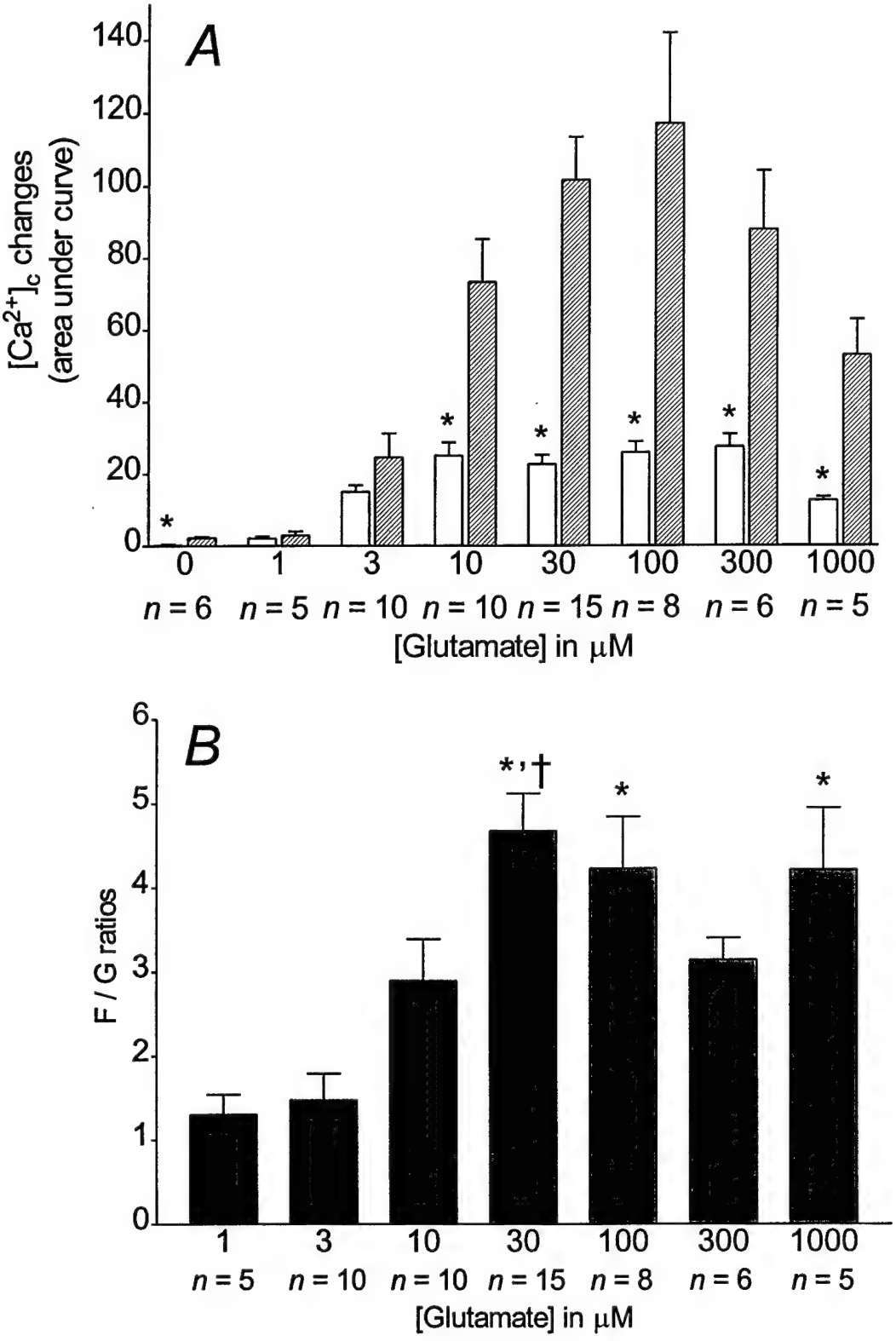
A
[Ca2+]c changes (area under curve)
140
120
100
80
60
40
20
0
*
0
1
3
10
30
100
300
1000
n = 6 n = 5 n = 10 n = 10 n = 15 n = 8 n = 6 n = 5
[Glutamate] in μM
B
F / G ratios
6
5
4
3
2
1
0
*,†
*
*
1
3
10
30
100
300
1000
n = 5 n = 10 n = 10 n = 15 n = 8 n = 6 n = 5
[Glutamate] in μM

Figure 4

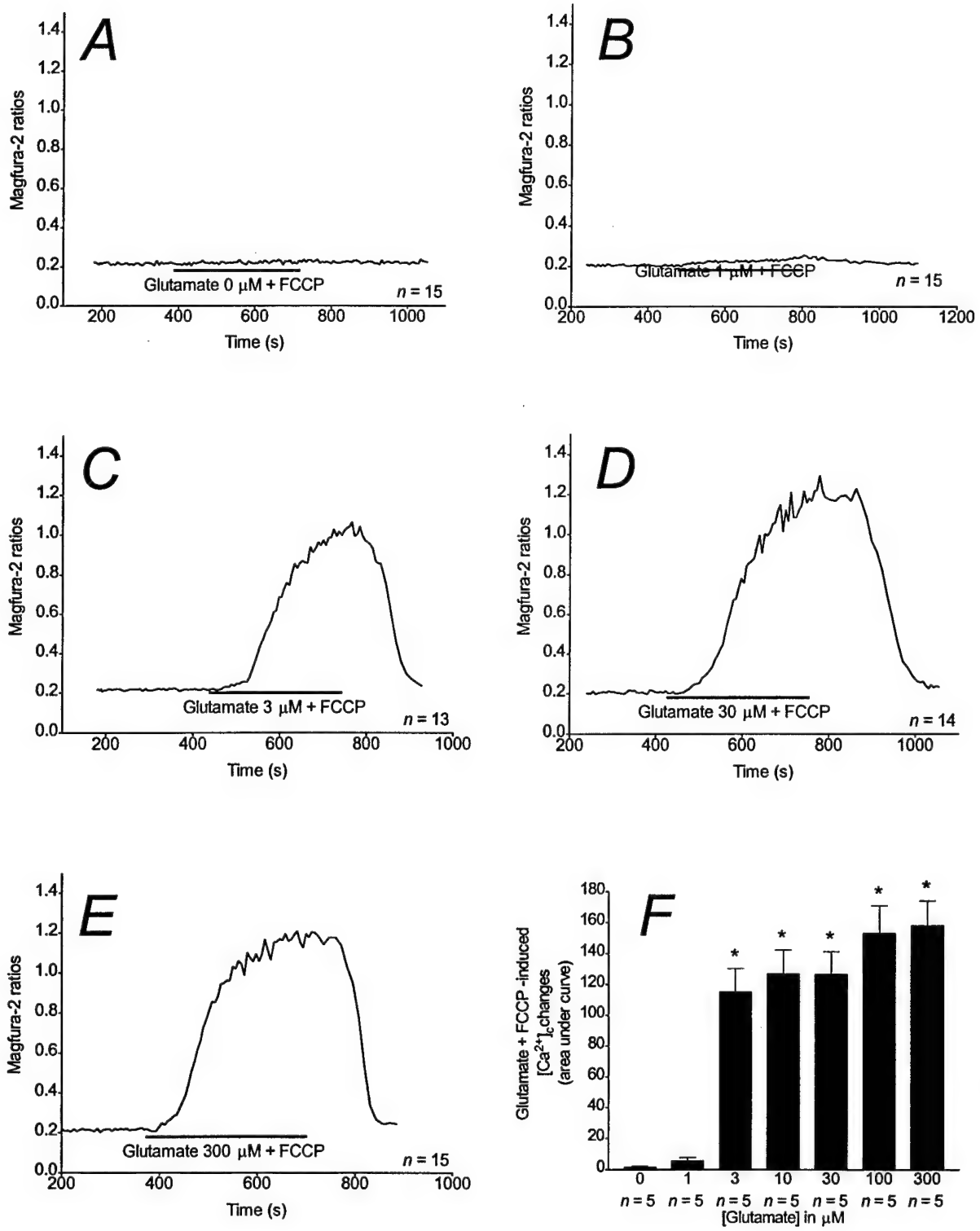
A
Magfura-2 ratios
Glutamate 0 μM + FCCP
n = 15
Time (s)
B
Glutamate 1 μM + FCCP
n = 15
C
Glutamate 3 μM + FCCP
n = 13
D
Glutamate 30 μM + FCCP
n = 14
E
Glutamate 300 μM + FCCP
n = 15
F
Glutamate + FCCP -induced
[Ca2+]c changes
(area under curve)
[Glutamate] in μM

Figure 5

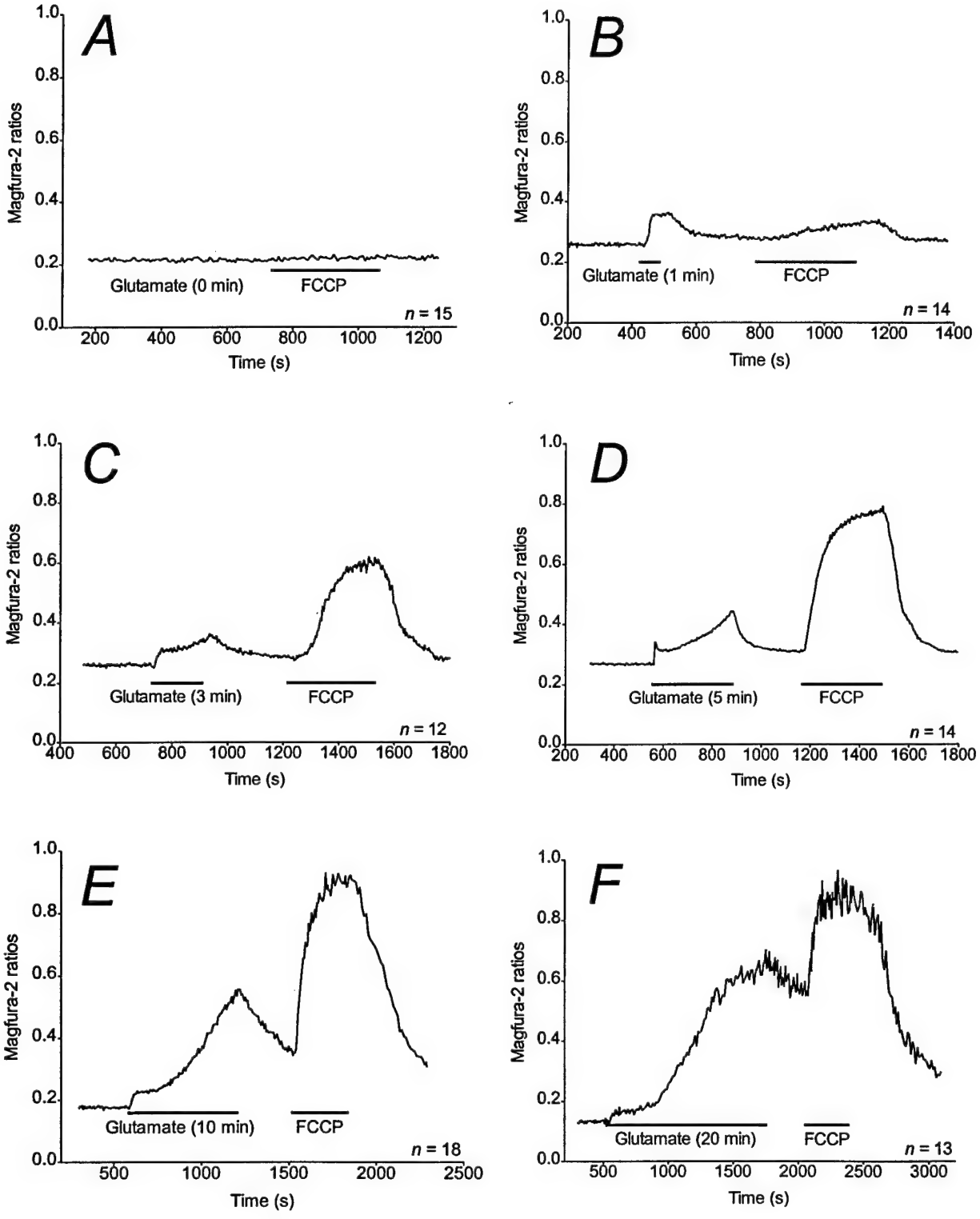
A
Magfura-2 ratios
Glutamate (0 min)
FCCP
n = 15
Time (s)
B
Glutamate (1 min)
FCCP
n = 14
C
Glutamate (3 min)
FCCP
n = 12
D
Glutamate (5 min)
FCCP
n = 14
E
Glutamate (10 min)
FCCP
n = 18
F
Glutamate (20 min)
FCCP
n = 13

Figure 6

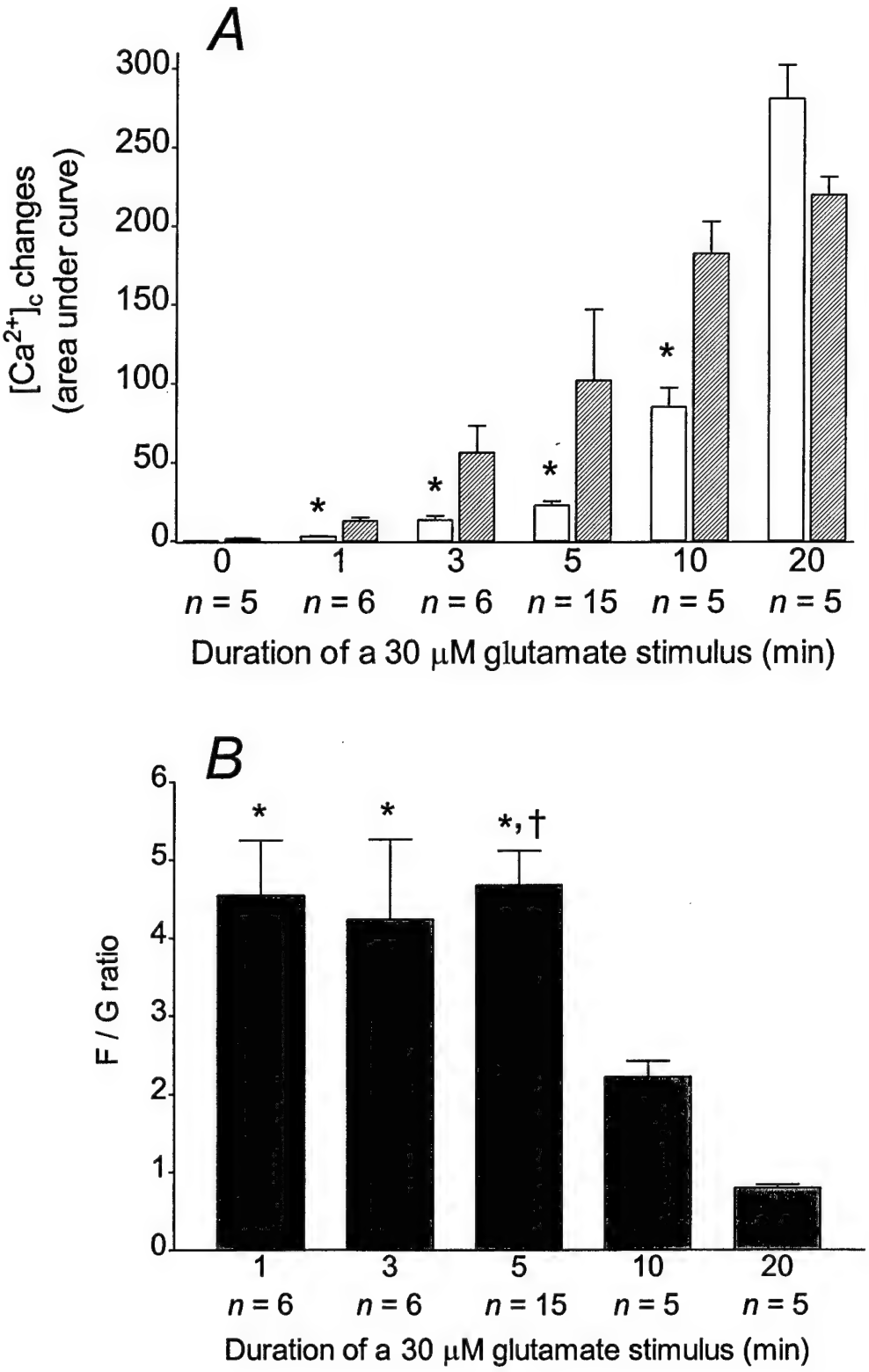
A
300
250
200
150
100
50
0
[Ca2+]c changes
(area under curve)
*
*
*
*
0
1
3
5
10
20
n = 5
n = 6
n = 6
n = 15
n = 5
n = 5
Duration of a 30 μM glutamate stimulus (min)
B
6
5
4
3
2
1
0
F / G ratio
*
*
*,†
1
3
5
10
20
n = 6
n = 6
n = 15
n = 5
n = 5
Duration of a 30 μM glutamate stimulus (min)

Figure 7

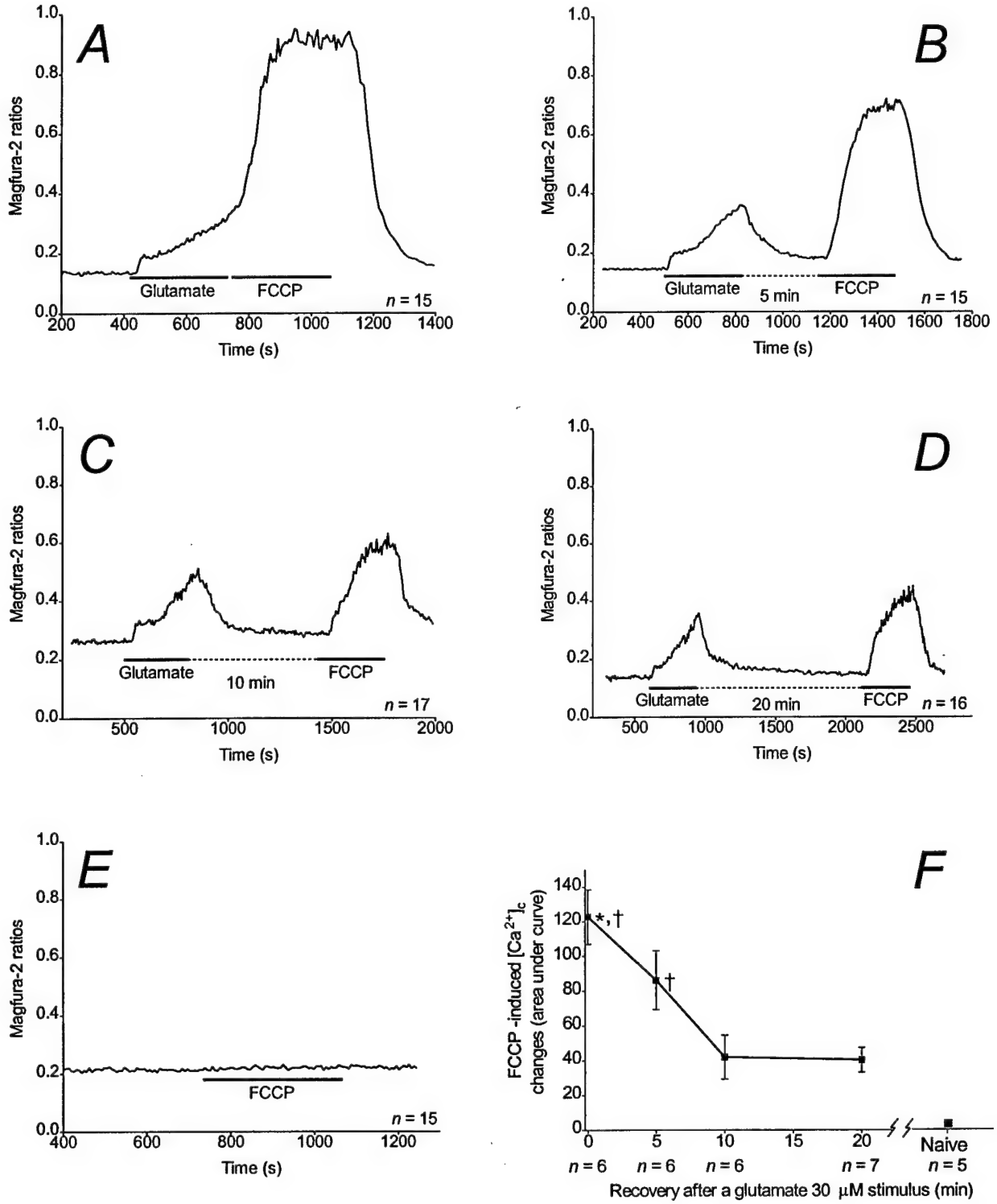
A
Magfura-2 ratios
Glutamate
FCCP
n = 15
Time (s)
B
Glutamate
5 min
FCCP
n = 15
Time (s)
C
Glutamate
10 min
FCCP
n = 17
Time (s)
D
Glutamate
20 min
FCCP
n = 16
Time (s)
E
FCCP
n = 15
Time (s)
F
FCCP -induced [Ca2+]c changes (area under curve)
*,†
†
n = 6
n = 6
n = 6
n = 7
n = 5
Naive
Recovery after a glutamate 30 µM stimulus (min)

Figure 8

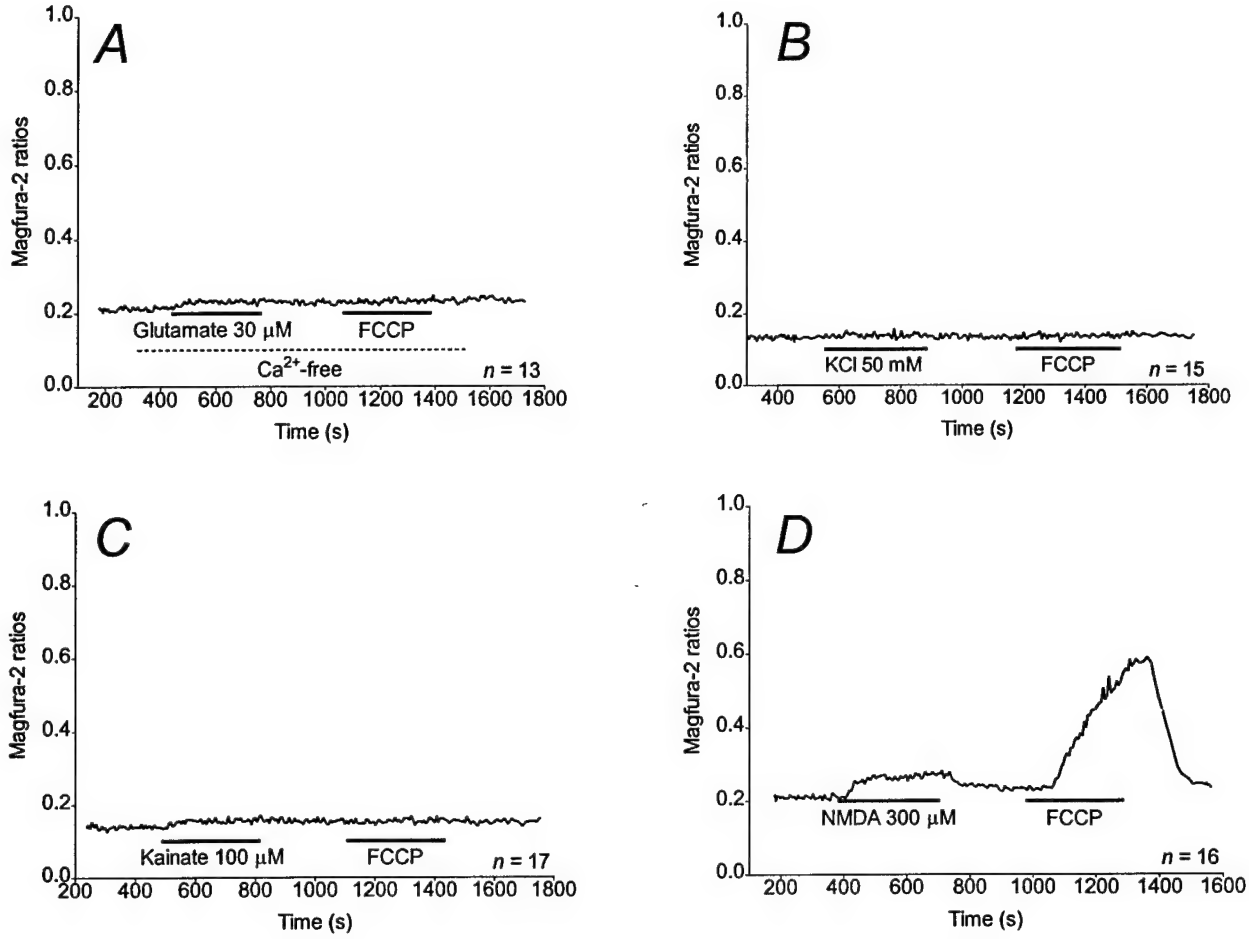
A
Magfura-2 ratios
1.0
0.8
0.6
0.4
0.2
0.0
Glutamate 30 µM
FCCP
Ca2+-free
n = 13
200 400 600 800 1000 1200 1400 1600 1800
Time (s)
B
Magfura-2 ratios
KCl 50 mM
FCCP
n = 15
400 600 800 1000 1200 1400 1600 1800
Time (s)
C
Magfura-2 ratios
Kainate 100 µM
FCCP
n = 17
200 400 600 800 1000 1200 1400 1600 1800
Time (s)
D
Magfura-2 ratios
NMDA 300 µM
FCCP
n = 16
200 400 600 800 1000 1200 1400 1600
Time (s)

Figure 9

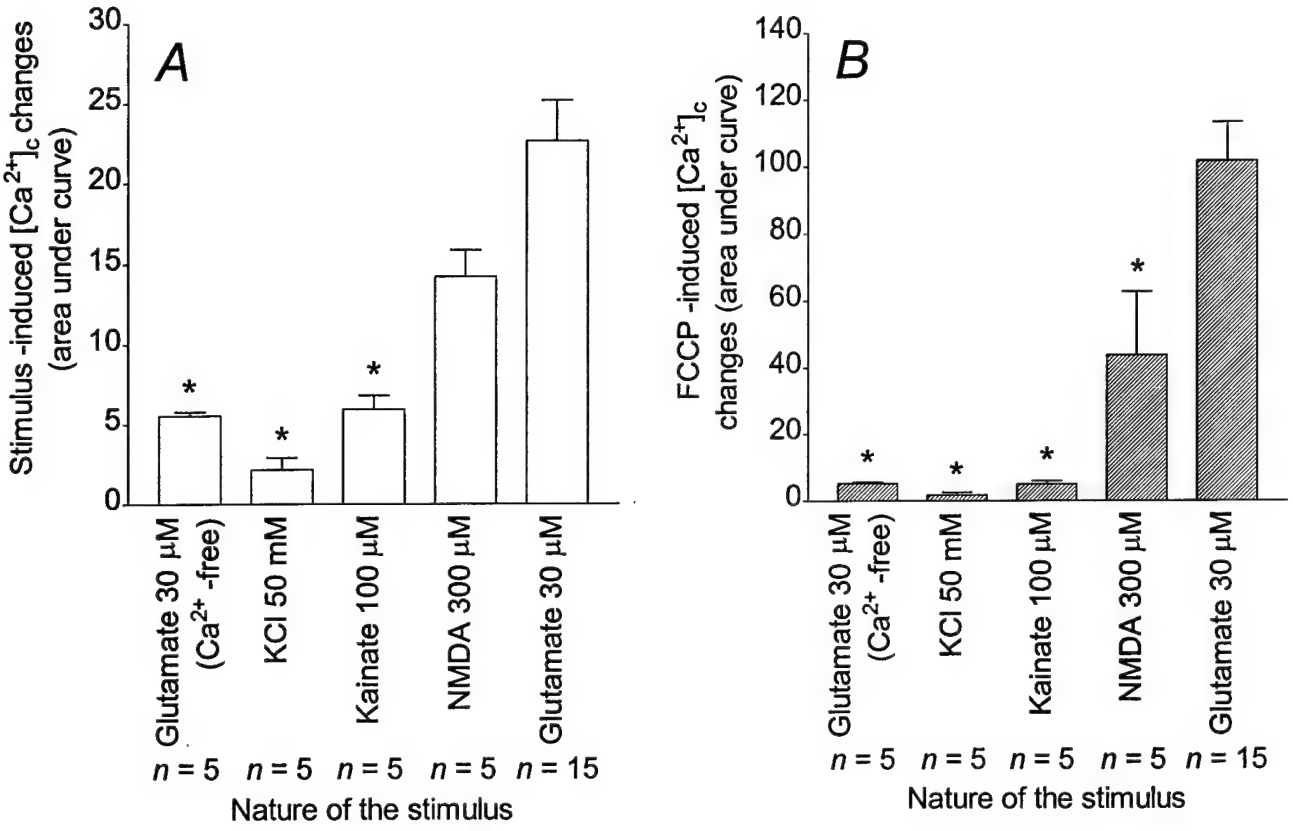
A
Stimulus -induced [Ca2+]c changes (area under curve)
30
25
20
15
10
5
0
*
*
*
Glutamate 30 µM (Ca2+ -free)
KCl 50 mM
Kainate 100 µM
NMDA 300 µM
Glutamate 30 µM
n = 5 n = 5 n = 5 n = 5 n = 15
Nature of the stimulus
B
FCCP -induced [Ca2+]c changes (area under curve)
140
120
100
80
60
40
20
0
*
*
*
*
Glutamate 30 µM (Ca2+ -free)
KCl 50 mM
Kainate 100 µM
NMDA 300 µM
Glutamate 30 µM
n = 5 n = 5 n = 5 n = 5 n = 15
Nature of the stimulus

SOCIETY FOR NEUROSCIENCE
2000 ABSTRACT FORM

Read all instructions before typing abstract.
See *Call for Abstracts* and reverse of this sheet.
Complete abstract and **all boxes at left and below.**
(Please type or print in black ink.)

_____ Check here if this is a **REPLACEMENT** of abstract submitted earlier. Remit a nonrefundable **$50** for each replacement abstract. Replacement abstracts must be **RECEIVED** by Wednesday, May 3, 2000.

SMALLEST RECOMMENDED TYPE SIZE: 10 POINT

SAMPLE:
2000 Annual Meeting
New Orleans, La.
November 4–9, 2000

POSTMARK DEADLINE:

MONDAY, APRIL 24, 2000

First (Presenting) Author

Provide full name (no initials), address, and phone numbers *of first author on abstract. You may present (first author) only one abstract.* (Please type or print in black ink.)

TANYA VOTYAKOVA
DEPT. PHARMACOL.
UNIV PITTSBURGH
W1313 BST PITTSBURGH
PA 15261 Fax: (412) 624 0794
Office: (412) 648 2135 Home: ( )
E-mail: TVOTYAK@HOTMAIL.COM

An asterisk must be placed after the sponsor's (signing member) name on the abstract.

MANDATORY: The present scientific work may involve a real or perceived financial conflict of interest. (See page 4, item 11.)
☐ yes ☒ no If yes: _____

Presentation Preference

Check one: ☒ poster only ☐ slide/poster

Themes and Topics

See list of themes and topics, pp. 17–18. Indicate below a first and second choice appropriate for programming and publishing your paper.

1st theme title: Disorders **theme letter:** J
1st topic title: Ex. amino acids: excitotox **topic number:** 125

2nd theme title: Disorders **theme letter:** J
2nd topic title: Neurotoxicity **topic number:** 141

Special Requests (for example, projection, video, or computer requirements)

Include nonrefundable **abstract handling fee** of **$50.** Fill out payment information form below. Purchase orders will not be accepted. Submission of abstract handling fee does not include registration for the Annual Meeting.

$\Delta\Psi_M$-DEPENDENT AND INDEPENDENT ROS PRODUCTION BY RAT BRAIN MITOCHONDRIA.

T.V. Votyakova and I.J. Reynolds*, Department of Pharmacology, University of Pittsburgh, Pittsburgh PA 15261.

In this study we investigated mitochondrial reactive oxygen species (ROS) generation by rat brain mitochondria. We studied two major mechanisms, $\Delta\Psi$m-dependent and –independent. $\Delta\Psi$m-dependent ROS production is supported by succinate oxidation in intact mitochondria. Rotenone (Rot), which blocks reverse electron transfer, completely inhibits ROS production. However, after a lag period of 5 min ROS production is resumed at the level of about 10% of the initial one apparently after the reduction of the quinone pool up to some threshold level. Inhibition of Complex III at the site of semiubiquinone reduction decreases the ROS production almost to zero, suggesting that some 90% of ROS generated by intact mitochondria oxidizing succinate originates at Complex I as a result of reverse electron transfer, and the rest are produced at the site of ubiquinones. Agents decreasing $\Delta\Psi$m at least below the level of ATP-ase operation (ADP, Ca^{2+} ions or uncouplers) strongly inhibited ROS production. By the restoration of $\Delta\Psi$m (the transition to state 4 from state 3, or chelating Ca^{2+} ions) ROS production was resumed.

In our hands no ROS production was observed with incubations up to 20 min of intact brain mitochondria in the presence of NADH-linked substrates. However the addition of Rot greatly increased ROS generation. The lag period of Rot action was about 20 sec, after which $\Delta\Psi$m was collapsed. This ROS production is comparable to the reverse electron transfer component of succinate-supported ROS production. Antimycin (Ant) and myxothiazole (Myxo) had no effect. Ant depolarized mitochondria and inhibited ROS production supported by succinate but after a lag period of 2-3 minutes the rate of ROS generation was gradually restored to 10-15% of initial value. Rot had no effect on ROS production at this stage, while Myxo inhibited it, suggesting the only source of ROS in this case at the Complex III.

Supported by USAMRMC (IJR).

Key Words: (see instructions p. 4)

1. Reactive oxygen species
2. Intracellular calcium
3. Mitochondrial membrane potential
4.

Signature of Society for Neuroscience member required below. ***No member may sign more than one abstract. The signing member must be an author on the paper and an asterisk must be placed after the sponsor's (signing member) name on the abstract.***

The signing member certifies that any work with **human or animal subjects** related in this abstract complies with the guiding policies and principles for experimental procedures endorsed by the Society. This signature acknowledges that each author on this abstract has seen and approved the final version of the abstract and has given consent to appear as an author. Authors must comply with ethical guidelines for human and animal research and may be asked to supply added documentation.

Society for Neuroscience member's signature

Ian J. Reynolds
Printed or typed name

(412) 648 2134
Telephone number

0000113 15
Member ID number (mandatory)

Tear at perforation

SOCIETY FOR NEUROSCIENCE
2000 ABSTRACT FORM

Read all instructions before typing abstract.
See *Call for Abstracts* and reverse of this sheet.
Complete abstract and **all boxes at left and below.**
(Please type or print in black ink.)

_____ Check here if this is a **REPLACEMENT** of abstract submitted earlier. Remit a nonrefundable **$50** for each replacement abstract. Replacement abstracts must be **RECEIVED** by Wednesday, May 3, 2000.

SMALLEST RECOMMENDED TYPE SIZE: 10 POINT

SAMPLE:
2000 Annual Meeting
New Orleans, La.
November 4–9, 2000

POSTMARK DEADLINE:

MONDAY, APRIL 24, 2000

First (Presenting) Author

Provide full name (no initials), address, and phone numbers *of first author on abstract. You may present (first author) only one abstract.* (Please type or print in black ink.)

Jennifer Buckman
University of Pittsburgh
Dept. of Pharmacology, W1303BST
Pittsburgh, PA 15261
Fax: (412) 648-1945
Office: (412) 383-7667 Home: (412) 441-0216
E-mail: jfb6+@pitt.edu

An asterisk must be placed after the sponsor's (signing member) name on the abstract.

MANDATORY: The present scientific work may involve a real or perceived financial conflict of interest. (See page 4, item 11.)
☐ yes ☒ no If yes: _____

Presentation Preference

Check one: ☒ poster only ☐ slide/poster

Themes and Topics

See list of themes and topics, pp. 17–18. Indicate below a first and second choice appropriate for programming and publishing your paper.

1st theme title: Disorders of the Nerv. Sys. + Aging **theme letter:** J
1st topic title: Excit. Amino Acids: excitotox + cell death **topic number:** 125

2nd theme title: Disorders of the Nervous Sys + Aging **theme letter:** J
2nd topic title: Ischemia: cellular + molec. mech's **topic number:** 133

Special Requests (for example, projection, video, or computer requirements)

Include nonrefundable **abstract handling fee of $50.** Fill out payment information form below. Purchase orders will not be accepted. Submission of abstract handling fee does not include registration for the Annual Meeting.

SPONTANEOUS MITOCHONDRIAL DEPOLARIZATIONS AND MOTILITY IN NEURONS.

JF Buckman*, Y Han and IJ Reynolds Dept. of Pharmacology, Univ. of Pittsburgh, Pittsburgh, PA 15261.

There is an emerging appreciation for a role of mitochondria in several forms of neural cell death. However, uncertainty about the significance of many aspects of normal mitochondrial physiology and function remains. Many critical bioenergetic features of mitochondria are driven by $\Delta\Psi_m$. Cultured forebrain neurons were loaded with different concentrations of two $\Delta\Psi_m$-sensitive fluorescent dyes, JC-1 and TMRM, and imaged. Optimal low and high dye concentrations were chosen and dye distribution within the neurons, sensitivity to the depolarizing agents, mitochondrial motility and $\Delta\Psi_m$ stability were assessed. Noticeable differences in cell body and process labeling, which were contingent on the loading concentration of the dye, were observed. Mitochondrial depolarization by the uncoupler, FCCP, led to an increase in TMRM and JC-1 monomer fluorescence in both cell bodies and processes, whereas depolarization by glutamate/glycine led to a greater increase in fluorescence intensity within the cell bodies, as compared to the processes. Compelling evidence for a complex and dynamic role of mitochondria in normal cellular functioning was observed. At low concentrations of both TMRM and JC-1, a large percentage of fluorescent mitochondria within the neuronal culture exhibited extensive motility. Moreover, the loading concentration of the $\Delta\Psi_m$-sensitive fluorescent dyes was inversely related to the percentage of mitochondria that appeared to move. At higher concentrations of TMRM and JC-1, mitochondria exhibited spontaneous oscillations in fluorescent intensity in small regions of the neuronal processes, indicative of partial, transient mitochondrial depolarizations We are currently investigating the impact of mitochondrial motility and $\Delta\Psi_m$ oscillations to determine the relationship of these phenomenon to cellular and synaptic signaling, ATP availability and usage, and permeability transition

Supported by USAMRMC, Scaife Family Foundation and T32NS07391.

Key Words: (see instructions p. 4)

1. excitotoxicity
2. JC-1
3. _____
4. _____

Signature of Society for Neuroscience member required below. ***No member may sign more than one abstract. The signing member must be an author on the paper and an asterisk must be placed after the sponsor's (signing member) name on the abstract.***

The signing member certifies that any work with **human or animal subjects** related in this abstract complies with the guiding policies and principles for experimental procedures endorsed by the Society. This signature acknowledges that each author on this abstract has seen and approved the final version of the abstract and has given consent to appear as an author. Authors must comply with ethical guidelines for human and animal research, and may be asked to supply added documentation.

Society for Neuroscience member's signature

Jennifer Buckman
Printed or typed name

(412) 383-7667
Telephone number

00016731 1
Member ID number (mandatory)

QUANTITATIVE EVALUATION OF MITOCHONDRIAL CALCIUM CONTENT FOLLOWING NMDA RECEPTOR STIMULATION. J. B. Brocard*, M. Tassetto and I. J. Reynolds. Department of Pharmacology, University of Pittsburgh, Pittsburgh PA 15261.

Recent observations showed that mitochondrial calcium accumulation is necessary for a NMDA (N-Methyl-D-Aspartate) receptor stimulus to be toxic to cortical neurons [Stout et al. (1998) *Nat. Neurosci.* 1: 366]. In an attempt to determine the magnitude of the calcium fluxes involved in this phenomenon, we used carbonyl cyanide *p*- (trifluoromethoxy) phenyl-hydrazone (FCCP), a mitochondrial proton gradient uncoupler, to release the mitochondrial calcium store during and following a glutamate stimulus, and magfura-2 to monitor cytoplasmic calcium. This method revealed a mitochondrial calcium concentration much larger than the cytoplasmic calcium changes observed during glutamate exposure, suggesting a very large accumulation of calcium in the mitochondria. Mitochondrial calcium uptake is dependent on glutamate concentration. In contrast, the changes in the overall quantity of calcium entering the cell, as measured by simultaneously treating neurons with glutamate and FCCP, showed an 'all-or-nothing' response. Mitochondrial calcium uptake is also dependent on the nature and duration of a given stimulus as shown by comparing mitochondrial calcium accumulation associated with depolarization, kainate and NMDA compared to glutamate. Thus, although mitochondrial calcium content is low in naïve cortical neurons, these organelles buffer large quantities of calcium during and after a glutamatergic stimulus. *Supported by the Human Frontier Science Program Organization (J. B. B.), NS34138 and DAMD 17-98-1-8627 (I. J. R.).*

SOCIETY FOR NEUROSCIENCE
2000 ABSTRACT FORM

Read all instructions before typing abstract.
See *Call for Abstracts* and reverse of this sheet.
Complete abstract and **all boxes at left and below.**
(Please type or print in black ink.)

_____ Check here if this is a REPLACEMENT of abstract submitted earlier. Remit a nonrefundable **$50** for each replacement abstract. Replacement abstracts must be RECEIVED by Wednesday, May 3, 2000.

First (Presenting) Author

Provide full name (no initials), address, and phone numbers *of first author on abstract. You may present (first author) only one abstract.* (Please type or print in black ink.)

Dr Geraldine J Kress
Univ Pittsburgh -- Pharmacology
W1313 BST
Pittsburgh, PA 15261
Fax: (412) 648-1945
Office: (412) 648-2135 Home: ( )
E-mail: gjk2+@pitt.edu

SMALLEST RECOMMENDED TYPE SIZE: 10 POINT

SAMPLE:
2000 Annual Meeting
New Orleans, La.
November 4–9, 2000

POSTMARK DEADLINE:

MONDAY, APRIL 24, 2000

An asterisk must be placed after the sponsor's (signing member) name on the abstract.

MANDATORY: The present scientific work may involve a real or perceived financial conflict of interest. (See page 4, item 11.)
☐ yes ☒ no If yes: _____

Presentation Preference

Check one: ☒ poster only ☐ slide/poster

Themes and Topics

See list of themes and topics, pp. 17–18. Indicate below a first and second choice appropriate for programming and publishing your paper.

1st theme title: Disorders
theme letter: J
1st topic title: Neurotoxicity
topic number: 141

2nd theme title: Disorders
theme letter: J
2nd topic title: Degenerative disease Parkinson's
topic number: 131

Special Requests (for example, projection, video, or computer requirements)

Include nonrefundable **abstract handling fee of $50.** Fill out payment information form below. Purchase orders will not be accepted. Submission of abstract handling fee does not include registration for the Annual Meeting.

INTRACELLULAR Fe^{2+} FLUORESCENCE MEASUREMENTS AND INTRACELLULAR Fe^{2+} INDUCED NEUROTOXICITY

G. J. Kress*, K.E. Dineley, and I. J. Reynolds.
Dept. of Pharmacology, Univ. of Pittsburgh, Pittsburgh, PA 15261.

Iron dependent processes may play a pivotal role in the development of oxidant-induced cell injury as is observed in Parkinson's disease, Alzheimer's disease, and ischemia. To study this phenomenon in neurons, astrocytes, and oligodendrocytes, it is our goal to develop a selective method for measuring intracellular iron (II) ($[Fe^{2+}]_i$) with fluorescence microscopy.

Previous studies have utilized calcein to measure $[Fe^{2+}]_i$. Calcein can be quenched by various ions, including iron and cobalt. A novel technique is proposed in which Fura-2 AM or Mag-Fura-2 AM can be used to study $[Fe^{2+}]_i$ relevant to cell injury. Fura-2 AM and Mag-Fura-2 AM are primarily utilized for calcium measurements, in which both wavelength of these ratiometric dyes increase intensity and the excitation wavelength shifts with increased intracellular calcium. In the presence of sodium pyrithione, an ionophore, and elevated extracellular $[Fe^{2+}]$, $[Fe^{2+}]_i$ can completely quench both wavelength of Fura-2 and Mag-Fura-2 in primary cultures of rat neurons, astrocytes, microglia, and oligodendrocytes. Thus, the spectral characteristics of Fura-2 and Mag-Fura-2 bound to Fe^{2+} are distinct from intracellular calcium. Also, it is observed that Fura-2 has a higher affinity for Fe^{2+} than Mag-Fura-2. Thus, utilizing Fura-2 and Mag-Fura-2 to measure $[Fe^{2+}]_i$ allows estimation of $[Fe^{2+}]_i$ over a range of values.

It is known that astrocytes are more resistant to glutamate, oxidative, and zinc exposures than neurons or oligodendrocytes. In preliminary experiments, we have noticed a concentration dependence curve of Fe^{2+} toxicity in the presence of sodium pyrithione, which caused complete death of neurons within 8 hrs while astrocytes were essentially still viable. Future experiments will further investigate the relationship between acute Fe^{2+} exposure to neurons, astrocytes, oligodendrocytes, and cytotoxicity.

(Supported by NS 34138)

Key Words: (see instructions p. 4)

Iron Ion Fura-2 Imaging Astrocyte

Signature of Society for Neuroscience member required below. ***No member may sign more than one abstract. The signing member must be an author on the paper and an asterisk must be placed after the sponsor's (signing member) name on the abstract.***

The signing member certifies that any work with **human or animal subjects** related in this abstract complies with the guiding policies and principles for experimental procedures endorsed by the Society. This signature acknowledges that each author on this abstract has seen and approved the final version of the abstract and has given consent to appear as an author. Authors must comply with ethical guidelines for human and animal research, and may be asked to supply added documentation.

Geraldine J Kress
Society for Neuroscience member's signature

Geraldine J. Kress
Printed or typed name

(412) 648-2135
Telephone number

10000529 7
Member ID number (mandatory)